Investigating Break Induced Replication and Template Switching in Fission Yeast

DEPARTMENT OF BIOCHEMISTRY
UNIVERSITY OF OXFORD

A thesis presented to the Faculty of Medical Sciences Division, University of Oxford for the degree of MSc by Research in Biochemistry

Yassine Laksir

Corpus Christi College
University of Oxford
Department of Biochemistry

Michaelmas term, 2022

Declaration

I hereby declare that this thesis entitled “Investigating Break Induced Replication and Template Switching in Fission Yeast” has been originally carried out by me under the supervision of Professor Matthew Whitby. This work has not formed the basis for award of any degree or diploma previously. The particulars given in this thesis are true to the best of my knowledge.

Yassine Laksir

Department of Biochemistry,
Corpus Christi College,
University of Oxford

Acknowledgments

I would like to thank my supervisor, Prof Matthew Whitby, for his support throughout my course. He has always been available and happy to help me in any possible way, both in my MSc degree and in enhancing my career progress. Overall, he has made me a better scientist, and I will forever be grateful to him. I would also like to thank Dr Christos Andreadis and Prof Stephan Uphoff, whose support and guidance was key for the completion of my degree.

I am grateful to Bushra Senin and Anja Bitterwolf, colleagues who made my journey a lot more enjoyable and pleasant. I would like to thank Dr Ian Gibbs-Seymour, Prof Neil Brockdorff and Prof Nicholas Lakin for their helpful advice and comments on my work. They have improved the quality of my thesis and made my progress towards my goals more efficient. I am grateful to my parents for their love and financial support to complete this degree. They believed in me even when I was not sure I could make it.

Lastly, I would like to thank Dr Fekret Osman whom I never met in person, but I would have loved to. His previous work at the Whitby lab was crucial for my research, and I am extremely grateful for it.

Abstract

Single-stranded DNA breaks (SSBs) are the most common DNA lesion a cell can suffer with ~1 SSB formed every 5 seconds in a mammalian cell under normal conditions. Hence, a significant number of SSBs are encountered by replication forks in S-phase and these encounters can result in double-stranded DNA breaks (DSBs), which are highly toxic lesions. Determining how DSBs are formed from such encounters and how these are repaired has been an important area of research for many years. Until recently, the prevailing hypothesis was that fork encounter of a SSB in the leading-strand template resulted in a single-ended DSB (seDSB) by "replication runoff", whereas encounter of a lagging-strand template SSB could be successfully "skipped over" by the fork leaving behind a double-ended DSB (deDSB) in one of the replicated sister chromatids. However, recent work, using the *Xenopus* egg extract system to study replication fork-SSB collisions *in-vitro*, has shown that both leading and lagging template strand SSBs cause seDSBs. An important goal is to establish whether this new paradigm holds true *in-vivo*. Unlike deDSBs, seDSBs are thought to be repaired mainly by a highly mutagenic process termed break-induced replication (BIR). Our understanding of the molecular mechanism of BIR has come mainly from studies of the repair of non-S-phase associated DSBs in budding yeast. How well these reflect what happens during the repair of replication-associated DSBs, and whether BIR is well-conserved amongst eukaryotes, are largely unanswered questions.

Here, I establish for the first time the Flp-nick system in fission yeast. This experimental tool utilises a re-engineered version of the Flp recombinase to induce irreversible SSBs at Flp Recognition Target (*FRT*) sites inserted into the genome of interest. Following nick induction, the re-engineered Flp protein remains covalently attached to the 3'-end of the SSB via a phosphotyrosyl DNA linkage, essentially

mimicking a trapped Topoisomerase 1. In my set-up, the *FRT* site is inserted at the *ade6* locus on chromosome 3 of fission yeast, where DNA replication occurs almost always in the same direction. This allows us to designate whether the SSB is in the leading or lagging template strand based on the *FRT* site orientation. I use this system to study the recombination events generated following the encounter of the SSB in both leading and lagging template strands by the replication fork.

I show that a Flp-nick generated SSB does not affect viability in fission yeast. However, as expected, it does induce recombination in its immediate vicinity. It also induces template switching at a genetic reporter positioned “downstream” of the SSB, which is indicative of BIR. Importantly, both leading and lagging template strand SSBs induce template switching suggesting that both give rise to seDSBs upon fork encounter, which in turn lead to BIR. I confirm these findings using another system to induce site-specific SSBs, the M13 filamentous bacteriophage gpII protein. With both the Flp-nick system and gpII systems, I find that converging forks limit BIR-associated template switching. I confirm that template switching is dependent on Rad52 and requires Rad51, and I determine the importance of several candidate proteins on Flp-nick-induced recombination.

Abbreviations

SSC	Saline Sodium Citrate
N3-MeA	3-MethylAdenine
AO	Active Orientation (*RTS1)*
ATP	Adenosine TriPhosphate
ALT	Alternative Lengthening of Telomeres
ARS	Autonomously Replicating Sequences
BER	Base Excision Repair
bp	base pair
BS	Bottom Strand
BIR	Break Induced Replication
CPT	Camptothecin
Chr	Chromosome
CFSs	Common Fragile Sites
CO	Crossover
DNA	DeoxyriboNucleic Acid
dNTP	DeoxyriboNucleotide TriPhosphate
DMSO	DiMethylSulphOxide
D-loop	Displacement loop
DTT	DiThioThreitol
DDR	DNA Damage Response
DDT	DNA Damage Tolerance
Pol	DNA Polymerase
dHJ	double Holliday Junction

DSB	Double-Stranded Break
DSBR	Double-Stranded Break Repair
EMMG	Edinburgh Minimal Media Glutamate
EDTA	EthyleneDiamineTetraAcetic acid
FRT	Flp Recognition Target
FPC	Fork Protection Complex
GCRs	Gross Chromosomal Rearrangements
HJ	Holliday Junction
HR	Homologous Recombination
HU	HydroxyUrea
IO	Inactive Orientation (*RTS1*)
ICL	Inter-Strand Crosslink
IR	Ionising Radiation
kb	kilo base pair
LA	Low Adenine
LB	Luria-Bertani
MEA	Malt Extract Agar
MMS	Methyl MethaneSulfonate
MCM	MiniChromosome Maintenance
MiDAS	Mitotic DNA Synthesis
nmt	no message in thiamine
NCO	Non-crossover
NHEJ	Non Homologous End Joining
NER	Nucleotide Excision Repair
NLS	Nucleus Localisation Sequence

PCR	Polymerase Chain Reaction
Pu-seq	Polymerase usage sequencing
PCNA	Proliferating Cell Nuclear Antigen
ROS	Reactive Oxygen Species
RDR	Recombination Dependent Replication
RFC	Replication Factor C
RFB	Replication Fork Barrier
RTS1	Replication Termination Sequence 1
RC	Replicative Complex
RPM	Revolutions Per Minute
rDNA	ribosomal DNA
SSA	Single Strand Annealing
SSB	Single-Stranded Break
ssDNA	Single-stranded DNA
SDS-PAGE	Sodium Dodecyl Sulphate PolyAcrylamide Gel Electrophoresis
SSBR	SSB Repair
SDSA	Synthesis Dependent Strand Annealing
TS	Top Strand
TLS	TransLesion Synthesis
TBE	Tris Buffered EDTA
TBS	Tris Buffered Saline
UV	Ultra Violet
YE	Yeast Extract
YES	Yeast Extract with Supplements

Table of Contents

Chapter 1

Introduction

The replisome is a multi-protein complex responsible for accurate genome duplication. DNA replication is exquisitely modulated to ensure the genome is duplicated only once every cell cycle, and prior to entering mitosis. The mechanistic processes involved in DNA replication are highly conserved across eukaryotes, although there are variations in DNA replication regulatory mechanisms and the complexity of the factors involved (Kearsey and Cotterill, 2003). The movement of the DNA replication fork is regularly challenged by obstacles including, among others, long-lived DNA-protein complexes, DNA breaks and transcription intermediates (**Fig. 1.1).** To overcome such obstacles, cells have developed a wide variety of mechanisms. Initially, cells may prevent the activity of replication fork barriers (RFBs). Should cells fail to preclude the activity of RFBs, they (*i.e.* RFBs) can cause the replisome to stall. In such scenario, the replisome can be stabilised to resume DNA replication once the barrier is removed or to allow merging with a replication fork travelling in the opposed direction. Should the replisome be unable to protect the replication fork structure, fork collapse (*i.e.* replisome proteins dissociation) can occur. Homologous recombination (HR) is pivotal to the repair and restart of collapsed/broken replication forks. Yet, HR can pose a significant threat to genomic stability and restart DNA replication at incorrect, non-contiguous DNA sequences and thus, cause deleterious genomic rearrangements when recombination is performed between ectopic homologous DNA sequences. These genomic rearrangements include, among others, inversions, deletions, duplications and translocations, which can cause altered gene expression and lead to further chromosomal instability that can drive the development of life-threatening diseases such as cancer (Carr and Lambert, 2013).

In this project, I utilise as a model system the fission yeast *Schizosaccharomyces pombe* (*S. pombe*) to investigate the homologous

recombination events implemented when replication forks encounter site-specific single-stranded DNA breaks (SSBs). In Chapter 1, I will review the mechanism of DNA replication and diverse challenges that physically impede the movement of the replication fork. I will also review various HR-based repair mechanisms required for the repair and restart of replication forks. A particular focus will be dedicated to the repair of SSBs in the context of a replication fork.

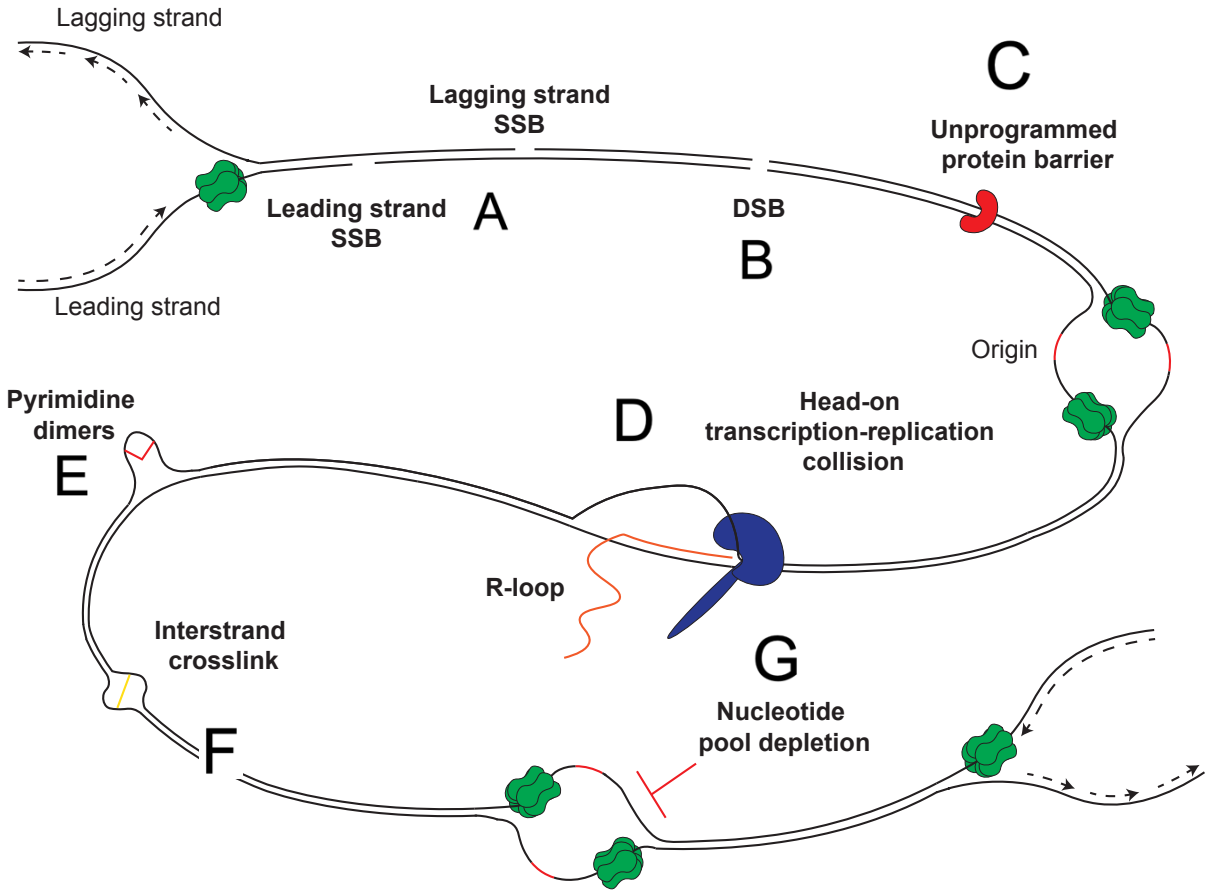

Figure 1.1. DNA replication barriers encountered by the replisome*. Replication forks are fired from the origins of replication. As the DNA is unwound to enable DNA synthesis from the parental DNA, replication forks can encounter a variety of replication fork barriers. These can be DNA breaks, which can affect either the template leading- or lagging-strand (SSBs)* ***(A)*** *or both simultaneously (DSBs)* ***(B)****. Replication fork barriers include also unprogrammed protein barriers* ***(C)****, transcription machinery* ***(D)****, pyrimidine dimers* ***(E)*** *and interstrand crosslinks* ***(F)****. An additional form of replication stress consists in the depletion of nucleotides* ***(G)*** *which causes the replication forks to stall.*

1.1 An Overview of DNA Replication

1.1.1 DNA replication origins

At each replication origin, a pair of replication forks is assembled and fired with the two replication forks travelling in opposing directions. In *Escherichia coli* (*E. coli*), DNA replication starts from a single replication origin (*i.e. OriC*) and travels bi-directionally through the circular genome. Replication termination occurs at specific DNA replication termination sequences (*i.e. TER*) (Leonard and Méchali, 2013). In eukaryotes, DNA replication is initiated from multiple replication origins scattered in the genome. Whilst in the budding yeast *Saccharomyces cerevisiae* (*S. cerevisiae*) replication origins are sequence specific, in *S. pombe* and humans replication origins lack such specificity and are scattered across wider genome areas. In budding yeast, replication origins are approximately 100-150 bp in size and are dubbed autonomously replicating sequences (ARS) (MacAlpine and Bell, 2005). Conversely, fission yeast replication origins possess no specific DNA sequence yet are A-T rich; furthermore, they are larger in size, approximately 1000 bp (Hayashi et al., 2007). Whilst in budding yeast replication origins are distinguished as “early” and “late” firing, in fission yeast and humans origin firing is stochastic, with replication origins differing in the frequency with which they fire. Importantly, all organisms have an excess of replication origins with no defect in viability when a replication origin is deleted, indicating that replication origins are utilised with some degree of flexibility, especially under conditions of stress (Woodward et al., 2006; Wyrick et al., 2001). Origin activation and initiation is tightly modulated to ensure that replication origins fire once only per cell division (Yeeles et al., 2015).

1.1.2 DNA replication initiation

In all organisms, a minimal replisome should present a core helicase to unwind the double-stranded DNA helix, a primase for primer synthesis, a DNA polymerase for nascent strand synthesis, a clamp sliding onto DNA which tethers the replisome to the DNA duplex, and finally a clamp loading factor. During DNA replication initiation, the origin recognition complex (ORC) binds to replication origins (Yuan and Li, 2020). Origin licencing occurs in G1-phase of the cell cycle and is the process which activates DNA-bound ORCs. In brief, this is achieved by binding of the ORC to Cdc6 and the subsequent loading of the ring-shaped Mcm2-7 hexamer onto DNA, and enables the stepwise assembly of the pre-replicative complex (pre-RC). This stepwise assembly of the pre-RC is also dependent on Cdt1, which is an essential licensing factor responsible for stabilising Mcm2-7 prior to loading onto DNA (Duzdevich et al., 2015). Prior to loading the second Mcm2-7 onto the DNA at the origin site, ORC and Cdc6 are released from the C-tier of the previously loaded Mcm2-7, hence leaving it encircled around the DNA duplex. Finally, ORC and Cdc6 re-bind to the loaded Mcm2-7 at the N-tier side and recruit the second Mcm2-7 in a Cdt1-mediated process, in a similar fashion to the loading of the first Mcm2-7 (**Fig 1.2**).

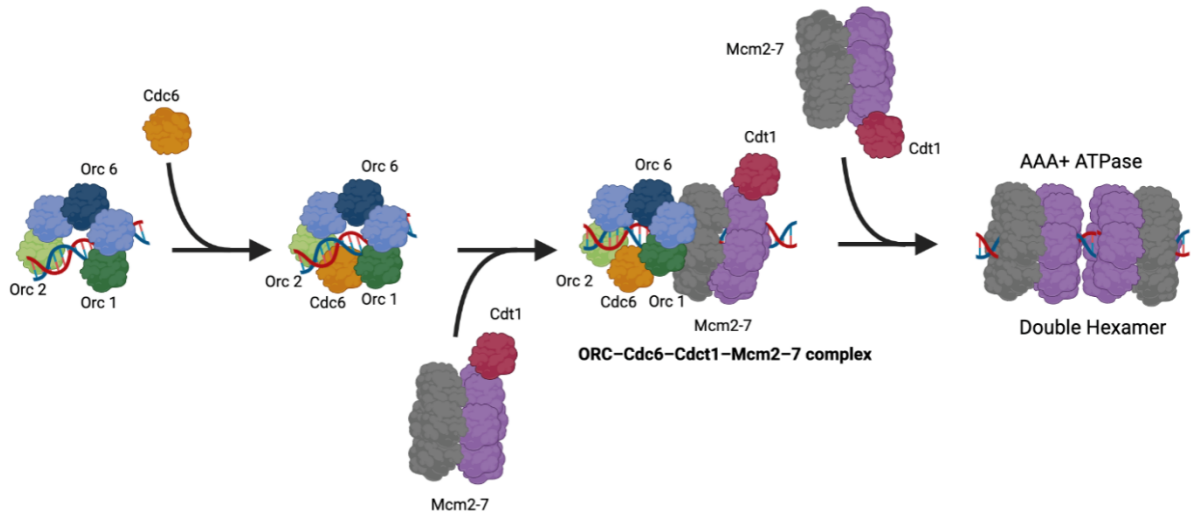

Figure 1.2. Mcm2-7 loading onto DNA replication origin mediated by ORC-Cdc6. *Cdc6 (yellow) binds to ORC (light green, dark green, light blue, dark blue subunits) "filling the gap" between Orc2 (light green) and Orc1 (dark green). This enables the ORC to serve as a landing platform for the first Mcm2-7 complex (C-tier, grey; N-tier purple). Thus, ORC-Mcm2-7 form an AAA+ protein complex which encircles the DNA duplex. The loading of the first Mcm2-7 by ORC-Cdc6 is not direct but mediated by the Mcm2-7 – bound essential licensing factor Cdt1 (red). This process is independent of ATP hydrolysis. Loading of the second Cdt1-bound Mcm2-7 complex requires ATP hydrolysis (not shown) by the ORC-Cdc6-Cdt1-Mcm2-7 complex and leads to the release of the Cdt1, Cdc6 and ORC in a sequential manner to finally assemble a functional AAA+ ATPase Mcm2-7. It is important to note that the assembled Mcm2-7 double hexamer is yet to be activated.*

The first step in the assembly of the CMG (Cdc45–Mcm2–7–GINS) helicase is the activation of the Mcm2-7 double hexamer. This process involves several components including, among others, Dbf4-dependent kinase (DDK), several Cyclin-dependent kinases (CDKs), Sld3–Sld7, Sld2, Mcm10 and Cdc45. DDK is responsible for phosphorylating Mcm2 and Mcm4. This chemical modification leads to the binding of Cdc45 and Sld3–Sld7 to the AAA+ double hexamer. Lastly, ATP hydrolysis by the CMG helicase and binding to Mcm10 extrudes the lagging-strand from the CMG central channel (Parker et al., 2017). Both CMG helicases must encircle their respective leading-strand and extrude the lagging-strand to enable the firing of two replication forks in opposing orientations. Furthermore, the CMG helicase contains two zing-finger domains which are in contact with the lagging-strand throughout the DNA replication process (Jenkyn-Bedford et al., 2021).

1.1.3 The elongation stage of DNA replication

The CMG helicase is essential in DNA replication elongation, and it unwinds the DNA to enable leading and lagging-strand synthesis. In yeast, the clamp-loading complex RFC is responsible for loading PCNA onto DNA at single-stranded/double-stranded junctions. PCNA is the key DNA polymerase clamp and regulates its processivity and rate of synthesis during DNA replication (Majka and Burgers, 2004). The first step of DNA replication elongation consists in the synthesis of short (10-15 bp) RNA sequences by Polα termed primers. Subsequently, DNA synthesis is continued by Polδ on the lagging-strand and Polε on the leading-strand (Miyabe et al., 2011). Both leading and lagging-strands are synthesised in the 5'→3' orientation since DNA polymerases can add nucleotides only to the 3'-OH. Thus, whilst the leading-strand is synthesised in a continuous manner in the direction of the replication fork, the lagging-strand is looped and synthesised discontinuously. Lagging-strand synthesis necessitates firstly

primer synthesis and secondly short tract elongation to generate DNA sequences termed Okazaki fragments. On the lagging-strand, primers are displaced by Polδ before being processed by Dna2 (RPA coated flaps) and flap endonuclease 1 FEN1 (uncoated flaps) (Kang et al., 2000; Stewart et al., 2008). Finally, DNA ligase I generates a continuous DNA strand by ligating the multiple Okazaki fragments. However, it should be noted that there is evidence challenging this canonical model of DNA replication. In the alternative model, Polδ acts as the main DNA polymerase for both leading and lagging-strands and Polε acts simply as a proof reading factor for Polδ synthesised DNA (Johnson et al., 2015).

1.1.4 DNA replication termination

DNA replication termination occurs when two replication forks from adjacent origins of replication merge. The completion of DNA replication involves the disassembly of the replisome and decatenation of the sister chromatids which are products of genome duplication. The failure of even a single pair of replication forks to merge prior to entering mitosis generates an area of unreplicated DNA, which can cause catastrophic genomic rearrangements during chromosome segregation in anaphase. Nevertheless, recovery pathways to complete genome duplication as cells enter mitosis exist, albeit these are prone to mutagenic synthesis (See section 1.5.4). In *E. coli*, DNA replication termination occurs at specific DNA sequences termed "*ter*". During canonical DNA replication, topological stress builds ahead of the replication fork which is relieved by DNA topoisomerases I and II. Therefore, it would be plausible to envisage that topoisomerases may be required to relieve the topological stress generated when two replication forks are at a short distance apart, and about to merge. Indeed, in *E. coli* and the SV40 virus, precatenanes are removed by topoisomerase II and this is crucial to enable fork convergence (Ishimi et al., 1992). In eukaryotes, the process of DNA

replication termination is less well understood. Indeed, topoisomerase II activity is dispensable in budding yeast (Baxter and Diffley, 2008). The Pif1-family of DNA helicase was shown the be among the main factors responsible for unwinding the final stretch of DNA between the two converging replication forks and thus, enabling DNA replication termination. This approach utilised an *in-vitro* reconstitution system of DNA replication termination including budding yeast proteins (Deegan et al., 2019). Recent studies in *Xenopus* egg extracts identified two key pathways for replication termination. The primary pathway involves Topoisomerase II to resolute the topological stress associated with fork convergence (Heintzman et al., 2019). In the alternative pathway, the activity of both the helicase RTEL1 and the replisome component Mcm10 are required for fork convergence under conditions of topological stress (Campos et al., 2022, Preprint)

During DNA replication termination, the two CMG helicases travelling towards each other pass each other with no detectable stalling or slowing down. Thus, CMG helicases continue translocating until reaching the single-stranded/ double-stranded DNA junction of the downstream Okazaki fragment. Subsequently, the final Okazaki fragment is processed by FEN1 and Polδ as indicated in section 1.1.3 (Deegan et al., 2019; Low et al., 2020). Finally, once CMG helicases encircle the double-stranded DNA, they are subject to polyubiquitination on the Mcm7 subunit by SCF^{Dia2} [SCF (Skp1/Cullin/F-box protein)] in budding yeast (Maric et al., 2014) or $CUL2^{LRR1}$ [CUL2 (Cullin-2)] in humans (Le et al., 2021). This enables the p97-mediated extraction of CMG helicases from chromatin (Le et al., 2021; Maric et al., 2014) (**Fig.1.3**).

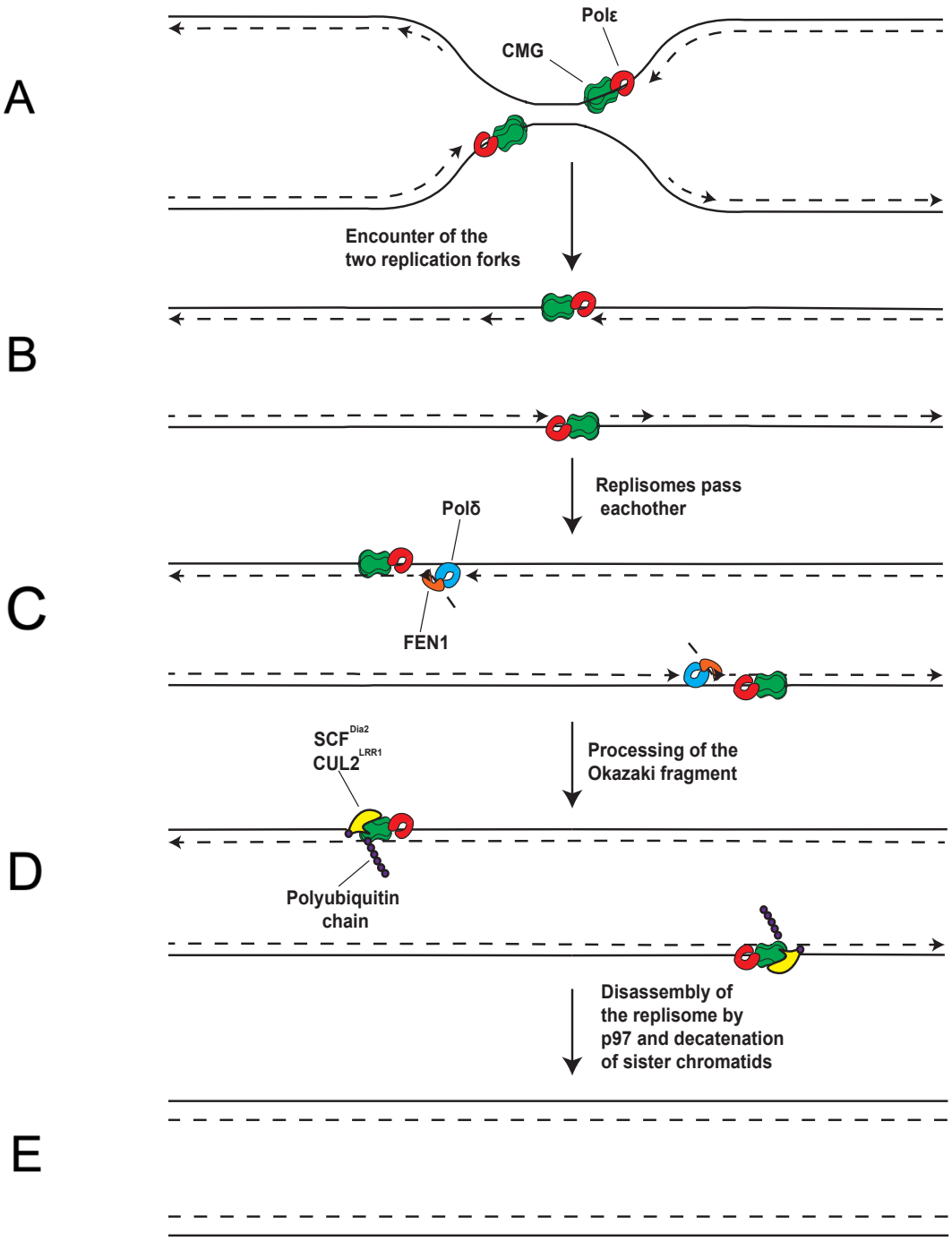

Figure 1.3. DNA replication termination in eukaryotes. A) *Towards the end of the replicon, replisomes arrive in proximity to each other.* ***B)*** *Replisomes pass each other without slowing down.* ***C)*** *Replisomes continue translocating until reaching the single-stranded/double-stranded DNA junction of the downstream Okazaki fragment, which is processed by FEN1 and Polδ.* ***D)*** *$CUL2^{LRR1}$ in humans and SCF^{Dia2} in budding yeast polyubiquitinate the Mcm7 subunit of the CMG helicase which is disassembled by p97.* ***E)*** *Decatenation of the sister chromatids is performed resulting in two copies of the same genetic material (not shown).*

1.2 DNA replication roadblocks

As mentioned in section 1.1.4, DNA replication must be completed prior to cells entering mitosis. A major challenge for the timely completion of DNA replication is the presence of replication fork barriers (RFBs) which can cause replication fork stalling or even collapse. DNA replication fork stalling is where a replication fork transiently arrests with its replisome components remaining attached to the DNA whilst the barrier is bypassed or removed from the chromatin – DNA replication can then resume (Hu et al., 2012). If DNA replication cannot resume, the fork structure can be stabilised to enable the merging with the fork travelling from the adjacent origin. Failure to stabilise an arrested replication fork can lead to its collapse, which likely involves the partial or complete disassembly of the replisome and consequent loss in ability to perform DNA synthesis. In such a scenario, restart of DNA replication necessitates additional factors for resumption of DNA synthesis and/or reassembly of the replisome (Cobb et al., 2005). Importantly, a collapsed fork can develop into a broken fork (*i.e.* a DNA double-stranded break (DSB) is formed), but fork breakage is not essential for replication restart (Carr and Lambert, 2013). RFBs can be caused by both endogenous and exogenous factors and include both damages to DNA bases and barriers which are specific to chromosomal features. In section 1.2, I discuss some of the common DNA lesions and RFBs which can impede DNA replication.

1.2.1 Replication fork barriers and DNA breaks

DNA bases can be damaged via both endogenous and exogenous factors. Endogenous causes include oxidative stress which can be generated by the by-products of normal physiological processes such as reactive oxygen species (ROS), whilst exogenous causes are generally genotoxic agents. Such damaged DNA bases can compromise the replisome progression since the main replicative DNA

polymerases are unable to add new nucleotides opposite to damaged or chemically modified bases. Importantly, such barriers do not necessarily compromise the progression of the replication fork *in vivo* and can be overcome by the replisome in some instances (Branzei and Foiani, 2010). A wide variety of genotoxins can compromise replisome progression. UV light damages the DNA by inducing a chemical reaction between two adjacent molecules of thymine/cytosine, hence generating photolesions termed cyclobutane pyrimidine dimers which can affect DNA fork progression (Saini et al., 2021). Similarly, methyl methanesulfonate (MMS) treatment induces the formation of 3-methyladenine (N3-MeA) products which block replisome progression (Wyatt and Pittman, 2006). Ionising radiation (IR) causes DSBs and promotes the generation of ROS which can induce a range of other DNA lesions that can impede replisome progression. Cisplatin causes the formation of interstrand crosslinks (ICLs), which preclude the separation of the DNA strands and impede the movement of the replication fork. Hydroxyurea (HU) is a ribonucleotide reductase inhibitor and transiently depletes the nucleotide pool which the replisome requires for DNA synthesis (Carr and Lambert, 2013). Lastly, camptothecin (CPT) treatment inhibits the religation step of topoisomerase I thereby generating long-lived SSBs with Top1 bound to the 3' end of the DNA via a phosphotyrosine linkage (Hsiang et al., 1985).

1.2.2 Replication-transcription collision

Collision between the transcription and replication machinery represents a significant threat for genomic stability and can cause collapse or breakage of the replication fork, especially when transcription and replication are not codirectional (Gaillard et al., 2013). Furthermore, excessive torsional stress is generated by replication-transcription collision. As a result, a large number of replication forks undergo reversal, hence both

delaying the completion of DNA replication and enhancing genomic instability due to the effect of nucleases on the reversed replication fork structure (García-Muse and Aguilera, 2016). In addition, especially in GC-rich DNA sequences, nascent RNA hybridises with one of the DNA strands thereby displacing the other DNA strand and forming an RNA-DNA hybrid structure termed R-loop. R-loops are often found near transcription regulatory regions and regulate gene expression yet also impede replisome progression. However, under hypoxia conditions and in tissues highly sensitive to oxygen depletion (*e.g.* brain), R-loops are found in excessive amounts and cause genomic instability and diseases such as cancer and neurodegeneration (Gaillard et al., 2013).

1.2.3 Programmed replication fork barriers

Throughout evolution, cells have developed programmed polar RFBs to ensure DNA replication is performed unidirectionally in certain chromosomal regions and towards specific loci. Usually, these RFBs are required to preclude DNA replication of specific DNA regions more than once per cell cycle, and to prevent potentially fatal transcription-replication collisions (Labib and Hodgson, 2007).

In *E. coli*, as mentioned in section 1.1.1, a pair of replication forks is fired bi-directionally from the *OriC* through the genome. Approximately halfway through in both directions, specific termination sequences (*i.e. terA-F*) are found. These specific sequences are bound by the Tus (terminus utilization substance) protein which transiently blocks replication forks by inhibiting the activity of the main replicative helicase DnaB (Larsen et al., 2014). This system coordinates DNA replication with chromosomal segregation and ensures that both replication forks converge at the correct terminator sequence, hence precluding over-replication events (Hiasa and Marians, 1994).

Similarly, budding yeast utilises a programmed RFB mediated by the Fob1 protein to maintain genome integrity. As mentioned in section 1.2.2, head-on collision between transcription and replication machinery is a serious threat to genomic stability and can cause replication fork collapse. Fob1 binds near a highly repetitive and highly transcribed ribosomal DNA (rDNA) sequence and it is important to block all replication forks traveling in the opposite direction to transcription (Labib and Hodgson, 2007) (**Fig.1.4A**).

In fission yeast, a replication coupled recombination process termed mating-type switching is promoted by the Replication Terminator Sequence-1 (*RTS1*) (Dalgaard and Klar, 2001) **(Fig 1.4B)**. In brief, mating-type switching is a kind of cell differentiation where cells express one of two sexual markers or mating-types (h^+ or h^-), with cells capable of switching between the two in a programmed fashion (Arcangioli and de Lahondès, 2000). *RTS1* is a polar RFB which blocks replication forks travelling in the centromere-distal direction and ensures that the mating-type locus (*mat1*) is replicated unidirectionally in the centromere proximal direction, which is necessary for the mechanism of mating-type switching (Dalgaard and Klar, 2001). This RFB has been utilised to investigate the recombination-dependent mechanisms implemented to repair replication forks following the encounter of the *RTS1* barrier and to demonstrate that such forks are likely to collapse (Ahn et al., 2005; Lambert et al., 2005; Pryce et al., 2009; Nguyen et al., 2015).

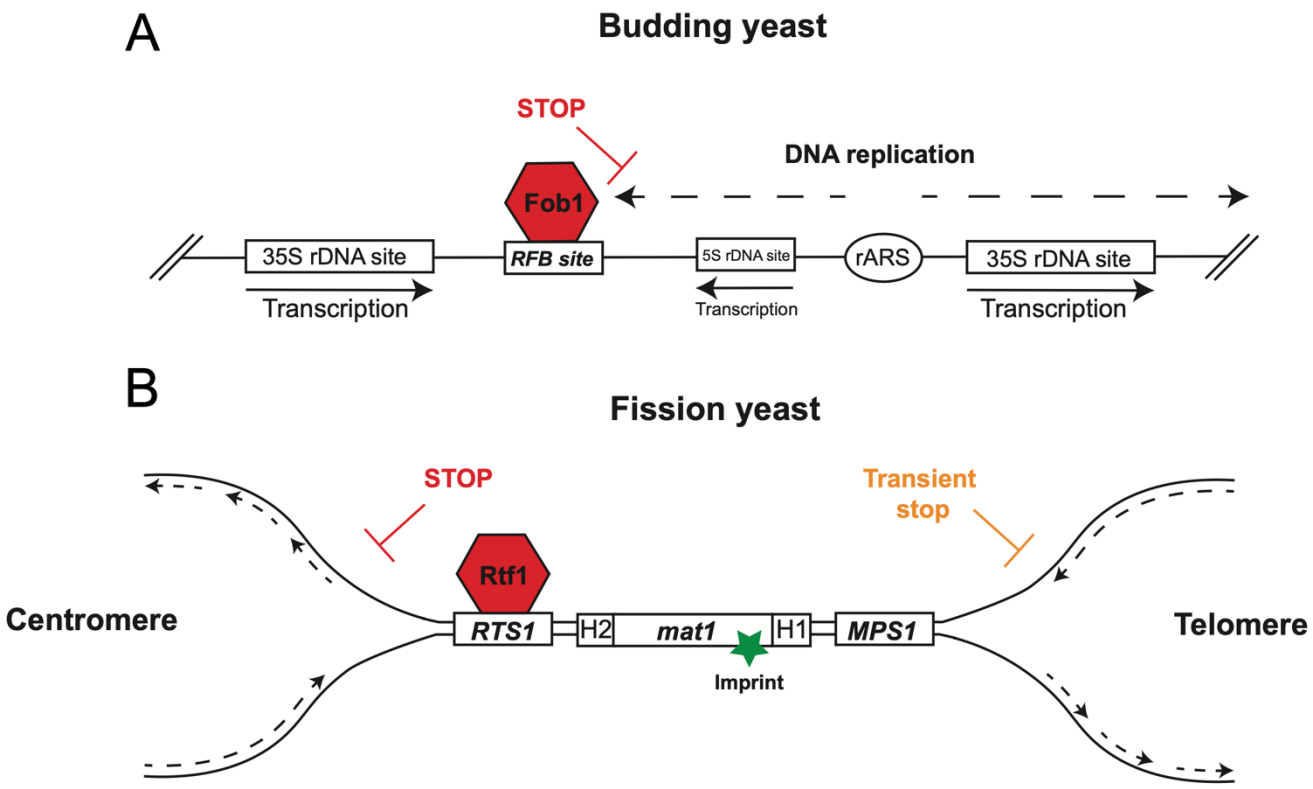

Figure 1.4. Programmed replication fork barriers. A) *Fob1 is a programmed replication fork barrier (RFB) in budding yeast. Its role is to block replication forks travelling in the opposite direction to 35S ribosome transcription. Replication forks originate from the ribosome Autonomously Replicating Sequence (rARS). Only the left-forward replication fork is blocked by Fob1.* ***B)*** *In fission yeast, at the mating-type locus (mat1), Rtf1 binds to the Replication Terminator Sequence-1 (RTS1) to block the replication fork travelling in the centromere-to-telomere direction. The replication fork travelling in the telomere-to-centromere direction pauses briefly at the Mating Pausing Site-1(MPS1) where it induces an imprint in the lagging strand (green star). Pausing at the MPS1 requires additional factors including Swi1, Swi3 and Mrc1 (not shown). The imprint, which consists in the incorporation of a DNA nick, generates a "switchable" cell. The DNA nick is converted into a DSB by the next round of DNA replication, which initiates homologous recombination (HR) and mating-type switching. DSB repair involves HR between the mat1 locus and the transcriptionally silent and heterochromatic mat1-P and mat3-M cassettes (not shown).*

1.3 The response to unprogrammed replication fork barriers and the role of homologous recombination

In mammalian cells, unprogrammed RFBs pose a significant threat to genomic stability, and if not promptly cleared in an efficient and error-free manner they increase the risk of development of a wide variety of diseases. To counteract replication stress, cells implement genome surveillance mechanisms which orchestrate cell cycle, replication origin firing, replication fork stabilisation and DNA repair. Collectively, all strategies implemented are known as the DNA damage response (DDR). The cell cycle stage is a prime determinant on the repair pathway choice. The entry into the different stages of the cell cycle is modulated by various CDKs, including Cdc28 in yeast, which is a master cell cycle regulator, and various other proteins. Deficiencies in CDKs cause DNA end resection problems and HR defects. In S-phase and G2 of the cell cycle, when an intact sister chromatid is available, DNA repair is usually performed by utilising a homologous DNA template via HR (Huertas et al., 2008).

HR is an evolutionary conserved process that, together with DNA synthesis, is key for restarting collapsed replication forks and repairing DSBs throughout the genome. Dysfunction in HR can manifest a range of problems, including underreplicated genomes, gross chromosomal rearrangements, and genomic mutations. At the DNA level, key HR proteins, including Rad51 and Rad52, have been implicated in stabilising stalled replication forks and preventing excessive end-resection (Errico and Costanzo, 2012). The first step of HR usually consists in 5'→3' end resection of the DNA ends, followed by the invasion of the donor DNA template by single-stranded DNA from the broken DNA template. These steps are termed DNA end processing and strand invasion, respectively. Strand invasion is usually performed by the 3' end of the non-resected DNA strand since nucleotides cannot be added to the

5’-end phosphate group. In the second step, the invading strand acts as a primer for new DNA synthesis enabling temporarily lost information from the damaged sister chromatid to be retrieved from the donor homologous template. HR has been best studied in the context of DSB repair and various types of HR repair in this context were proposed. These include, among others, break-induced replication (BIR), synthesis-dependent strand annealing (SDSA) and single strand annealing (SSA) (**Fig 1.5**). Whilst BIR and SDSA are usually Rad51-dependent (Liu et al., 2021; Dupaigne et al., 2008), SSA is Rad51-independent (Vu et al., 2022). Furthermore, SDSA is believed to be the predominant DSB repair pathway implemented by eukaryotic cells and is also the least-error prone (Andersen and Sekelsky, 2010; Verma and Greenberg, 2016). The main three steps of HR repair consist in pre-synapsis, synapsis and post-synapsis and are discussed in the following three subchapters. A multitude of recombination proteins are required to catalyse different steps of HR repair. For the purpose of this thesis, the yeast homologues in mammals and bacteria are listed (See **Table 1.1** for reference).

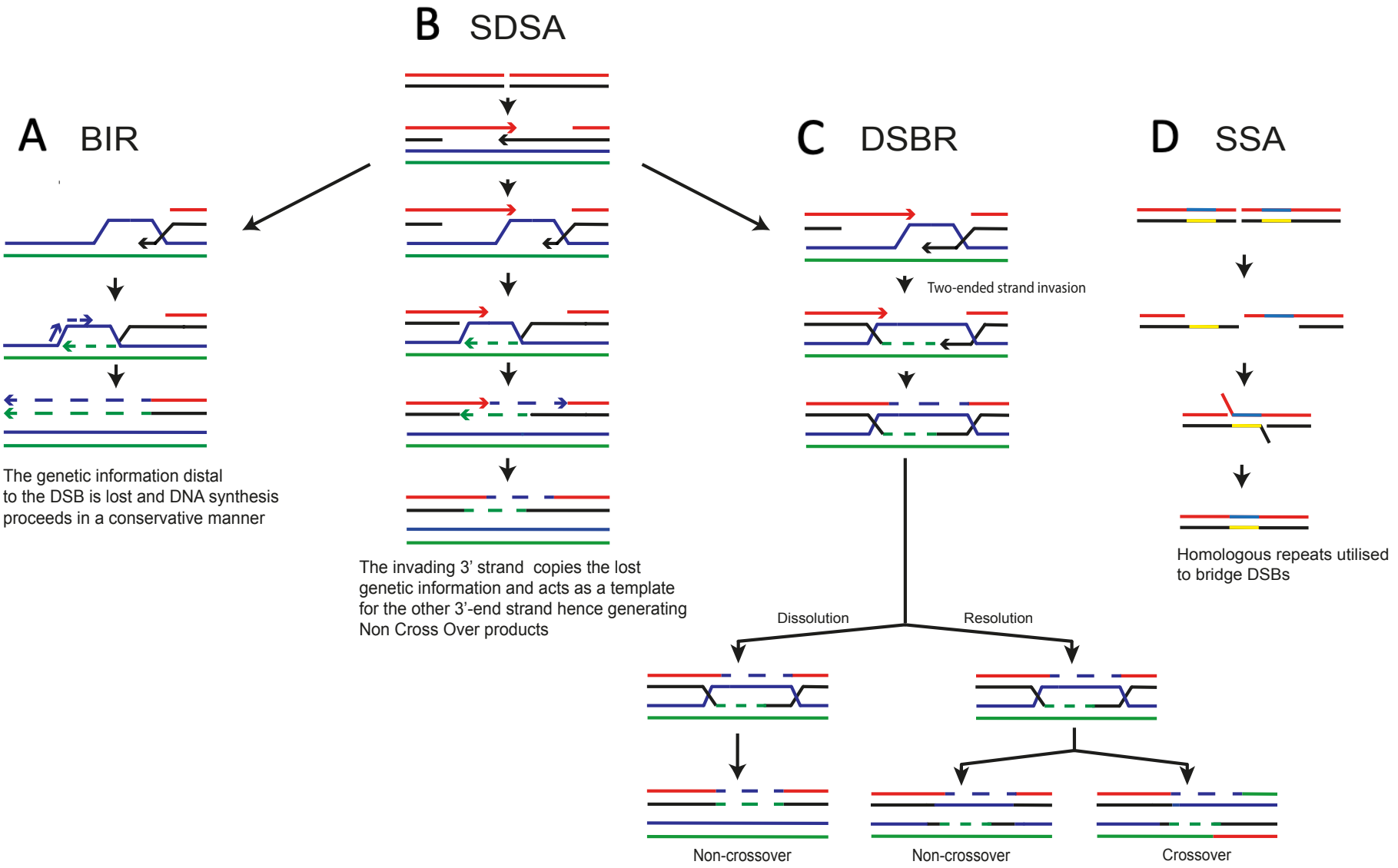
A BIR
B SDSA
C DSBR
D SSA
The genetic information distal to the DSB is lost and DNA synthesis proceeds in a conservative manner
The invading 3' strand copies the lost genetic information and acts as a template for the other 3'-end strand hence generating Non Cross Over products
Two-ended strand invasion
Dissolution
Resolution
Non-crossover
Non-crossover
Crossover
Homologous repeats utilised to bridge DSBs

Figure 1.5. The mechanistic steps of the main DNA repair pathways in S- and G2-phases of the cell cycle. A) *Break induced replication (BIR) is utilised to repair single-ended DSBs (seDSBs). Following 5'→ 3' end-resection and 3'-end strand invasion of the non-resected DNA strand, DNA synthesis proceeds conservatively, potentially until the end of the chromosome.* ***B)*** *In synthesis-dependent strand annealing (SDSA), the kinetics of end-resection and strand invasion are the same as per BIR. SDSA repairs double-ended DSBs (deDSBs). As opposed to BIR, in SDSA the nascent DNA strand pairs with the other 3' single-stranded DNA end and thus retrieves the lost genetic information.* ***C)*** *In the DSB repair (DSBR) model, the kinetics of end-resection is same as per SDSA and BIR. Consequently, strand invasion is performed by both ends of the DSB. Double Holliday Junction intermediates are processed either through dissolution or resolution and generate either non-crossover (NCO) or crossover (CO) events.* ***D)*** *The single strand annealing (SSA) pathway consists of an initial extensive resection to expose 3' single-stranded homologous DNA sequences. Consequently, the homologous sequences anneal, the 3' tails are cleaved, and the nicks are ligated, resulting in deletion of the intervening DNA sequence.*

Table 1.1. ***Recombination proteins in different species.*** *Functionally equivalent and homologous proteins are indicated in the same row.*

	Mammals	***S. cerevisiae***	***S. pombe***	***E. coli***
Pre-synapsis	MRE11-RAD50-NBS1	Mre11-Rad50-Nbs1	Mre11 (Rad32) - Rad50 - Nbs1	RecBCD SbcD-SbcC
	BLM	Sgs1	Rqh1	RecQ
	CtIP1	Sae2	Ctp1	-
	DNA2	Dna2	Dna2	-
	PARI	Srs2	Srs2	UvrD
	EXO1	Exo1	Exo1	RecE, RecJ
	FBH1	-	Fbh1	-
	RPA	RPA	RPA	SSB
Synapsis	RAD51	Rad51	Rad51 (Rhp51)	RecA
	RAD52	Rad52	Rad52 (Rad22)	RecO
	XRCC2 - SWS1 - RAD51D - SWSAP1	Shu1-Shu2-Psy3-Csm2	Rlp1-Sws1-Rdl1	-
	SWI5 - SFR1	Sae3-Mei5	Swi5-Sfr1	-
	RAD51B, RAD51C - XRCC3	Rad55-Rad57	Rad55 (Rhp55) - Rad57 (Rhp57)	RecF-RecR
	RAD54	Rad54	Rad54 (Rhp54)	-
Post-synapsis	TopoIIIα	Top3	Top3	TopoIII
	MUS81-EME1	Mus81-Mms4	Mus81-Eme1	-
	FANCM	Mph1	Fml1	-
	FBH1	-	Fbh1	-
	PARI	Srs2	Srs2	UvrD RuvAB
	BLM, RECQ1, RECQ4, RECQ5, WRN	Sgs1	Rqh1	RecQ
	GEN1	Yen1	-	RuvC
	SLX1 - SLX4	Slx1-Slx4	Slx1-Slx4	-

1.3.1 Pre-synapsis: DNA end-resection

Pre-synapsis is the first step of HR repair and consists in the 5'→3' end resection of the strand not involved in invasion of the homologous sequence. This process is performed in a two-step manner and exposes a single-stranded DNA arm involved in strand invasion of the homologous sequence with its 3'-OH end (Zhu et al., 2008). Short-range resection, the first step of pre-synapsis, is performed by Mre11-Rad50-Nbs1 (MRN) and Ctp1 in fission yeast, Mre11-Rad50-Xrs2 (MRX) and Sae2 in budding yeast, and MRN and CtIP in humans. Rad50 is an important support in short-range resection by Mre11, especially in processing protein-bound ends, whilst Nbs1 is responsible for recruiting the entire complex to the DSB ends. Similarly, in *S. cerevisiae* MRX-mediated short-range resection is improved by the Sae2 nuclease. Subsequently, long-range resection is performed by two alternative pathways: I) DNA helicase Sgs1 (Rqh1 in *S. pombe*) working with Dna2; or II) exonuclease Exo1-mediated resection (Symington, 2016; Zhao et al., 2020; Mimitou and Symington, 2011).

1.3.2 Synapsis: strand invasion into the intact DNA homologous template

Single-stranded DNA is unstable and susceptible to cleavage by nucleases, therefore, once end resection to expose a single-stranded DNA arm has occurred, it becomes coated with replication protein A (RPA) (Binz et al., 2004). Subsequently, Rad51 a key recombination protein, loads onto the DNA whilst displacing the previously bound RPA proteins, hence forming a single-stranded nucleoprotein filament. The displacement of RPA proteins is mediated by Rad52 (Benson et al., 1998; Kurokawa et al., 2008). The nucleoprotein filament is stabilised further by Rad55 and Rad57 (Rad51 paralogues) (Liu et al., 2011). Once assembled, the nucleoprotein filament conducts a search for a homologous DNA sequence and, once this has been located, it catalyses strand

invasion of the intact homologous template to form a displacement loop (hereafter referred to as D-loop) (Baumann et al., 1996). DNA homology sequences shorter than 9 nucleotides are disregarded by Rad51 (Qi et al., 2015). The subsequent DNA synthesis for HR repair is initiated from the 3' end and involves a variety of enzymes including Polδ, Polε and various translesion synthesis (TLS) polymerases (McVey et al., 2016).

1.3.3 Post-synapsis: resolution of the homologous recombination intermediates

The D-loop is a crucial component of the HR-mediated repair of DSBs and is exquisitely coordinated by the activity of a variety of enzymes, often helicases and translocases. Such enzymes control in part the fate of the D-loop by facilitating branch migration of the four-way junction, hence promoting DNA synthesis. Nevertheless, such enzymes may also have inhibitory effects on the D-loop and, for instance, promote its dissociation from the donor homologous template. FANCM-like helicases, Fbh1, Srs2 and RecQ-like helicases have all been implicated in D-loop processing. It is believed that often their activity disrupts the activity of the D-loop to promote SDSA, a more reliable and error-free repair mechanism (Bernstein et al., 2010; Dupaigne et al., 2008; Lorenz et al., 2009, 2012). Some of these factors also act to remove Rad51 from DNA, for example the human RecQ-like helicases BLM and RECQ5 have been shown to remove Rad51 from single-stranded DNA *in vitro* (Bugreev et al., 2007; Hu et al., 2007), and Srs2, a 3'-->5' helicase, inhibits D-loop formation by stripping Rad51 off the single-stranded DNA. This DNA helicase possesses anti-recombinase activity *in vivo* and is believed to promote SDSA over other HR-mediated repair pathways (Dupaigne et al., 2008; Lorenz et al., 2009; Doe and Whitby, 2004; Krejci et al., 2003).

If the D-loop is not dissociated by a DNA helicase/translocase, then a double Holliday junction may form by so-called second-end capture in which the single-

stranded DNA at the other end of the DSB anneals to the displaced strand of the D-loop. Processing of the double Holliday junction can be done by Holliday junction resolvases, such as RuvC in *E. coli* and Yen1 or Mus81 in eukaryotes, which are structure-specific endonucleases that generate either non-crossover or crossover recombinant products depending on which junction strands are cut (**Fig 1.2**). Alternatively, the double Holliday junction can be "dissolved", through the action of a RecQ-like helicase working in conjunction with Top3, to generate non-crossover recombinants (Jasin and Rothstein, 2013; Bizard and Hickson, 2014).

1.4 Single-stranded breaks

SSBs are very common DNA lesions which, unless repaired promptly and efficiently, compromise the progression of the DNA replication fork. Each mammalian cell genome suffers more than 10,000 SSBs per day (approximately 1 SSB every 5 seconds), making it by far the most common DNA lesion (Hossain et al., 2018). The sources of SSBs can be both direct (disintegration of the sugar-phosphate backbone) and indirect (long-lived intermediates of DNA metabolic mechanisms or DNA repair processes). The most common direct cause of SSBs is the oxidation of deoxyribose and subsequent fragmentation of the sugar by ROS which eventually generates SSBs with 3' damaged termini (section 1.4.2) (Demple and Harrison, 1994). Indirect causes of SSBs include apyrimidinic/apurinic endonuclease (e.g. APE1 in humans and Apn1 in yeast) - mediated base excision repair (BER) following removal of a damaged base by a DNA glycosylase (or bifunctional DNA glycosylase) (section 1.4.1) (Caldecott, 2020). A final source of SSBs, which is highly relevant to this study, is the abortive action of topoisomerases which, as discussed in section 1.4.3, can occasionally remain trapped to the 3'-end of the DNA and generate a long-lived SSB (Pommier et al., 2016).

1.4.1 Indirect Single-Stranded Breaks - Base Excision Repair

BER is implemented to repair minor base lesions and indirect SSBs which cause minimal distortions of the DNA helical structure. A wide variety of DNA glycosylases sense damaged bases and cleave the glycosidic bond between the base and the backbone sugar phosphate. Subsequently, an AP endonuclease starts the repair by inducing a DNA incision at the 5' end of the resulting abasic lesion, hence leaving a 3'-OH group and 5'- 2-deoxyribose-5-phosphate (dRP) moiety flanking the nucleotide gap (Mitra et al., 1997). APE1 and Apn1 are the major AP endonucleases in humans and yeast, respectively. Intriguingly, they share no similarities in terms of structure. In addition to the ability to hydrolyse the phosphodiester backbone 5' to the AP site, both APE1 and Apn1 possess a 3' phosphodiesterase activity required to remove blocking damages at the 3'-end such as 3'-phosphoglycolate, which can be generated following IR exposure (Mol et al., 2000). In mammalian cells, the mechanism continues either with short-patch BER with a single nucleotide being replaced, or long-patch BER in which 2-13 nucleotides are replaced. Short-patch BER requires the activity of DNA polymerase ß (Polß) and the 3' diesterase activity of APE1, to remove the 5'-dRP and 3'-abasic ends, respectively. Next, gap-filling is performed by Polß and nicks are sealed by DNA ligase I and III. In long-patch BER, DNA synthesis from the 3'OH is carried out by Polε or Polγ to displace the DNA strand containing the 5'-dRP. Subsequently, FEN1 cleaves the flap structure formed at the displaced 5'-dRP end, to allow ligation of the nick by DNA ligase I and III. Long-patch BER necessitates the activity of additional proteins, namely PCNA and RFC which stimulate the activity of Polε or Polγ. It is important to note that whilst both budding and fission yeast contain homologues to the mammalian proteins PCNA, FEN1 and RFC (Lieber, 1997; Yoder

and Burgers, 1991; Waseem et al., 1992) long-patch BER was never demonstrated in these organisms.

1.4.2 Direct Single-Stranded Breaks – Sugar Damage

In mammalian cells, direct SSBs are usually rapidly sensed and bound by PARP1 which consequently modifies itself and various target proteins with chains of poly(ADP-ribose) (pADPr) many hundred units long. Interestingly, in yeast no PARP1 orthologue is present, and the mechanism of SSB repair (SSBR), as opposed to humans, is not clear. This is partly due to only little amount of work being performed on SSBR in yeast. In humans, PARP1 promotes the recruitment of multiple protein complexes including XRCC1 which acts as a scaffold protein for other proteins involved in SSBR (Hanzlikova et al., 2017). Direct SSBs present most of the times damaged 3' or 5' termini which must be restored to normal 3'-OH and 5'-phosphate termini. 3' ends are processed by APE1 in a reaction stimulated manyfold by XRCC1 (Whitehouse et al., 2001). In humans, among the set of proteins which are recruited by XRCC1, PNK is responsible for processing both 3'-phosphate and 5'-OH ends, via both its kinase and phosphate activities hence restoring them to 3'-OH and 5'-phosphate termini. Similarly, in yeast PNKP (orthologue of mammalian PNK) is responsible for restoring 3'-OH and 5'-phosphate termini however, as opposed to humans, only its phosphatase domain is retained in this organism (Sanchez et al., 2017; Caldecott, 2003). The next steps, gap filling and ends ligation, were mostly investigated in the context of BER (section 1.4.1), nevertheless a significantly similar mechanism likely exists to repair direct SSBs.

1.4.3 Abortive Topoisomerase generate protein-bound single-stranded breaks

Top1 releases topological stress by inducing a SSB in one of the DNA strands, passing the two broken DNA ends across the intact strand, and rapidly religating the DNA ends. The initial SSB is generated by a catalytically active tyrosine residue, hence generating

a DNA-Top1 3'-phosphotyrosine intermediate prior to religating the DNA ends (Stewart et al., 1998). Occasionally, Top1 can remain covalently bound to the 3'-end of the DNA, hence generating long-lived SSBs, especially near DNA lesions. In such scenario, the SSBR machinery intervenes to repair the break. Trapped Top1 enzymes are removed by the tyrosyl-DNA phosphodiesterase TDP1 in humans and yeast (Pouliot et al., 2001; Wang, 2002). In mammalian cells, SSBs covalently bound to Top1 can be repaired also by the SSBR polypeptides PARP1 and XRCC1 in collaboration with TDP1 (Das et al., 2014). Top1-bound SSBs are generated also following the treatment with the drug CPT, which inhibits the Top1 religation step hence generating long-lived protein-bound SSBs (Liu, 1989). Notably, CPT-derivative poisons such as topotecan and irinotecan are widely utilised anticancer drugs for the past two decades (Thomas and Pommier, 2019).

1.5 The repair of Single-Stranded Breaks in S-phase

As previously mentioned, trapped Top1 cleavage complexes generate protein-bound single-stranded breaks. There is extensive literature indicating that Top1-inhibition via CPT treatment generates DSBs when a replication fork encounters a trapped Top1 enzyme (Avemann et al., 1988; Hsiang et al., 1985; Strumberg et al., 2000; Ray Chaudhuri et al., 2012). Under CPT treatment, the replisome was shown to "fall-off" at Top1-bound SSBs via a replication run-off mechanism (Strumberg et al., 2000). Nevertheless, electron microscopy studies showed that CPT-mediated Top1 inhibition can also induce fork reversal hence generating a four-way junction (Ray Chaudhuri et al., 2012).

In another study utilising a reengineered version of the Flp-recombinase to induce site-specific protein-bound SSBs, it was shown that leading-strand SSBs generated in S-phase in budding yeast were converted into single ended DSBs

(seDSBs) by the incoming replication fork. Such seDSBs were repaired by break induced replication (BIR) (section 1.5.2). However, in this study the structure of a lagging-strand nick encountered by a replication fork was not elucidated (Mayle et al., 2015). Exactly what happens when a replication fork encounters a SSB has been the subject of investigation for a number of years and diverse pathways have been suggested (**Fig. 1.6**).

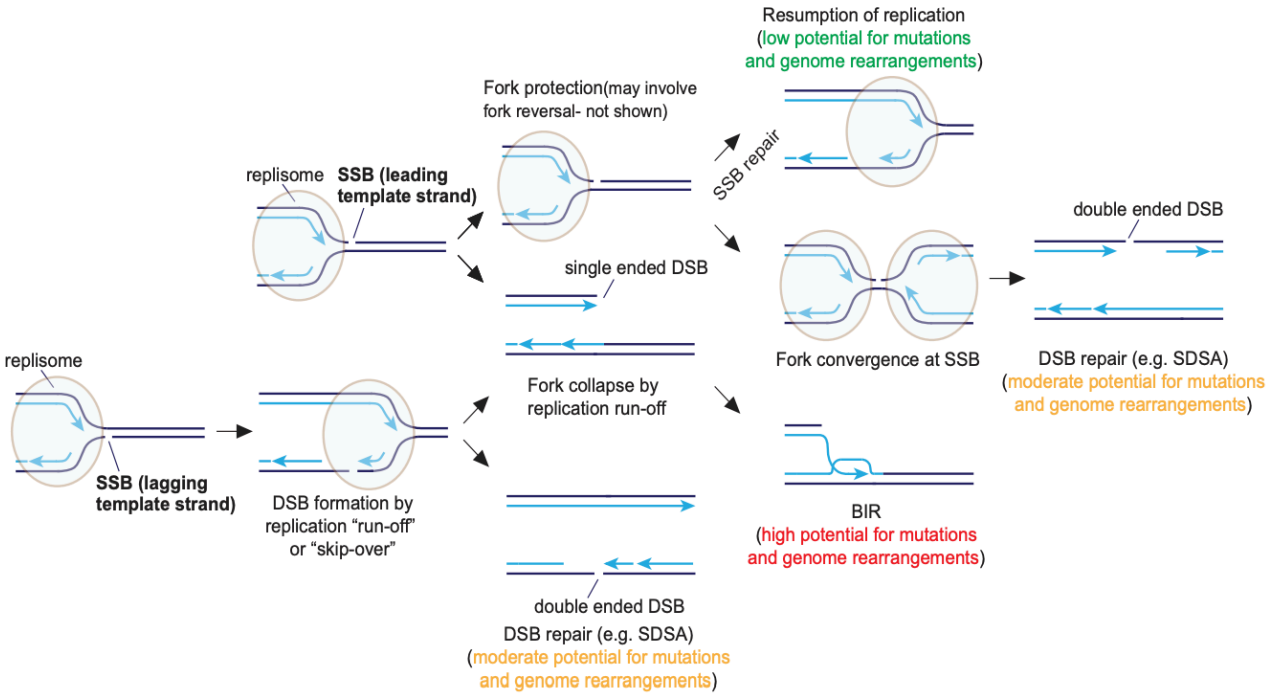

Figure 1.6. Possible outcomes following a replication fork-single-stranded break encounter. *Upon encountering a leading-strand single-stranded break (SSB), the replication fork can run-off, generating a single-ended double-stranded break (seDSB) which is repaired via break induced replication (BIR). Alternatively, the replication fork can be protected while the SSB is repaired - DNA replication can then resume. Fork protection can also enable the arrival of the replication fork travelling in the opposing direction which generates a double-ended DSB (deDSB) which is repaired via synthesis dependent strand annealing (SDSA). Conversely, a lagging-strand SSB can be successfully skipped over and converted to a deDSB which is repaired via SDSA. Alternatively, the lagging-strand SSB is converted to a seDSB which is repaired via BIR.*

Until recently, the prevailing model was that the encounter of a nick in the continuously replicated leading-strand generated a seDSB via a replication run-off mechanism. In contrast, a nick in the discontinuously replicated lagging-strand was thought to generate double-ended DSBs (deDSBs) (Caldecott, 2008). However, recent findings using the *Xenopus* egg extract model system have challenged this model by showing that nicks in both leading and lagging-strand generate seDSBs (Vrtis et al., 2021). Vrtis et. al., utilised single molecule electron microscopy imaging approaches to follow the fate of the CMG helicase upon encountering SSBs induced by the nickase Cas9 (nCas9-H840A). GINS, a key subuit of the CMG helicase, was labelled with Alexa Fluor 647 in egg extracts containing Fen1 fluorescently labelled with mkikGR (to follow nascent DNA synthesis). They demonstrated that leading-strand nicks generate a near blunt seDSBs with an approximately 3 nt - long 5' ssDNA overhang in the leading-strand by a replisome run-off mechanism (**Fig. 1.7A)**. In contrast, lagging-strand nicks generate seDSBs with an approximately 70 nt 3' ssDNA overhang. Interestingly, at lagging-strand nicks the replisome stalls and is disassembled in a ubiquitination/removal mechanism near-identical to the replication termination mechanism discussed in section 1.1.4 (Vrtis et al., 2021) (**Fig. 1.7B**). Seemingly, leading and lagging-strand nicks are more similar than otherwise expected and are both converted into seDSBs in *Xenopus* egg extracts. These results remain to be confirmed *in vivo*. In addition, it remains to be confirmed which pathway is performed to repair the seDSBs generated following the encounter of a lagging-strand SSB by a replication fork.

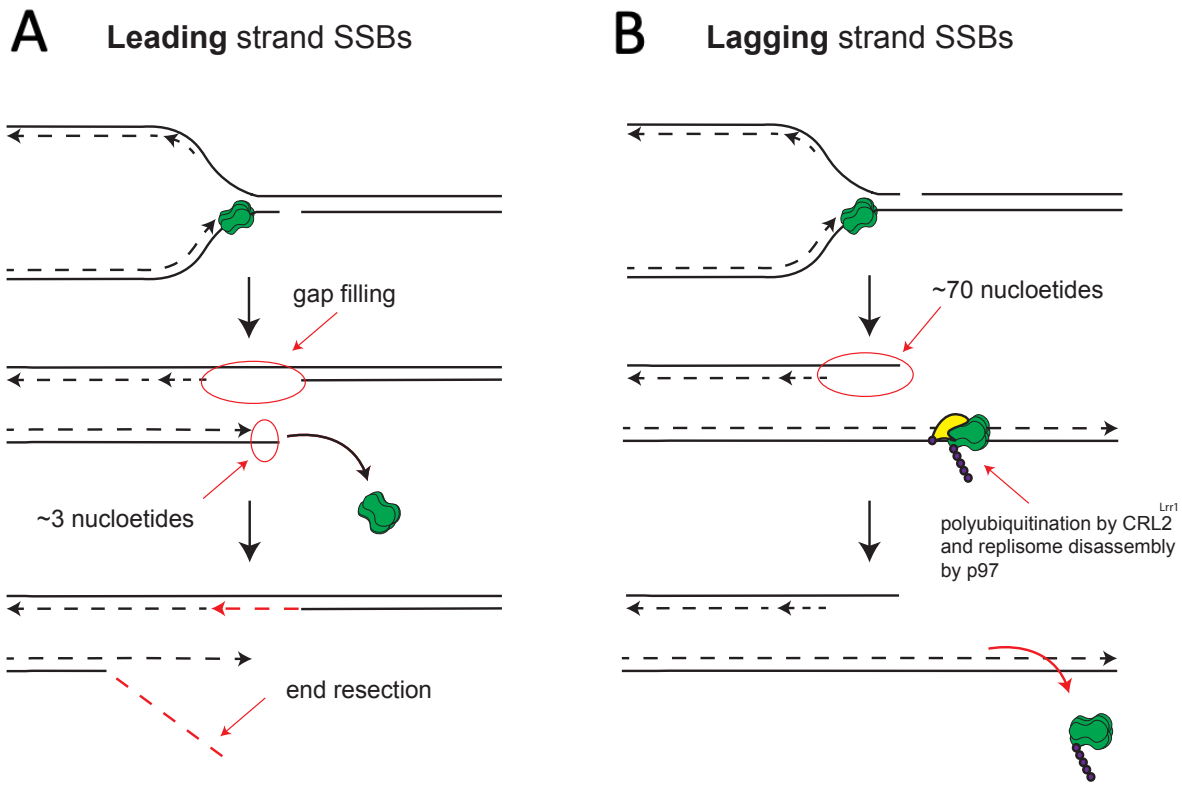

Figure 1.7. Experimental findings in Xenopus egg extracts by Vrtis et. al. A) *Leading strand nicks are converted into seDSBs by replisome run-off leaving behind a nearly blunt (~3 nucleotides) overhang. End resection exposes a single strand filament for HR mediated repair. On the lagging strand, a ~70 nucleotides gap is repaired by gap filling.* ***B)*** *Lagging strand nicks cause the replisome to stall leaving behind a ~70 nucleotides overhang on the lagging strand. In a similar fashion to canonical DNA replication termination, the CMG helicase is then polyubiquitinated by* $CRL2^{Lrr1}$ *and dismantled by p97.*

1.5.1 The nature of the replication associated DSB determines the HR repair pathway utilised

The simplest HR pathway to repair deDSBs by gene conversion is SDSA. In SDSA, a single end of the DSB invades the homologous template, hence generating a D-loop. The process continues with DNA synthesis and is completed when the newly synthesised DNA is unwound and annealed to the other DSB end (Ira et al., 2006). Conversely, in BIR, which is required to repair seDSBs, DNA synthesis is performed extensively and can proceed to the end of the chromosome. SDSA and BIR share numerous similarities. Firstly, the kinetics of strand invasion and homology search are identical in both BIR and SDSA. Secondly, both SDSA and BIR proceed via D-loop mediated DNA synthesis (Donnianni and Symington, 2013; Saini et al., 2013). This leads to conservative inheritance of the newly synthetised DNA and a significant number of point mutations in the area of DNA replicated by the D-loop (McGill et al., 1989; Ponder et al., 2005; Hicks et al., 2010; Sakofsky et al., 2014). The D-loop is less stable than a canonical DNA replication fork and introduces increased mutations of up to 10^2 – 10^3 fold (Deem et al., 2011), as well as increased template switching leading to chromosomal rearrangements (Smith et al., 2007). Thirdly, leading -synthesis in both SDSA and BIR proceeds at the same rate and kinetics (Jain et al., 2009), whilst lagging-strand synthesis is performed afterwards (Liu et al., 2021). These facts suggest that pathway choice is carried out after leading-strand synthesis is performed. Identifying the key elements driving pathway choice is crucial since SDSA is relatively error-free, whilst BIR is highly mutagenic due to a far longer region being subject to low-fidelity D-loop mediated DNA synthesis. Indeed, pathways have been proposed to be responsible for inhibiting BIR and channelling the HR-mediated repair to SDSA. Particularly, second-end capture, driven by Rad52, was suggested to be the crucial

step channelling BIR into SDSA (Pham et al., 2021; Jain et al., 2009). The D-loop employed in BIR undergoes multiple rounds of invasion-dissolution-reinvasion, at each round, second-end capture is not possible since the structure of the DSB is single ended. On the other hand, SDSA is utilised to repair double-ended DSBs and thus, second-end capture is possible (**Fig. 1.8**) (Štafa et al., 2014; Mayle et al., 2015; Pham et al., 2021).

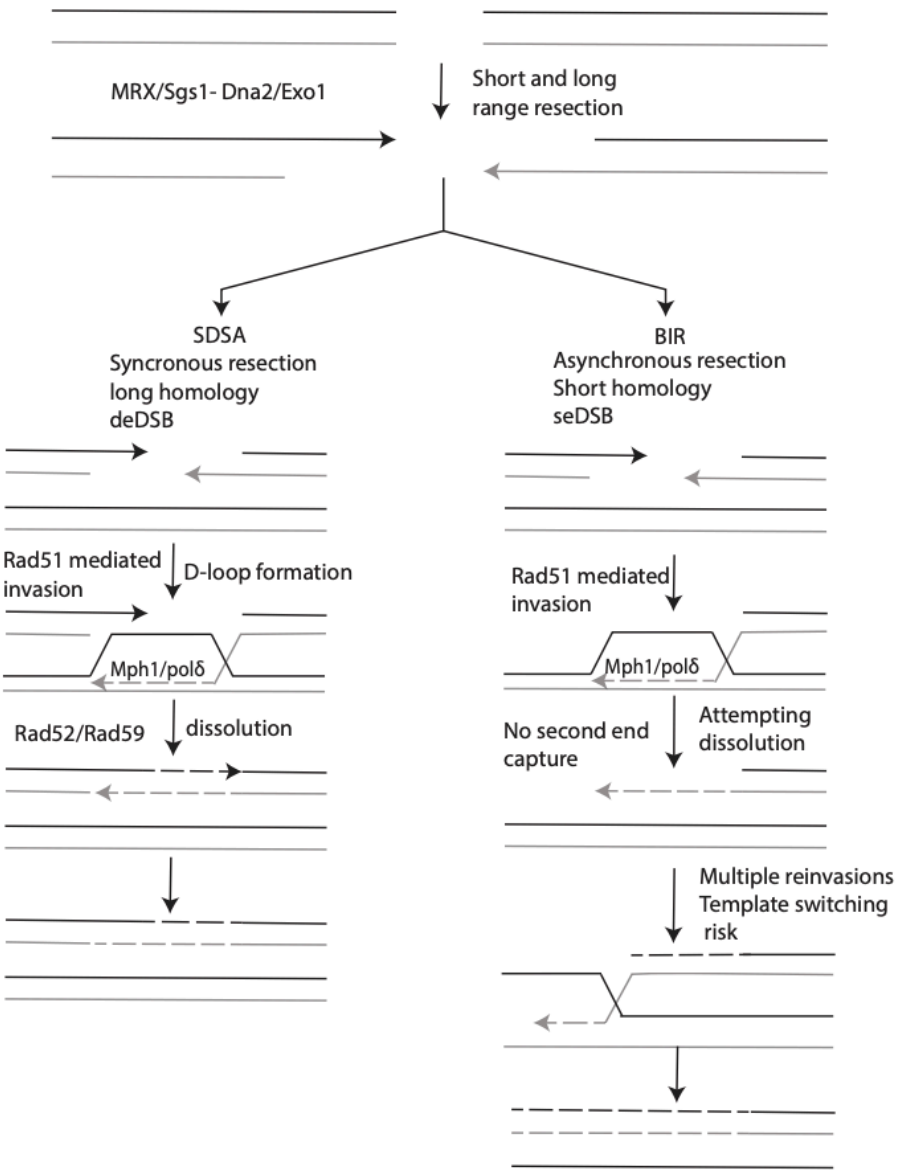

Fig. 1.8. ***Repair pathway choice: SDSA or BIR.*** *The kinetics of strand invasion and leading-strand synthesis are very similar between BIR and SDSA. SDSA (left) is utilised to repair deDSBs, hence following leading-strand synthesis and dissolution, second-end capture (dissociation from DNA template and annealing to the second broken end) is performed. Conversely, BIR (right) is utilised to repair seDSBs and consists in conservative DNA replication. The D-loop undergoes multiple rounds of invasion-dissolution-reinvasion and no second-end capture occurs. This phenomenon increases the risk of invading and copying the wrong DNA sequence (template switch).*

Importantly, in budding yeast, second-end capture for SDSA required at least 150bp of homology as well as the strand annealing activity of the Rad52/Rad59 complex; alternatively, BIR is performed (Mehta et al., 2017). Other factors influencing pathway choice between SDSA and BIR include the activity of Mph1 helicase in interrupting D-loop mediated DNA synthesis and asynchronous resection of the DSB by the MRX complex (Štafa et al., 2014; Pham et al., 2021).

1.5.2 An overview of BIR

Most of our understanding of BIR comes from studies in budding yeast utilising site-specific DSBs. Often deDSBs were generated via the HO endonuclease expressed from the galactose inducible promoter. In these experiments, only one end of the deDSBs had homology with a region located on another chromosome, hence "forcing" the cell to repair the DNA lesion by BIR (Malkova et al., 1996; Lydeard et al., 2007; Malkova et al., 2005; Stivison et al., 2020). In a similar fashion to other HR repair mechanisms, BIR involves the exposure of a 3' ssDNA tail by 5'→3' end resection which is bound by RPA proteins. Consequently, RPA proteins are removed, and Rad51 is loaded onto DNA in a Rad52-dependent manner hence generating a nucleoprotein filament. Homology search by the nucleoprotein filament is rapidly initiated, however, there is contradicting evidence on whether D-loop mediated low-fidelity DNA synthesis is performed immediately or delayed for up to several hours (Anand et al., 2017; Jain et al., 2009; Mehta et al., 2017). Importantly, most of the evidence indicates that BIR is delayed enough to trigger the G2/M arrest checkpoint implying that most of the BIR repair processes occur in the G2/M phase of the cell cycle (Davis and Symington, 2004; Malkova et al., 2005; Jain et al., 2009; Donnianni and Symington, 2013).

There are two main BIR pathways that share a dependence on Rad52 but are distinguished by their reliance on Rad51 (Malkova et al., 1996; Lydeard et al., 2007).

Whilst some factors are essential for the Rad51-dependent pathway, others are dispensable for the Rad51-independent one, and vice versa. In budding yeast, Rad51-independent BIR relies on Rad59, Rdh54 and MRX (Signon et al., 2001) whereas the Rad51-dependent pathway is dependent on Rad54, Rad55 and Rad57 (Malkova et al., 2005). Rad51 is believed to prevent extensive 5'→3' end resection which would expose long ssDNA tails. Rad52, which possesses strand annealing activity, could utilise these long ssDNA tails to drive homology search and start Rad51-independent BIR. Therefore, Rad51 inhibits Rad51-independent Rad52-dependent BIR. Moreover, usually Rad51-independent BIR involves genomic rearrangements between homeologous DNA repetitive regions. Such rearrangements are not prevalent in Rad51-dependent BIR (VanHulle et al., 2007; Downing et al., 2008). The rest of the chapter will focus on Rad51-dependent BIR, which is the canonical and better understood type of BIR.

1.5.3 The mechanism of BIR-mediated DNA synthesis

As mentioned in section 1.5.2, BIR proceeds via a migrating D-loop, which displaces the newly synthesised DNA strand via branch migration of an unresolved Holliday junction. As opposed to canonical DNA replication, BIR-mediated DNA synthesis in leading and lagging-strands is asynchronous. During D-loop migration, the leading-strand is extended from its 3'-OH end. Consequently, the lagging-strand utilises the newly synthetised leading-strand as template for repair. Due to its particular mode of repair, BIR results in conservative inheritance of the newly synthesised DNA (Saini et al., 2013; Donnianni and Symington, 2013; Wilson et al., 2013).

Pif1 is thought to be the main helicase responsible for unwinding the DNA and enabling D-loop progression (Wilson et al., 2013), and without it DNA synthesis is limited to approximately 5 kb (Liu et al., 2021). It remains unclear whether the other

Pif1-family helicase in budding yeast, Rrm3, is involved in BIR. Both Pif1 and Rrm3 were shown to cooperate in DNA replication termination (Deegan et al., 2019), yet no deficiencies in BIR were detected when Rrm3 was deleted (Wilson et al., 2013). Other helicases, including Srs2 and Mph1, affect the successful completion of BIR by supporting the unwinding of toxic DNA intermediates (Elango et al., 2017).

Polδ is the main replicative polymerase involved in both leading and lagging-strand synthesis in BIR (Vasan et al., 2014; Donnianni et al., 2019). Furthermore, unlike canonical DNA replication, BIR depends on Pol32, which is a non-essential subunit of Polδ. Some BIR synthesis (approximately 20kb) can be performed in the absence of Pol32 and presence of the Pif1 helicase. The absence of both blocks BIR completely (Liu et al., 2021). Another polymerase, Polε, was detected at the BIR complex via ChIP analysis (Wilson et al., 2013), yet BIR ribonucleotide incorporation analysis in strains defective in Polε did not show any deficiencies in BIR or evidence of Polε involvement (Donnianni et al., 2019). Therefore, the participation of Polε is yet to be confirmed. A third polymerase, Polα primase, is essential for BIR. More precisely, deletion of Polα primase precludes the successful completion of BIR as it is required for lagging-strand synthesis in budding yeast. Interestingly, inactivation of Polα primase precluded both leading- and lagging-strand synthesis, whilst leading-strand synthesis was believed to be primase independent and utilise the 3' end of the invading ssDNA arm as primer (Lydeard et al., 2007). Liu et al. demonstrated that leading-strand synthesis can occur independent of Polα primase up to 25kb, following this site Polα primase is required to synthesise the lagging-strand and create a duplex DNA molecule (Liu et al., 2021). However, it remains unclear why lagging-strand synthesis requires an approximately 25kb-long leading-strand to initiate synthesis.

1.5.4 Common Fragile Sites and Mitotic DNA Synthesis

BIR is an evolutionary conserved DNA repair mechanism. In a similar fashion to BIR in eukaryotes, BIR plays an essential role in bacteria and bacteriophage T4 (Mosig, 1998; Kogoma, 1997). As previously mentioned, in bacteria DNA replication is initiated from a single replication origin (*OriC*). Hence, bacteria are particularly susceptible to replication fork collapse and rely completely on BIR for replication restart (Kogoma, 1997; Marians, 2000). Conversely, eukaryotes possess multiple replication origins, which makes them less reliant on BIR. Indeed, convergence with replication forks travelling in the opposite direction was shown to limit the extent of low-fidelity BIR in yeast. Furthermore, the structure specific endonuclease Mus81 was shown to limit BIR-mediated mutagenic synthesis in budding yeast (Mayle et al., 2015).

DNA repair mechanisms similar to BIR have been reported in humans following replication collapse at common fragile sites (CFSs) (Minocherhomji et al., 2015; Bhowmick et al., 2016). CFSs regions can be under-replicated during DNA synthesis and, under conditions of replication stress, can lead to replication fork collapse. DNA breaks due to CFSs are generated due to a multitude of reasons. Inhibition of main replicative polymerases by aphidicolin treatment generates replication stress and causes DNA breakage at CFSs. Furthermore, their propensity to be replicated late, the presence of large coding regions, and scarcity of replication origins are all factors that contribute to CFSs fragility (Durkin and Glover, 2007; Glover et al., 2017). Intriguingly, CFSs, which are enriched in late replication origins, generate breaks which are often repaired during mitosis via a process termed mitotic DNA synthesis (MiDAS), albeit the exact features that lead to MiDAS remain to be elucidated. The mechanistic process of MiDAS is nearly identical to BIR and is thought to require the activity of Mus81 to cleave a stalled DNA replication fork. In a similar fashion to BIR, MiDAS proceeds by

conservative DNA synthesis (Bhowmick et al., 2016). Implementing MiDAS, a significantly error prone recovery pathway, during mitosis and shortly prior to chromosomal segregation can be envisaged as a desperate remedy to complete genome duplication at the expense of fidelity. Seemingly, undergoing chromosome segregation with an underreplicated genome represents a far greater threat compared to low-fidelity DNA repair by MiDAS (Bhowmick et al., 2016).

1.5.5 Oncogene overexpression causes high frequency of DNA replication forks collapse

Oncogenes are a group of genes which regulate cell proliferation, differentiation and cell cycle. Dysregulation in these genes potentially causes cancer. Activation of oncogenes induces replication stress in human tissues (Di Micco et al., 2006). Upon oncogene overexpression, the DNA replication-specific checkpoint kinase ATR is activated (Cimprich and Cortez, 2008) and the number of DNA DSBs increases in human cells (Bartkova et al., 2006). Several DNA fibre analysis studies have shown that, upon oncogene activation, replication forks stall or collapse. Consequently, dormant replication origins are fired, likely to rescue the stalled or collapsed replication fork (Di Micco et al., 2006; Bartkova et al., 2006; Bester et al., 2011; Jones et al., 2013; Srinivasan et al., 2013). Moreover, there is strong evidence indicating that oncogene overexpression causes deletions and loss of heterozygosity (LOH) within CFSs. These genomic rearrangements following oncogene induced replication collapse at CFSs resemble the changes generated following DNA polymerase inhibition via aphidicolin and can be repaired via MiDAS (Di Micco et al., 2006; Arlt et al., 2009; Arlt et al., 2011). The exact mechanisms via which oncogene activation induces replication stress is not clear, nevertheless, factors affecting it include dysregulated origin firing, scarcity of

dNTPs, elevated levels of transcription travelling in the opposing orientation of DNA replication (Macheret and Halazonetis, 2018).

1.5.6 Alternative Lengthening of Telomeres is utilised to repair eroded telomeres

As previously mentioned, seDSBs are a substrate for BIR-mediated repair. Importantly, seDSBs are not generated solely in the context of a replication fork, but also at eroded telomeres. At each round of DNA replication, genetic information is lost at the end of the chromosomes due to the “end replication problem”. Under normal circumstances, telomerase performs progressive synthesis of telomeric repeats extended from the 3’-OH ends of linear chromosomes, thereby reversing the genetic information loss. When telomerase is not present, telomeres are gradually eroded. Consequently, alternative lengthening of telomeres (ALT) is the mechanism responsible for extending eroded telomeres by copying telomere repeats from other chromosomes (McEachern and Haber, 2006). In yeast, two different ALT pathways exist. Type I depends on Pol32, Rad52 and Rad51 whereas type II relies only on Pol32 and Rad52 (Lydeard et al., 2007; Lundblad and Blackburn, 1993; Teng and Zakian, 1999; Teng et al., 2000). In addition, Type II relies on the MRX complex to process the seDSBs ends and Rad59 to support Rad52 strand annealing activity (Teng and Zakian, 1999; Teng et al., 2000; Le et al., 1999). Interestingly, ALT significantly resembles BIR in G2/M phase of the cell cycle. Type I and Type II ALT are potentially initiated by Rad51-dependent strand invasion and Rad52-mediated strand annealing with homologous DNA regions, respectively. In a similar fashion to yeast, in humans ALT is performed by a BIR-like mechanism and leads to conservative inheritance of the newly synthesised DNA (Dilley et al., 2016; Roumelioti et al., 2016). Approximately 15% of all cancers utilise ALT to maintain telomeres (Dilley and Greenberg, 2015; Neumann and Reddel, 2002).

1.5.7 Similarities between break induced replication and recombination dependent replication

The *RTS1* polar replication fork barrier was utilised to study the recombination events implemented to overcome protein-DNA RFBs. Recombination dependent replication (RDR) is a BIR-like mechanism implemented to restart collapsed yet unbroken DNA replication forks (Carr and Lambert, 2013). However, as opposed to BIR, RDR follows a mode of DNA synthesis which is semiconservative (Miyabe et al., 2015). *RTS1* is the RFB most utilised in fission yeast to study DSB-free RDR (Ahn et al., 2005). During RDR, since no DSB is formed following the replication fork collapse, sister chromatids are attached throughout the repair process (*i.e.* RDR) (Ait Saada et al., 2017). Hence, in a similar fashion to Rad51-dependent BIR, RDR proceeds in a Rad51-vand Rad52-dependent manner (Ahn et al., 2005; Lambert et al., 2005; Mizuno et al., 2009). Similarly to BIR, in *RTS1*-induced RDR the restarted replication fork is highly mutagenic, prone to template switching and replication slippage (Nguyen et al., 2015; Iraqui et al., 2012).

1.6 Aims of this study

It was shown previously that SSBs can be passively converted into DSBs by an incoming replication fork in S-phase (Vrtis et al., 2021; Mayle et al., 2015). Furthermore, it was demonstrated that seDSBs breaks generated following the encounter of leading-strand SSBs by replication forks are repaired by BIR, a highly mutagenic homologous recombination-based repair process (Mayle et al., 2015). However, in this study, the repair of seDSBs was performed only in a leading-strand scenario. Furthermore, virtually all studies focused on BIR were performed in budding yeast (Mayle et al., 2015; Liu et al., 2021; Malkova et al., 1996; Lydeard et al., 2007; Malkova et al., 2005; Stivison et al., 2020) an organism only very distantly related to

humans and fission yeast (Laurent et al., 2020; Sipiczki, 2000). Moreover, much of our knowledge on BIR comes from studies performed in budding yeast were DSBs were generated not in the context of an active replication fork (Malkova et al., 1996; Lydeard et al., 2007; Malkova et al., 2005).

Therefore, in this project I aimed to set up the Flp-nick system, a tool to study the repair of SSBs in the context of a replication fork in fission yeast. The Flp-nick system was previously utilised in budding yeast to study BIR, however the repair of lagging-strand SSBs in S-phase was not investigated (Mayle et al., 2015). Conservation of biochemical pathways in both fission and budding yeast will likely mean they are conserved in humans, especially regarding the DNA replication process which is highly conserved all the way from bacteria to humans (Oakley, 2019). I investigate the recombination events implemented following replication fork-SSBs encounters both in the vicinity and several kilobases downstream the break site. Importantly, I adapt my system to generate site-specific SSBs in either leading- or lagging-strands.

Converging replication forks were shown to limit the mutagenic synthesis characteristic of BIR in budding yeast (Mayle et al., 2015). I genetically reengineer the fission yeast genome to delete a critical replication origin (*ori1253)* to study the effect on BIR-mediated repair. In the same study, structure specific endonucleases were shown to limit BIR-mediated synthesis to few kilobases downstream (Mayle et al., 2015). I check for evolutionary conservation of this mechanism in fission yeast. Finally, I studied the role of several candidate proteins in BIR-mediated repair.

Chapter 2

Materials and Methods

2.1 Media

2.1.1 *Escherichia coli* media

E. coli was cultured in Lysogeny Broth (LB) (5 g/l NaCl, 5 g/l yeast extract (YE), 10 g/l tryptone) or on LB-agar (15 g/l) at 37 °C. Liquid cultures were incubated with shaking at 200 rpm on an orbital shaker. Ampicillin was supplemented to the media to a final concentration of 50 µg/ml. Prior to use, the antibiotic was filtered sterilised using a 0.2 µm Millipore syringe filter and then stored at 4 °C (Sambrook and Russell, 2001).

2.1.2 *S. pombe* media

Salts (50X in 1 l ddH_2O: 52.5 g magnesium chloride hexahydrate, 0.735 g calcium chloride dihydrate, 50 g potassium chloride, 2 g sodium sulphate), vitamins (1000X in 1 l ddH_2O: 1 g pantotheric acid, 10 g nicotinic acid, 10 g myo-inositol, 10 mg biotin) and minerals (10000X in 100 ml ddH_2O: 1 g citric acid, 0.04 g copper sulphate, 0.1 g potassium iodide, 0.16 g molybdic acid, 0.2 g ferric chloride, 0.4 g zinc sulphate heptahydrate, 0.4 g manganese sulphate, 0.5 g boric acid) were autoclaved before use, and stored at 4 ˚C. Edinburgh Minimal Media was supplemented with 3.7 mg/ml L-glutamic acid monosodium salt (EMMG) (1 l in ddH_2O: 1 ml vitamins 1000 X, 0.1 ml minerals 10000X, 20 ml salts 50X, 30 g D-Glucose, 3.7 g sodium glutamate, 2.2 g anhydrous Na_2HPO_4, and 3 g potassium hydrogen phthalate). The complete media was Yeast Extract either without (YE) or with all amino acid supplements (YES) (Sabatinos and Forsburg, 2010). Solid media was prepared by adding Difco™ agar to a final concentration of 18 g/l. Cells were grown at 30 ˚C unless mentioned differently. Liquid cultures were incubated with shaking at 200 rpm. Auxotrophic strains were grown on selective EMMG supplemented accordingly with at least one of the following: uracil, leucine, arginine, adenine, histidine, and lysine; to a final concentration of 225

mg/l. Low adenine (LA) levels were generated by adding to the media adenine to a final concentration of 10 mg/l to distinguish between Ade^- and Ade^+ colonies. Under LA conditions, Ade^+ colonies appear white whilst Ade^- colonies appear red. For selection of Ade^+ recombinants, YE media was supplemented with all amino acids at the abovementioned concentrations except adenine. Furthermore, guanine (dissolved in 1 M NaOH) was added to a final concentration of 200 mg/l to preclude uptake of residual adenine (Osman and Whitby, 2009a). For strains carrying antibiotic selective markers, media contained hygromycin B (200 mg/l), nourseothricin (100 mg/l), and/or geneticin (100 mg/l) was used as required. Repression of the "no message in thiamine" (*nmt*) promoter was achieved via addition of 4 µM thiamine to minimal media. Complete de-repression was achieved by growing cells at 30 ˚C for at least 48 hrs in the absence of thiamine.

2.2 *S. pombe* strain construction

Standard genetic techniques were used to construct *S. pombe* strains (Sabatinos and Forsburg, 2010). **Table 6.1** illustrates the *S. pombe* strains utilised in this study together with their genotype and a simple description of the construction strategy.

2.2.1 *S. pombe* transformation

S. pombe strains were grown to exponential phase in selective liquid media and transformed at a concentration of $1x\ 10^7$ cells/ml. The procedure followed was based on the well-established lithium acetate high-efficiency transformation protocol (Rai et al., 2018). Cells were harvested via centrifugation for 3 min at 1,811 xg in 50 ml centrifugation tubes. Subsequently, cells were washed once with 50 ml of ddH_2O and twice with 5 ml LiAc/TE (0.1 M Lithium Acetate (pH 7.5), 10 mM Tris-HCl, 1 mM EDTA). Cells were resuspended in LiAc/TE to a concentration of $2x10^9$ cells/ml and transferred into a sterile 1.5 ml reaction tube. A DNA amount of 1 µg and 10 µg were utilised for

circular plasmids and linear cassettes, respectively. Therefore, the appropriate DNA amount and 2 µl of Sonicated Salmon Sperm (10 mg/ml) were added to the sterile reaction tube and incubated for 10 min at room temperature. Subsequently, 260 µl of polyethylene glycol (PEG) (40% m/v) in LiAc/TE were added to the mixture and the solution was incubated at 30 ˚C for 2.5 hrs. Finally, 43 µl of dimethylsulfoxide (DMSO) were added and cells were heat-shocked for 5 min at 42 ˚C in a water bath. Prior to plating, cells were washed with Milli-Q water to remove DMSO. Various dilutions down to 10^{-3} were plated onto appropriate media. For auxotrophic markers, cells were plated directly onto selective plates whereas for antibiotic markers cells were plated onto YES media for 24-48 hrs and then replica plated onto appropriate YES + antibiotic plates. Plates were incubated at 30 ˚C until colonies reached the appropriate size, and then colonies were screened via colony polymerase chain reaction (PCR) as described in section 2.2.3.

2.2.2 *S. pombe* crosses

Crosses were performed between two haploid strains with opposite mating-types (*i.e.,* h^- and h^+) by mixing equal amounts of cells suspended in sterile ddH_2O, and subsequently plating them in a “star shape” onto Malt Extract Agar (MEA) (20 g agar and 30 g malt extract in 1 l ddH_2O (pH>5.5)). Plates were incubated at 25 ˚C for 4 days until asci were clearly visible under a microscope and then spores were released from the parent tissue by Glusulase (PerkinElmer, USA) digestion at 30 ˚C for 14-18 hrs. Finally, spores were washed in 1 ml sterile ddH_2O and plated onto the appropriate selective media. Plates were incubated until colonies appeared and isolates were screened for appropriate auxotrophic markers and genotoxin resistance. Finally, the mating-type was determined by crossing the isolates to strains of known mating-type

(FO656 (h^+) – FO652 (h^-)). Diploid strains were not used at any stage in this study and instead, discarded immediately.

2.2.3 *S. pombe* colony PCR

Colony PCR was used to check the correct integration of the DNA cassette into the *S. pombe* genome. Where required, PCR products were sequenced via Source Bioscience to check the integrity of the target sequence. PCR primers were designed such that one annealed on the chromosome region flanking the inserted cassette and the other primer inside the inserted cassette. A very small amount (almost not visible) of the colony was placed in a PCR reaction mixture of 50 µl and boiled at 98 ˚C for 10 min to release in solution the chromosomal DNA. Amplification of DNA fragments via PCR was performed with Taq polymerase (New England Biolabs (NEB), Ipswich, MA) and with the Thermal Cycler (Biorad, C1000 Touch).

2.2.4 *S. pombe* genomic DNA isolation

Between 5 and 10 ml of an overnight culture of *S. pombe* was harvested and spheroplasted by incubation in 1 ml Citrate Phosphate buffer (50 mM Na_2HPO_4, 40 mM EDTA, 1.2 M sorbitol and 55 mM citric acid) supplemented with 2.5 mg Zymolyase 20T (MP Biomedical, UK) at 37 ˚C for 1 hr. A final concentration of 2% sodium dodecyl sulphate (SDS) was then added to the cells which were then visualised under the microscope to assess spheroplasting efficiency. Spheroplasts were gently resuspended in 550 µl TE with 1% SDS and placed in a 65 ˚C incubator for 1 hr. 175 µl of 5 M potassium acetate was then added to the sample, which was then centrifuged at 16,000 xg for 15 min at 4 ˚C. Following centrifugation, the pellet was discarded, and the supernatant transferred to a sterile microcentrifuge tube where an equal volume of isopropanol was added to precipitate the DNA. The DNA was pelleted by centrifugation at 4 ˚C for 15 min at 16,000 xg. Two consecutive washes of the DNA pellet with 70%

ice-cold ethanol were then performed and the pellet was allowed to air-dry. Finally, the DNA pellet was resuspended in 50-200 µl of TE including 20 µg/ml RNase A at room temperature for 30 min and stored at -20 °C.

2.3 Molecular biology techniques

2.3.1 Cloning procedures

Generally, for plasmid cloning the required DNA fragment was excised via restriction enzyme digestion from the parental plasmid vector. Then, the restriction digest mixture was run on a 0.7-1% agarose gel (Cambridge Reagents, UK) and purified using a QIAquick Gel Extraction Kit (Qiagen, Hiden, Germany). Ligation of DNA fragments was performed using T4 DNA ligase (NEB), incubating overnight at 16 °C. Correct plasmid construct were identified via diagnostic restriction digest analysis and sequencing (Source Bioscience). Plasmids used in this study are listed in **Table 6.2.** NEB supplied all restriction enzymes used in this study. Oligonucleotides were ordered from Merck Life Science UK Limited (Dorset, England) and are listed in **Table 6.3**. PCR analyses were performed using a Thermal cycler (Biorad, C1000 Touch).

2.3.2 *E. coli* transformation and plasmid miniprep

Competent *E. coli* cells (DH5α) were transformed with 50 to 100 ng plasmid DNA utilising the well-established heat shock protocol (Sambrook and Russell, 2001). Cells were plated onto LB media supplemented with 50 µg/ml ampicillin and grown at 37 ˚C overnight. Minipreps were performed following the Kit-free Alkaline Lysis Plasmid Miniprep protocol (Paalme and Speek, 2021). Colonies were inoculated into 5 ml of liquid LB supplemented with ampicillin and grown with aeration overnight at 37 °C. 4.5 ml of the overnight culture was then harvested, and the cell pellet was resuspended in 300 µl Buffer P1 (5 ml 1 M tris (pH 8.0), 5 ml 200 mM EDTA, make up volume to 100

ml). Subsequently, 3 µl of RNAseA (10 mg/ml) was added followed by 300 µl of Buffer P2 (10 ml 2M NaOH, 10 ml 10% SDS, make up volume to 100 ml). The solution was mixed by inversion and incubated for 5 min at room temperature before addition of 300 µl of Buffer P3 (29.4 g potassium acetate dissolved in 50 ml ddH_2O adjusted with concentrated acetic acid to pH 5.5, make up volume to 100 ml) to the tube which was mixed by inversion before placing it in a centrifuge for 15 min at 16,000 xg. The white pellet was discarded, and the supernatant was transferred to a fresh sterile microcentrifuge tube where a 0.8 volume (approx. 640 µl) of isopropanol was added to precipitate the DNA. The precipitated DNA was then harvested by centrifugation at 16,000 xg for 15 min and washed twice with 70% ice-cold ethanol to remove residual salt. Finally, the DNA was resuspended gently in 30 µl 1xTE.

2.4 Genetic assays

2.4.1 Spot assay for assessing growth/viability

Cells were grown in selective EMMG liquid cultures for 48 hrs either with (repressed *nmt* promoter) or without (derepressed *nmt* promoter) thiamine. Cells were harvested when the culture reached an OD_{600} 0.7, which approximately equates to mid-exponential phase. Subsequently, 3 serial 10-fold dilutions down to 10^{-3} were prepared and 10 µl from each suspension were plated onto the appropriate selection plates. Plates were incubated at 30 ˚C for 4 days and photographed every 24 hrs to record growth.

2.4.2 Spot assay for assessing genotoxin sensitivity

Cells were grown to mid-exponential phase and serially diluted as described in section 2.4.1. 10 µl of each serial dilution was then gently spotted onto a series of YES plates containing appropriate concentrations of genotoxin (HU, MMS or CPT). The cells were

also spotted onto a control YES plate without genotoxin, and onto YES plates that were subsequently irradiated with UV light using a Stratalinker (Stratagene). Plates were incubated at 30 ˚C and photographs taken every 24 hrs to keep a record of the relative growth of the strains being tested. The chronic exposure to genotoxins or acute exposure to UV light induces DNA lesions which can cause fork stalling and/or breaking as discussed in chapter 1.2.1.

2.4.3 Mitotic direct repeat recombination assay

The direct repeat recombination assay was carried out as indicated in a previous well-established protocol (Osman and Whitby, 2009a). The strain was streaked out from the freezer at -80 ˚C onto EMMG selective media lacking histidine and supplemented with LA and incubated at 30 ˚C for 4-5 days until single colonies reached an appropriate size. Subsequently, 3 different red non-recombinant colonies (biological replicates) were plated onto EMMG media including all supplements (*i.e.* Arginine, Histidine, Leucine, Lysine and Uracil) and either with or without thiamine (EMMG + 5S +T and EMMG + 5S -T, respectively). Regarding strains containing a plasmid, growth was performed on EMMG including all supplements except for leucine (to select for retention of the plasmid) and either with or without thiamine (EMMG -Leu +T and EMMG -Leu -T, respectively) (Osman et al., 2016). Subsequently, 5 colonies (technical replicates) from each of the 3 EMMG plates (biological replicates) were assayed by plating onto YE -adenine media supplemented with guanine to determine the recombination frequency. The recombination value was then normalised to the viability value by plating the 5 colonies also onto YE media supplemented with LA. Plates were incubated at 30 °C for 8 days to ensure all recombinant colonies had sufficient time to grow. The ratio between the recombination and viability value indicates the recombination frequency of the strain. Finally, the YE- adenine +guanine plates were

replica-plated onto EMMG -histidine to differentiate between deletion and gene conversion recombination events.

2.5 Data analysis and statistics

All statistical analysis was performed utilising Graphpad Prism version 9.0 for Macintosh (GraphPad Software, La Jolla California, USA). Initially, a one-way ANOVA test was performed to understand if there was statistical evidence that the population means were significantly different. Subsequently, data were tested for normal distribution via the Shapiro-Wilk normality test. Depending on the distribution of the data, mean values were compared via the appropriate independent-sample two-tailed t-test. P values below 0.05 were considered significant.

Chapter 3

Establishing the Flp-nick system to study Break Induced Replication

3.1 Introduction

Among the range of lesions a genome can suffer, SSBs are by far the most common (Hossain et al., 2018). SSBs can arise due to a multitude of reasons and are generally rapidly and efficiently repaired by the SSBR machinery (see section 1.4 for more details) (Caldecott, 2008). As discussed in section 1.5, SSBs are occasionally encountered by replication forks and converted into DSBs. Early studies utilising the Top1 inhibitor camptothecin indicated that following replication fork-SSB encounters, DSBs are generated via a runoff mechanism (Avemann et al., 1988; Hsiang et al., 1985; Strumberg et al., 2000). More recent studies suggested that replication forks undergo reversal upon encountering camptothecin-induced SSBs (Ray Chaudhuri et al., 2012). Subsequently, a study in budding yeast utilising a reengineered version of the Flp recombinase (Flp-nick) showed that leading-strand SSBs are converted into seDSBs by the incoming replication fork. In the same study, they demonstrated BIR to be responsible for repairing these replication-associated seDSBs. Yet, the repair of lagging-strand SSBs in S-phase was not investigated (Mayle et al., 2015). In this project, I wanted to emulate their work and establish the Flp-nick system to study BIR in fission yeast, an organism only distantly related to both humans and budding yeast (Laurent et al., 2020; Sipiczki, 2000). Here, I build on the work from Mayle et. al., (2015) by performing a side-by-side comparison of the pathways deployed to repair leading and lagging-strand protein-bound SSBs in the context of a replication fork. I also compare the ability of protein-bound SSBs to induce BIR with that of the *RTS1* protein-DNA RFB to induce RDR.

The Whitby lab previously utilised a direct repeat heteroallele reporter located at the fission yeast endogenous *ade6* locus on ChrIII to study the recombination events induced by the *RTS1* barrier in fission yeast (Ahn et al., 2005). *RTS1* is a native fission

yeast RFB which promotes mating-type switching (see section 1.2.3) (Dalgaard and Klar, 2001). The direct repeat heteroallele reporter consists of a *his3*$^{+}$ functional gene flanked by two loss-of-function *ade6*$^{-}$ heteroalleles (*ade6-L469* and *ade6-M375*) with a point mutation generating an early stop codon in the *ade6* coding sequence **(Fig. 3.1)**. Strains with an intact and unrecombined reporter accumulate red pigment in media supplemented with low adenine (LA). Cells with recombined reporters appear white in the same media supplemented with LA and can arise via ectopic non-allelic homologous recombination (NAHR) between the heteroalleles. This recombination mechanism restores the wild-type (WT) sequence in one or both heteroalleles. Qualitative and quantitative analysis of these recombination events can be performed via the mitotic direct repeat recombination assay outlined in section 2.4.3. Recombination between the direct repeat heteroalleles generates two different classes of functional Ade^{+} recombinants: deletions (Ade^{+}, His^{-}) and gene conversions (Ade^{+}, His^{+}), which can be quantified with precision, and arise via different mechanisms. It is important to note that some of the recombination events which occur are silent in our system of study and, therefore, cannot scored as part of this project. Nevertheless, this experimental setting enables a robust quantitative study of a good proportion of recombination events taking place at a specific genomic locus (Osman and Whitby, 2009).

Whether DNA replication in a specific DNA strand is performed continuously (leading-strand) or discontinuously (lagging-strand) depends on the directionality of the replication fork at that specific region of DNA. Since several early firing and strong origins of replication are located at the *ade6* telomere proximal region, at the *ade6* locus DNA replication is nearly unidirectional in the telomere-to-centromere direction (Ahn et al., 2005; Lorenz et al., 2009) **(Fig. 3.1A).** For simplicity, in this thesis I refer to

the leading-strand as the **top strand (TS)** and the lagging-strand as the **bottom strand (BS)**.

Flp recombinase is encoded by the *Saccharomyces cerevisiae* 2µ plasmid and catalyses recombination between two Flippase Recombination Targets (*FRT*) within the plasmid to promote a type of rolling circle replication that maintains the 2µ plasmid at a high copy number (Gronostajski and Sadowski, 1985). Importantly, Flp recombinase is not found in fission yeast. During the catalytic reaction, a crucial tyrosine residue at the Flp active site carries out the initial cleavage step generating 5'-OH ends and 3'-phosphotyrosyl linkages. Subsequently, the nucleophilic 5'-OH ends perform the strand exchange reaction with a second *FRT* site. A crucial histidine residue found in the Flp active site is required for activation of the OH^- group at the 5' end (Ma et al., 2007). In this study, I utilise a re-engineered Flp recombinase (Flp^{H305L}), lacking the above-mentioned key histidine residue required for the religation step, to induce long-lived site-specific nicks in the fission yeast genome. Following the induction of the SSB, Flp^{H305L} remains covalently bound to the 3' end of the DNA via a phosphotyrosyl linkage (Gronostajski and Sadowski, 1985; Nielsen et al., 2009). Hence, DNA cleavage by Flp^{H305L} mimics a topoisomerase cleavage complex in that it induces a SSB but instead of rapidly religating it, it remains covalently bound to the 3'-end of the DNA via a phosphotyrosyl linkage (Gronostajski and Sadowski, 1985; Nielsen et al., 2009). In a similar fashion to previous studies investigating *RTS1*-induced RDR (Ahn et al 2005; Nguyen et al 2015; Jalan et al 2019), I utilise the direct repeat *ade6* heteroallele reporter with an integrated *FRT* site to investigate Flp^{H305L}-induced recombination. Moreover, since DNA replication across the *ade6* locus is virtually unidirectional (Ahn et al., 2005), in my system it is possible to generate TS and BS SSBs by simply changing the orientation of the *FRT* site. Furthermore, by utilising

the same reporter systems at the same genomic locations used to characterize *RTS1*-induced RDR, I am able to directly compare Flp^{H305L}-induced BIR with *RTS1*-induced RDR.

3.2 Results

3.2.1 Establishing a system to monitor recombination induced by Flp^{H305L}-*FRT* site-specific single-stranded breaks.

I set out to establish a system which would enable us to study the recombination events in the vicinity of a stalled or collapsed replication fork at Flp^{H305L}-induced site-specific SSBs in fission yeast. Initially, the *FRT* site was subcloned in both TS and BS orientations into the plasmid pFOX2 (**Fig. 3.1A,B)**. Subsequently, the plasmid was linearised and integrated into fission yeast (**Fig. 3.1C**). Ends-in recombination generated a strain carrying the *FRT* site located within the recombination reporter in the short DNA region between the functional *his3*$^{+}$ gene and *ade6-M375* (**Fig. 3.1D**). Hereafter, I refer to these reporters as TS and BS "**0 kb reporters**". The correct integration of the reporter and presence of the *FRT* site as well as its orientation were verified by colony PCR and DNA sequencing (**Fig. 3.1E,F**). Off target insertion of the cassette would be via ends-out recombination and, therefore, not detected via colony PCR.

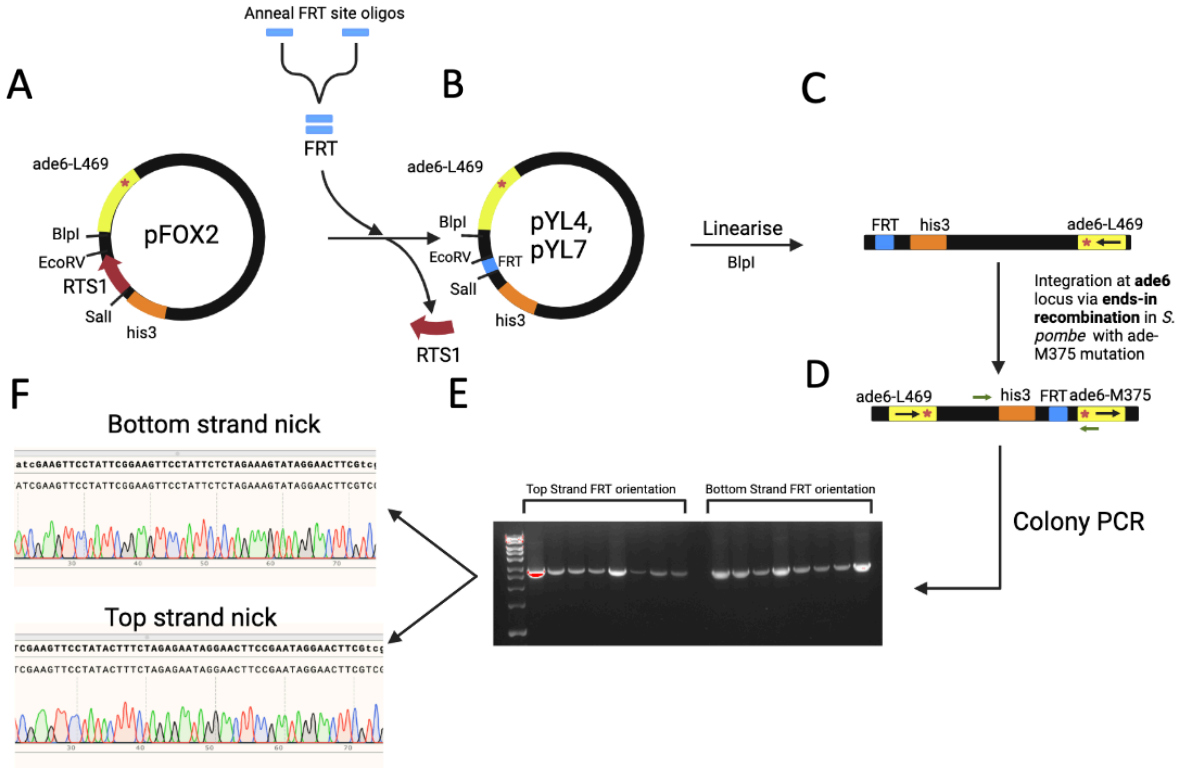

Figure 3.1. Integration of the FRT site at the ade6 locus on ChrIII. A) *FRT site oligos containing SalI/EcoRV overhangs were cloned into SalI/EcoRV digested pFOX2 hence replacing RTS1.* ***B)*** *The derivative plasmids pYL4 (BS orientation) and pYL7 (TS orientation) were linearised via BlpI digestion and transformed into S. pombe (ade6-M375 strain FO1236).* ***C)*** *Ends-in recombination generates a strain carrying a direct repeat reporter of ade6 heteroalleles integrated at the ade6 locus.* ***D)*** *The FRT site is located within the reporter in the short DNA region between the his3^{+} functional gene and the ade6-M375. Ade^{-} His^{+} progenies were selected and investigated further by colony PCR and Sanger sequencing. Primers for the diagnostic PCR shown in E are indicated by the green arrows.* ***E)*** *Agarose gel showing the products from a series of diagnostic colony PCR reactions (using primer oMW717 and oMW705) to identify transformants with correctly integrated pYL4/pYL7.* ***F)*** *Sanger sequencing (oMW717) to verify the correct integration and orientation of the FRT site (i.e. either TS or BS orientation).*

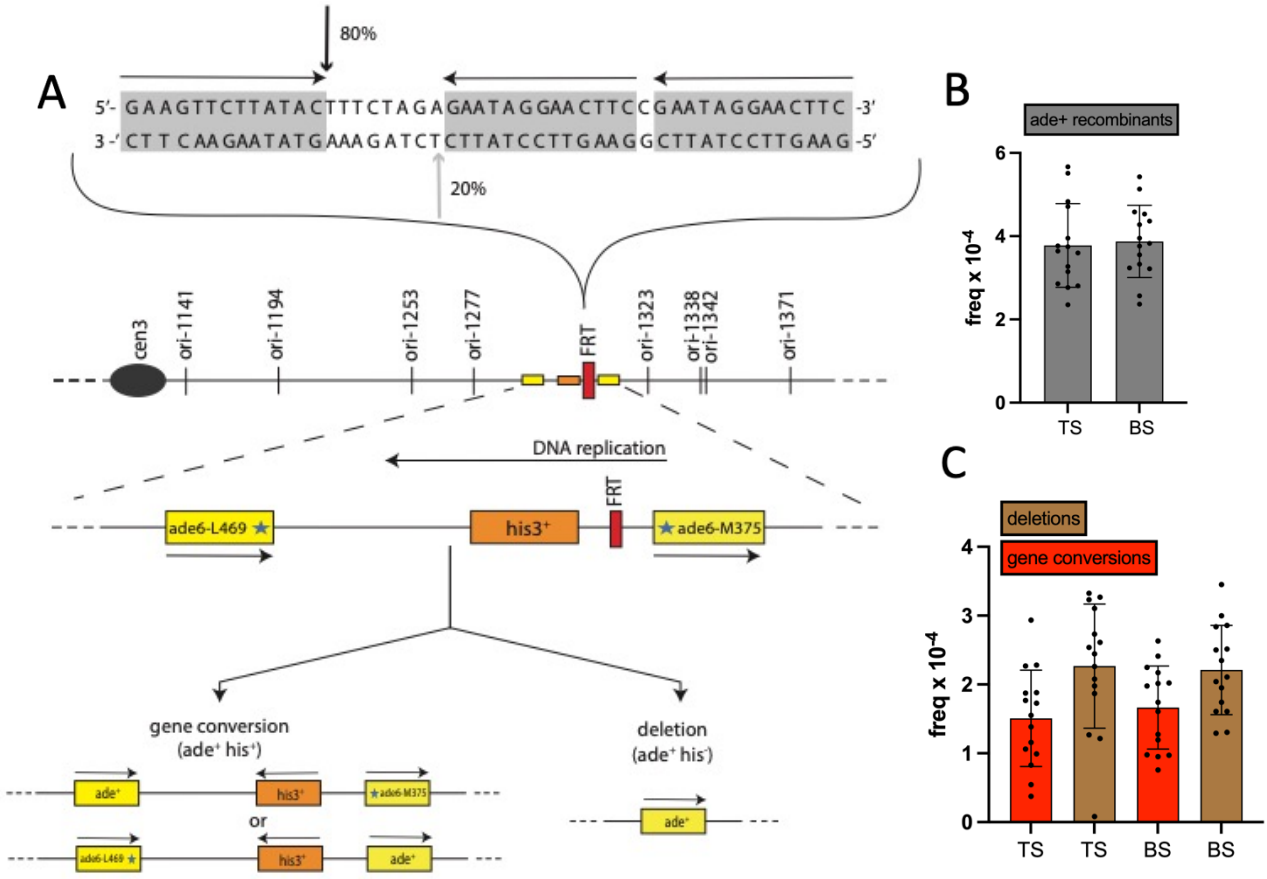

Figure 3.2. ***Experimental setting and spontaneous recombination levels for TS and BS "0kb reporters". A)*** *The FRT site, where protein-bound SSBs are generated by Flp^{H305L}, is located within the direct repeat heteroallele recombination reporter. Recombination between direct repeat heteroalleles generates two classes of Ade^{+} functional recombinants: gene conversions (Ade^{+} His^{+}) and deletions (Ade^{+} His^{-}).* ***B)*** *Bar chart indicating the measured spontaneous Ade^{+} frequencies for the TS and BS "0kb reporters".* ***C)*** *Illustrates the proportion of gene conversion and deletions. TS indicates that the FRT site is in the orientation in which the majority of Flp^{H305L} nicks will be in the top (leading) strand, whilst BS indicates that the FRT site is in the opposite orientation meaning that the majority of Flp^{H305L} nicks will be in the bottom (lagging) strand. Strains are MCW10107 and MCW10108. Error bars represent +/- standard deviation.*

Even under normal conditions, spontaneous recombination occurs throughout the genome with every cell division and this can be affected by the local chromatin architecture (Smith and Aladjem, 2014). Therefore, the spontaneous (baseline) recombination levels for the new TS and BS 0 kb reporters were measured. As expected, no significant difference in spontaneous recombination levels was detected between TS and BS. The total frequency of Ade^+ recombinants was ~3.7×10^{-4} for both TS and BS containing strains (**Fig. 3.2B**). Furthermore, in both cases the ratio of deletions to gene conversions was approximately 6:4 (**Fig. 3.2C**).

3.2.2 The Flp-nick system stimulates recombination between direct repeat heteroalleles in fission yeast

Having determined the spontaneous recombination levels, I next tested whether expressing Flp^{H305L} in fission yeast induced direct repeat recombination. Even though Flp^{H305L} was previously shown to induce BIR in budding yeast (Nielsen et al., 2009; Mayle et al., 2015), it was not certain that it would work efficiently in fission yeast. Therefore, I expressed Flp^{H305L} from a multi-copy pREP1 plasmid that carries the strong no message in thiamine 1 promoter (P*nmt1*) that can be de-repressed upon thiamine depletion. As plasmid copy number can vary amongst transformants (Karim et al., 2013), I obtained data from three independent transformants for each strain tested. In the presence of thiamine, there was approximately a four-fold increase in the frequency of Ade^+ recombinants in both TS and BS 0 kb reporter strains carrying the pREP1-*FLPH305L* plasmid, compared to the same strains carrying the empty pREP1 plasmid (**Fig. 3.3A**). This is likely due to "leaky expression" of *FLPH305L* from the repressed *nmt1* promoter. However, upon full expression of Flp^{H305L} in the absence of thiamine, the frequency of Ade^+ recombinants increased ~400-fold compared to spontaneous levels (**Fig. 3.3A**). Interestingly, the frequency of Ade^+ recombinants was

slightly higher (~0.25 -fold) in the strain carrying the BS reporter compared to the TS reporter (p=0.0137). Analysis of the ratio of deletions and gene conversions showed a similar pattern for both TS and BS reporters with deletions being far more abundant (~93% for BS and ~88% for TS) than gene conversions (~7% for BS and ~12% for TS). In both cases the skew towards deletions was significantly greater than seen for spontaneous recombination (7 – 12% vs ~30%). Overall, these data confirm that Flp-nick SSBs strongly induce recombination when present in either leading or lagging template strands.

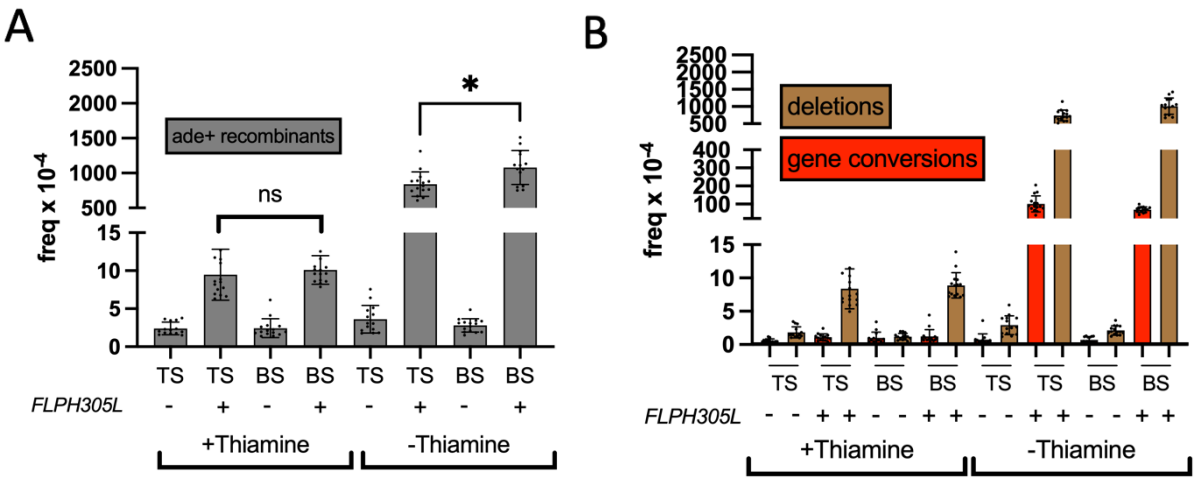

Figure 3.3. The Flp-nick system promotes direct repeat heteroallele recombination in fission yeast. A) *Indicates the frequency of total Ade^{+} recombinants.* ***B)*** *Illustrates the proportion of gene conversion and deletions. Flp^{H305L} is expressed from a pREP1 plasmid. Upon thiamine depletion (-thiamine) the Pnmt1 promoter is de-repressed and Flp^{H305L} expression is induced. As a negative control, strains were transformed with a pREP1 empty plasmid. TS indicates that the FRT site is in the orientation in which the majority of Flp^{H305L} nicks will be in the top (leading) strand, whilst BS indicates that the FRT site is in the opposite orientation meaning that the majority of Flp^{H305L} nicks will be in the bottom (lagging) strand. Strains are MCW10107, MCW10108, MCW10107 transformed with pREP1, MCW10107 transformed with pPC7, MCW10108 transformed with pREP1 and MCW10108 transformed with pPC7. Error bars represent +/- standard deviation. P<0.05 (*).*

3.2.3 Optimising *FLPH305L* expression levels

As mentioned in section 3.2.2, Flp^{H305L} expression levels driven from a plasmid are not stable as plasmids may be retained by different strains in different copy numbers, and may be lost occasionally (Caunt et al., 1988; Karim et al., 2013). Therefore, to ensure stable expression levels, I reengineered the *S. pombe* genome to express Flp^{H305L} from a single chromosomal copy located at the endogenous *lys1* locus. To identify the ideal promoter to drive expression from a single chromosomal copy, I inserted the *FLPH305L* coding sequence behind three different promoters: P*nmt81*, P*nmt41* and P*nmt1*. *Pnmt81-FLPH305L* expression was not sufficiently high to generate a significant increase in Ade^+ recombinants (**Fig. 3.4A**). A modest ~2.7-fold increase in recombination frequency was observed with *Pnmt41-FLPH305L* expression (**Fig. 3.4A**). However, expression of Flp^{H305L} from *Pnmt1* (the strongest promoter of the three tested) yielded the highest frequency of Ade^+ recombinants, which was ~50-fold higher than the spontaneous level (**Fig. 3.4A**). Both spontaneous recombination and recombination under *Pnmt81* levels of Flp^{H305L} gave rise to a similar ratio of deletions (~60%) to gene conversions (~40%) (**Fig. 3.4B**). Expression of *Pnmt41-FLPH305L* generated a more biased ratio with deletions more frequent (~75%) than gene conversions (~25%) (**Fig. 3.4B**). However, the highest level of Flp^{H305L} expression (*i.e. Pnmt1-FLPH305L*) caused an even bigger bias towards deletions (~80%) compared to gene conversions (~20%) (**Fig. 3.4B**). Seemingly, the HR-dependent mechanisms implemented to repair Flp^{H305L}-induced SSBs, are more prone to result in the deletion of the intervening sequence flanking the *ade6* heteroalleles. The bias towards deletions could be since deletions do not necessarily require invasion of the sister chromatid but can also arise by SSA. Additionally, gene conversions can still be converted into deletions whereas the inverse is not possible.

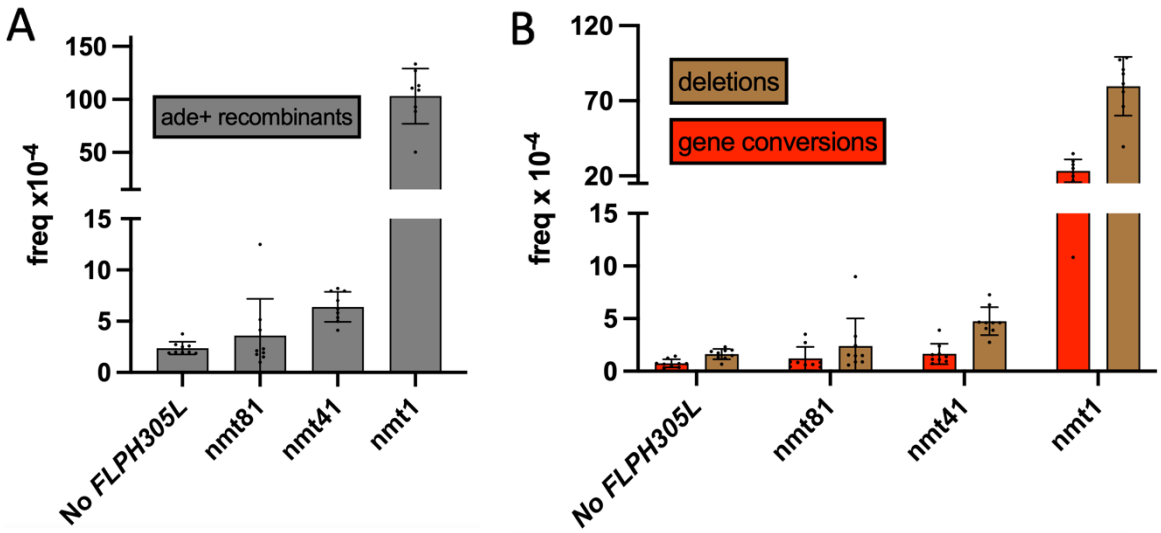

Figure 3.4. Optimising the Flp^{H305L} expression levels from a single chromosomal copy. *Bar charts showing the frequency of Ade^{+} recombinants generated following expression of Flp^{H305L} from Pnmt81, Pnmt41 and Pnmt1 promoters from a single chromosomal copy integrated at the lys1 locus.* ***A)*** *Indicates the frequency of total Ade^{+} recombinants.* ***B)*** *Illustrates the proportion of gene conversion and deletions. The FRT site is present in the TS orientation in all strains. Strains are MCW10107, MCW10116, MCW10117, MCW10118. Error bars represent +/- standard deviation.*

To confirm that the recombination induced by expression of Flp^{H305L} from the P*nmt1* promoter was indeed due to Flp^{H305L} cleaving the DNA at the *FRT* site, I repeated the experiment in a strain carrying a 0 kb reporter with no *FRT* site present. In this strain background, expression of Flp^{H305L} from the *nmt1* promoter resulted in no induction of Ade^+ recombinants (**Fig. 6.1**). Altogether these data show that expression of Flp^{H305L}, driven by an *nmt1* promoter from a single chromosomal locus, is sufficient to induce high levels of direct repeat recombination when there is an *FRT* site positioned between the DNA repeats.

3.2.4 Both leading and lagging-strand Flp-nicks induce similar levels of direct repeat recombination.

Having optimised Flp^{H305L} expression levels from a single chromosomal copy, I next re-evaluated whether a Flp-nick in the leading template strand (TS) induced direct repeat recombination to the same extent as one in the lagging template strand (BS). As mentioned in Section 3.2.2, when Flp^{H305L} was expressed from a multicopy plasmid, I detected a small (~1.28x) but significant (p=0.015) fold increase in the frequency of Ade^+ recombinants with *FRT* in the BS nick orientation compared to the TS nick orientation (**Fig. 3.3A**). However, when Flp^{H305L} was expressed from a single chromosomal copy, no significant difference in the frequency of Ade^+ recombinants between TS and BS was detected (**Fig. 3.5A**). Importantly, compared to the spontaneous level of recombination, the induced level (*i.e.* Flp^{H305L} expression from P*nmt1*) showed a stronger bias towards deletion-type recombinants (**Fig. 3.5B**). This was most pronounced with a BS nick where deletions formed ~93% of the total Ade^+ recombinants (**Fig. 3.5B**). Altogether these data show that both TS and BS Flp^{H305L}-induced SSBs stimulate direct repeat recombination to similar levels (**Fig. 3.5A**).

However, the level of induction is less than obtained when Flp^{H305L} was expressed from a multicopy plasmid (**Fig. 3.3A**) suggesting that the amount of Flp^{H305L} is insufficient to achieve cleavage of *FRT* site in every cell.

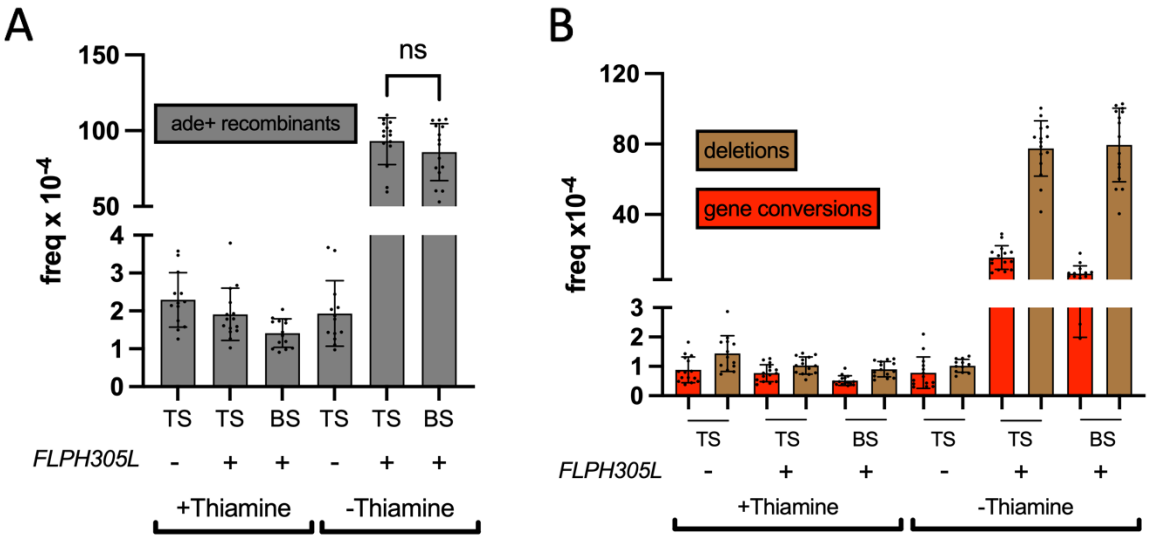

Figure 3.5. Both TS and BS Flp^{H305L}-induced SSBs stimulate recombination between direct ade6 heteroalleles. *Bar chart showing the frequency of Ade^{+} recombinants generated to repair Flp^{H305L}-induced SSBs in the context of a replication fork.* ***A)*** *Indicates the frequency of total Ade^{+} recombinants.* ***B)*** *Bar chart showing the frequency of gene conversions and deletions. TS indicates Top (leading) strand whilst BS indicates bottom (lagging) strand orientation. Strains are MCW10107, MCW10118, MCW10121. Error bars represent +/- standard deviation.*

3.2.5 The Flp-nick system stimulates template switching downstream of the site of replication fork SSB encounter

Mayle et al., (2015) reported that BIR-mediated mutagenic synthesis is limited to a few kilobases downstream of Flp-induced SSBs, and that converging replication forks are sufficient to suppress BIR. In their experimental system, SSBs were generated either between efficient replication origins or at subtelomeric positions where only dormant origins are located. I established a similar experimental set up in fission yeast by relocating the direct repeat of *ade6* heteroalleles 12.4 kb downstream of the *FRT* site (**Fig. 3.6A**). From hereafter, I will refer to this experimental set up as the "**12.4 kb reporter**". In a similar fashion to the system reported in Mayle et. al. (2015), in my system the restarted replication fork travelling in the telomere-to-centromere direction will merge with replication forks travelling in the opposite direction (mainly originating from *ori1253* and *ori1277*). Furthermore, the direct repeat of *ade6* heteroalleles positioned at the 12.4 kb locus measures the template switching events characteristic of BIR. Template switching is mainly due to the low stability of the migrating D-loop involved in BIR, which can occasionally switch to a different incorrect homologous repair template (Smith et al., 2007). One template switching event between the *ade6* heteroalleles can cause the loss of the intervening DNA region and formation of an *ade6*$^{+}$ gene. Two template switching events can stimulate the formation of an *ade6*$^{+}$ gene and retention of the intervening DNA region. Thus, the two events are distinguished by retention (gene conversions) or loss (deletions) of the intervening *his3*$^{+}$ functional gene (Jalan et al., 2019).

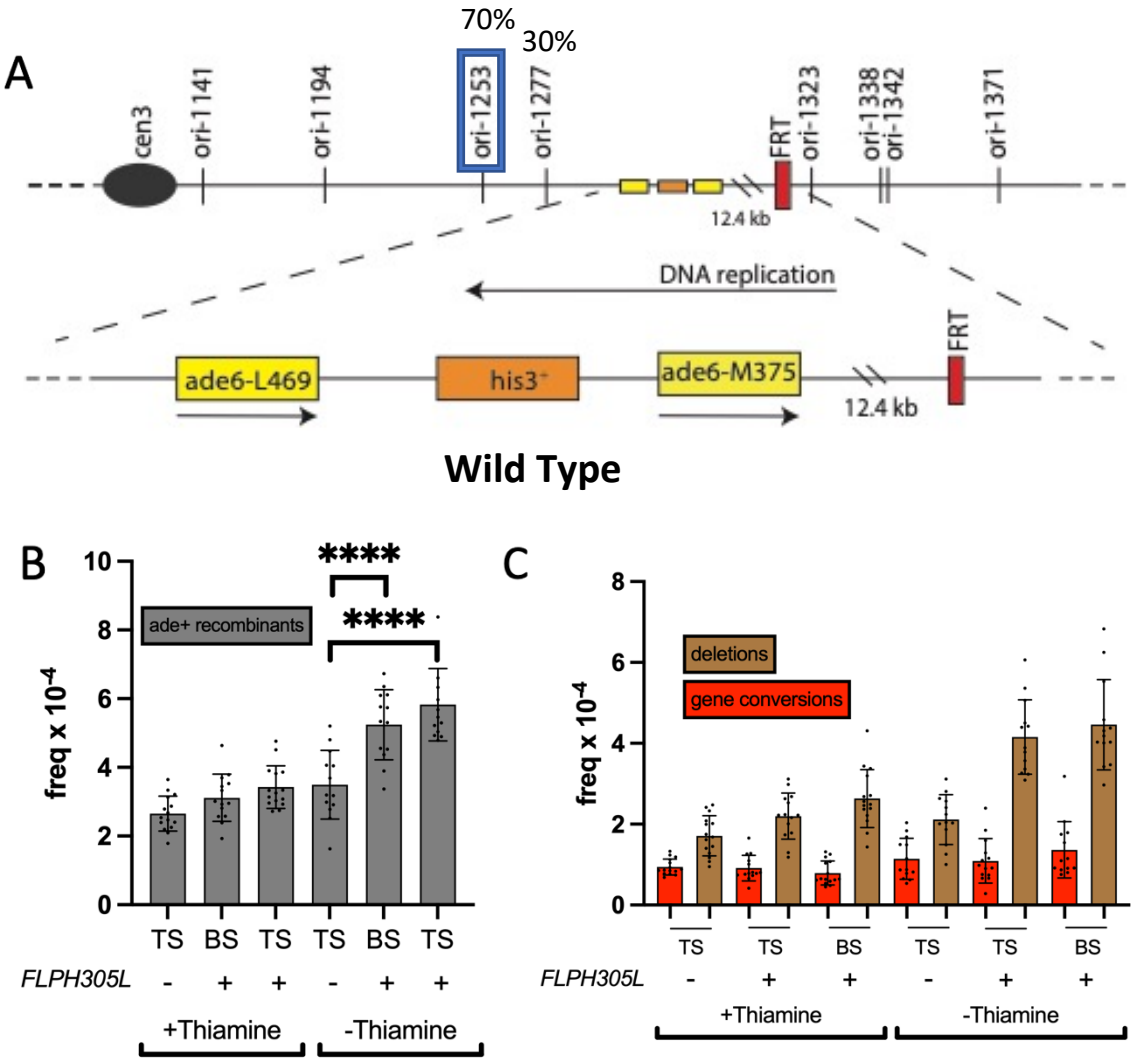

Figure 3.6. A system to monitor quantitatively the template switching events downstream of a Flp^{H305L}-induced SSB. A) *The FRT, where Flp^{H305L}-induced protein-bound SSBs are generated, is inserted at the endogenous ade6 locus. The ade6 heteroallele reporter is positioned 12.4kb downstream of FRT. The DNA replication directionality, indicated by a black arrow, is mainly in the telomere to centromere direction. Recombination between the ade6 heteroalleles generates two classes of recombinants Ade$^+$His$^-$ (deletions) and Ade$^+$His$^+$ (gene conversions) (not shown). ori1253, highlighted by a blue rectangular box, and ori1277, next to ori1253, fire in 70% and 30% of cell divisions, respectively (Jalan et al., 2019; Nguyen et al., 2015).* ***B)***

Total frequency of Ade$^+$ recombinants at 12.4 kb reporter downstream of FRT. ***C)*** *Frequency of gene conversions and deletions. TS indicates Top (leading) strand whilst BS indicates bottom (lagging) strand orientation. Strains are MCW10128, MCW10141, MCW10144. Error bars represent +/- standard deviation. P<0.0001 (****).*

As with the 0 kb system (section 3.2.1), once the 12.4 kb system was engineered, I initially quantified the spontaneous recombination levels for this chromosomal location (**Fig. 3.6B**). The total Ade$^+$ recombinant frequency was ~2.5 x 10^{-4}, which is slightly lower than at the 0kb reporter (~3.7 x 10^{-4}) ($p<0.0001$), and the proportion of gene conversions was also less (30% versus 40% at the 0 kb reporter). These differences might relate to differences in the chromatin architecture at the two genomic sites (Smith and Aladjem, 2014). Having measured the spontaneous level, I next assessed whether Flp^{H305L}-induced SSBs would lead to an increase in the frequency of Ade$^+$ recombinants at the 12.4 kb reporter (**Fig. 3.6B**). For both TS and BS orientations of the *FRT* site, a small (~2-fold) but significant ($p<0.0001$) increase in Ade$^+$ recombinants was observed. Also, for both TS and BS orientations, essentially all of the induced recombinants were deletions (**Fig. 3.6C**). These data suggest that both leading and lagging-strand SSBs can similarly give rise to BIR, which is associated with template switching that predominantly gives rise to deletions at the 12.4 kb reporter.

3.2.6 Converging forks limit BIR-mediated mutagenic synthesis

Converging replication forks are believed to suppress BIR (Mayle et al., 2015; Ait Saada et al., 2018; Pardo et al., 2020), which could explain the minimal increase in template switching detected at the 12.4 kb reporter (**Fig. 3.6A, B)**. According to this model, limiting the frequency of converging replication forks should promote BIR-mediated synthesis (**Fig. 3.7A**). To test this hypothesis, I genetically reengineered the fission yeast genome by deleting *ori1253*. It was previously demonstrated by 2-Dimensional Gel Electrophoresis that ~ 70% of cells in each cell cycle fire a pair of replication forks from *ori1253* (**Fig 3.6A**) (Jalan et al., 2019; Nguyen et al., 2015;

Nieduszynski et al., 2007). Therefore, Flp-nick strains carrying 12.4 kb reporters were crossed to strains established by the Whitby lab lacking only *ori1253*. In the absence of this origin of replication, a higher proportion of restarted replication forks should replicate the *ade6* heteroallele reporter located at the 12.4 kb site via BIR, instead of being rescued by merging with an opposing replication fork. Indeed, with *ori1253* deleted there was marked increase in the frequency of Ade^+ recombinants (7-fold for *FRT* TS; 12-fold for *FRT* BS) at the 12.4 kb reporter upon Flp^{H305L} expression, which is indicative of increased template switching and BIR (**Fig. 3.7B**). Interestingly, BIR-mediated repair of TS SSBs generated a higher (1.8-fold) frequency of Ade^+ recombinants than that induced by BS SSBs ($p<0.0001$). This difference was confirmed in multiple experiments and by testing two independent isolates for each strain (**Fig. 3.7B; Fig. 6.2A**). Most of the induced Ade^+ recombinants were deletions, which increased ~7-fold and ~12-fold upon BS and TS SSB induction, respectively (**Fig. 3.7C**). However, both TS and BS SSBs also induced gene conversions up by 2.7-fold and 2-fold ($p<0.0001$), respectively (**Fig. 3.7C**; **Fig. 6.2B**).

3.2.7 GpII-induced SSBs in both leading and lagging template strands also induce template switching at the downstream reporter

As mentioned in section 3.2.1, Flp^{H305L}-mediated cleavage is not performed entirely on a single DNA strand. Instead, there is evidence indicating that DNA nicking is performed ~80% on a strand and ~20% on the complementary strand. As a consequence, in the Flp-nick system, when the *FRT* site is orientated to generate nicks predominantly in one strand, an undesired proportion of SSBs is generated in the complementary one (**Fig. 3.2A**) (Mayle et al., 2015; Nielsen et al., 2012). If, unknowingly, the actual nicking range was more balanced in our system (e.g. 60%,

40%), the unwanted proportion (*i.e.* 40%) of SSBs generated from the BS *FRT* site orientation would be in reality TS nicks, and hence be repaired by BIR. I investigated this scientific question by utilising the M13 filamentous bacteriophage gene protein II, from hereafter referred simply as “gpII”.

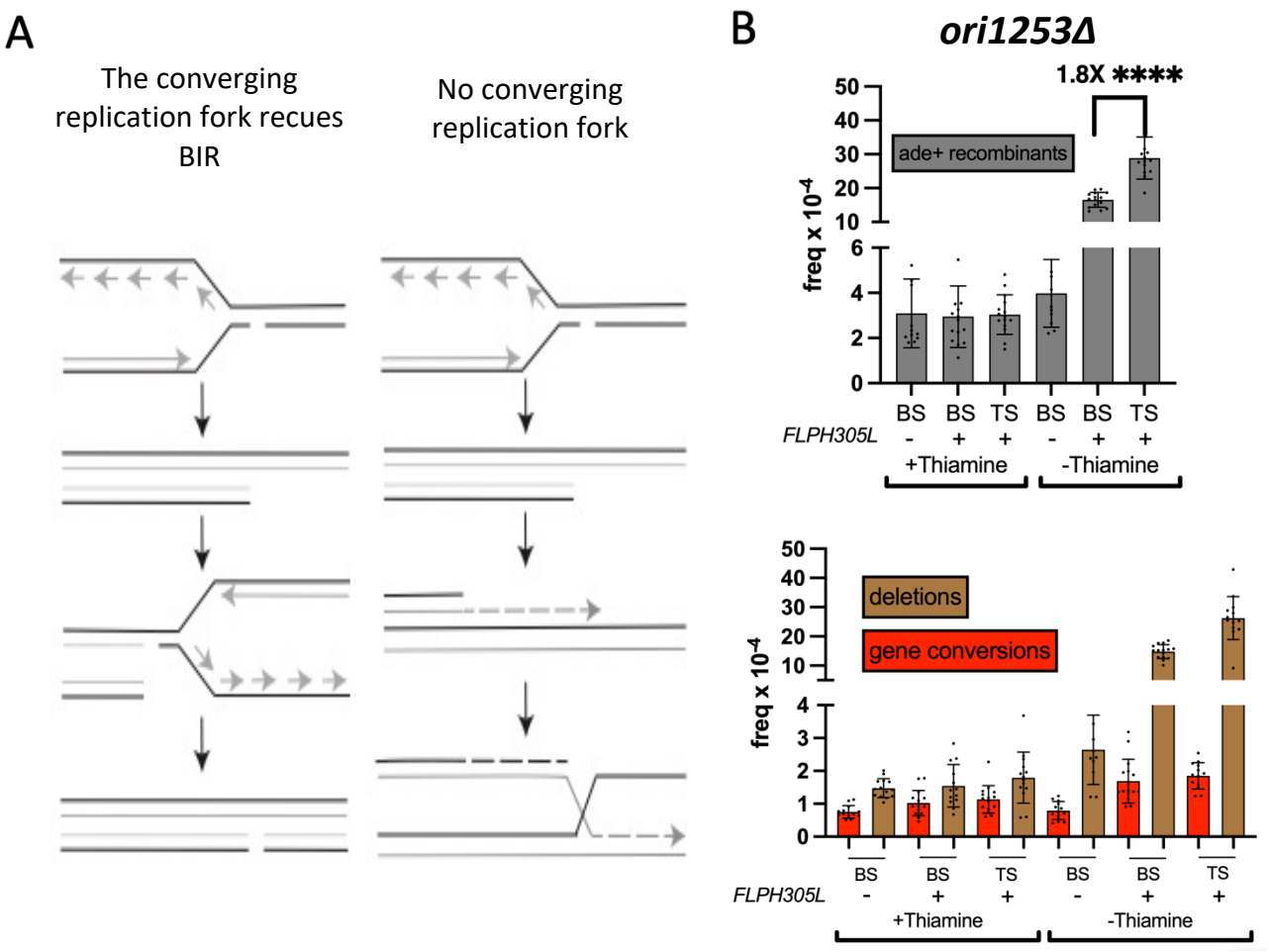

Figure 3.7 Converging forks limit BIR associated template switching.

A) *A converging replication fork travelling in the opposing direction merges with the stalled or broken replication fork, hence suppressing BIR. When no converging fork is present, the stalled or broken replication fork is restarted via BIR.* ***B)*** *Frequency of Ade$^+$ recombinants at 12.4 kb reporter downstream of the FRT site when ori1253 is deleted.* ***C)*** *Calculated proportion of gene conversions and deletions. TS indicates Top (leading) strand whilst BS indicates bottom (lagging) strand orientation. Strains are MCW10205, MCW10138, MCW10139. Error bars represent +/- standard deviation. P<0.0001 (****).*

In nature, the gpII protein is required to induce a SSB in the phage DNA and initiate rolling circle phage DNA replication in the host cell (Pratt and Erdahl, 1968). The gpII nickase was previously utilised to investigate replication-chromosome fragmentation at SSBs (Kuzminov, 2001). This system was also utilised by the Whitby group to investigate the role of long-range resection at stalled or collapsed replication forks (Osman et al., 2016). As opposed to Flp^{H305L} which remains covalently bound to the 3'- end of the DNA, the gpII nickase remains covalently bound to the 5'-end of the DNA (Asano et al., 1999). Importantly, the gpII nickase, as opposed to Flp^{H305L}, introduces SSBs solely on one DNA strand. I inserted the 40bp *gpII* site, where the gpII nickase introduces SSBs, in both TS and BS orientations at the endogenous *ade6* locus in fission yeast and positioned the *ade6* heteroallele reporter 12.4 kb downstream (**Fig. 3.8A**). In this experimental set up, the restarted replication fork travelling in the telomere-to-centromere direction will replicate the 12.4 kb reporter, which can be utilised to quantify the template switching events (**Fig. 3.8A**). In a similar fashion to the data obtained utilising the Flp-nick system 12kb reporters, both TS and BS nicks were repaired via BIR in the gpII-nickase system. The gpII nickase stimulated a modest but significant ($p<0.0001$) increase in template switching 12.4 kb downstream (2.8-fold for BS; 2.4-fold for TS) (**Fig 3.8B**), which was stimulated even further upon deletion of *ori1253* (7.8-fold for BS; 6.4-fold for TS) (**Fig. 3.8D**). Intriguingly, with *ori1253* present, BS nicks stimulated recombination 1.2-fold more than TS nicks ($p=0.041$) (**Fig. 3.8B**). A similar difference was observed when *ori1253* was deleted, but in this case the difference was not statistically significant ($p=0.155$) (**Fig. 3.8D**). These small differences could be due to plasmid copy number variations in different strains. In my experiments, *Pnmt81-NLS*-gpII was expressed from a multicopy pREP81 plasmid which may be retained in different copy numbers. Three different

transformants for each strain were tested during this experiment, in an attempt to account for plasmid copy number variations.

In a similar fashion to the Flp-nick system, with the gpII-nickase system, the majority of Ade$^+$ recombinants were deletions, which increased ~3.8- fold and ~2.7-fold upon BS and TS nick induction, respectively ($p<0.0001$) in a *ori1253*+ background (**Fig. 3.8C**). There was also a noticeable increase in gene conversions but only in the strain with a BS nick (~3.1-fold; $p<0.0001$) (**Fig. 3.8C**). In a *ori1253*Δ background, the majority of Ade$^+$ recombinants were again deletions, which increased ~5-fold and ~4-fold, when BS and TS nicks were generated, respectively (**Fig. 3.8E**). However, gene conversions also increased ~3-fold and ~2-fold upon BS and TS nick induction, respectively (**Fig. 3.8E**). Altogether these data provide further evidence that both leading and lagging-strand SSBs can give rise to BIR that is associated with template switching. They also suggest that fork convergence is a major limiting factor for BIR, as is the case in budding yeast.

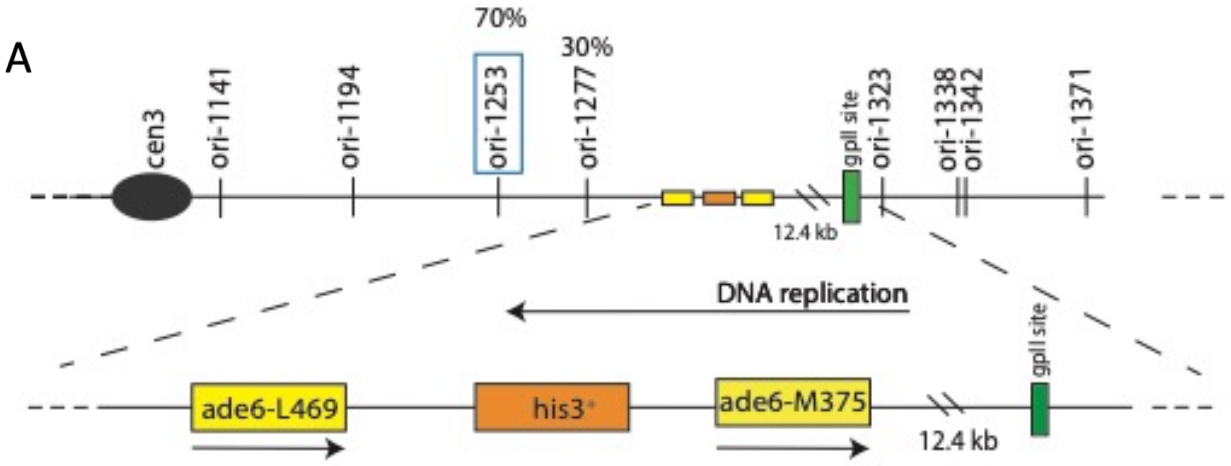

Wild Type

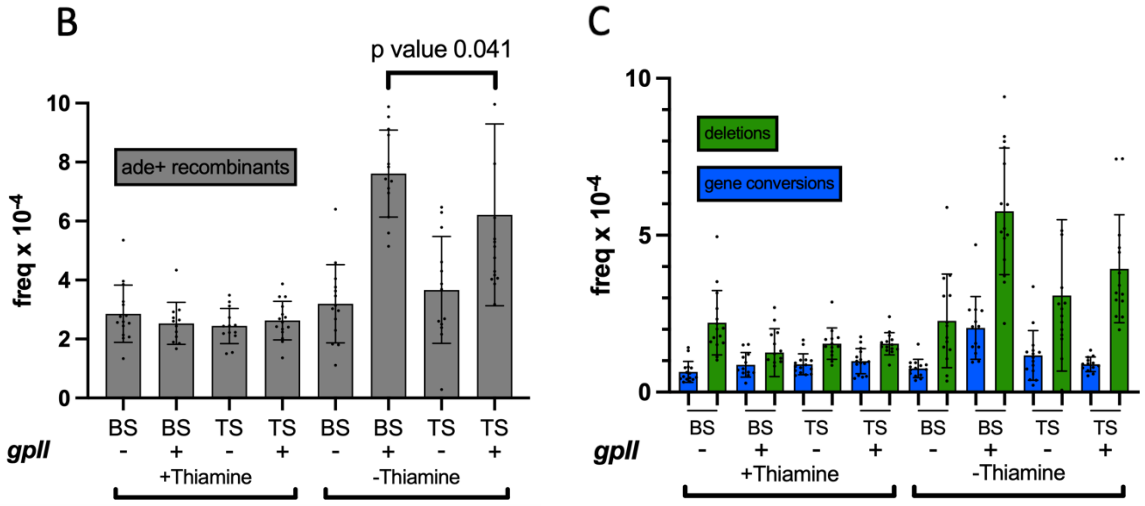

ori1253Δ

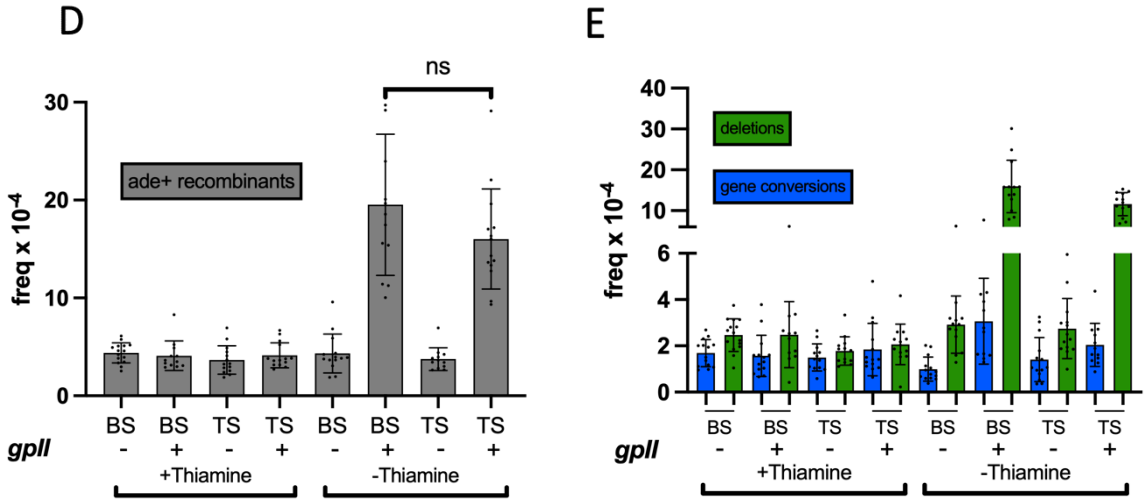

Figure 3.8 SSBs made by the M13 filamentous bacteriophage gene protein II (gpII) induce template switching at the 12.4 kb reporter. A) *Illustrates the experimental system used to investigate template switching associated with BIR. The gpII site is located 12.4 upstream of the direct repeat reporter. A blue rectangular box highlights the position of ori1253 which fires in the majority (70%) of cells in each cell cycle* (Jalan et al., 2019; Nguyen et al., 2015; Nieduszynski et al., 2007)*.* ***B)*** *Total Ade$^+$ recombinant frequency in strains with ori1253.* ***C)*** *Frequency of gene conversions and deletions in the same strains as in B.* ***D)*** *Total Ade$^+$ recombinant frequency in strains without ori1253.* ***E)*** *Frequency of gene conversions and deletions in the same strains as in D. TS indicates Top (leading) strand whilst BS indicates bottom (lagging) strand orientation. Strains with ori1253 are: MCW10151 transformed with pREP1; MCW10151 transformed with pMW2238; MCW10152 transformed with pREP1; and MCW10152 transformed with pMW2238. Strains with ori1253 deleted are: MCW10192 transformed with pREP1; MCW10192 transformed with pMW2238; MCW10194 transformed with pREP1; and MCW10194 transformed with pMW2238. Error bars represent +/- standard deviation.*

3.3 Discussion

3.3.1 The Flp-nick system stimulates direct repeat heteroallelic recombination in fission yeast.

To investigate SSB-induced recombination, the *FRT* site was placed in both BS and TS orientations between two *ade6* heteroalleles (*ade6-L469* and *ade6*-M375). Subsequently, Flp^{H305L} was expressed from a multicopy plasmid behind a strong inducible promoter (P*nmt1*) such that replication forks would encounter Flp^{H305L}-induced protein-bound SSBs predominantly in either BS or TS. A high frequency of direct repeat recombination was induced with both BS and TS SSBs confirming for the first time that the Flp-nick system works in fission yeast. To achieve a more consistent level of Flp^{H305L} between cells, I inserted *FLPH305L* at a single chromosomal site. Expression of Flp^{H305L} from P*nmt1* under these conditions yielded ~10-fold lower levels of direct repeat recombination than achieved with plasmid-expressed Flp^{H305L} (compare data in **Fig. 3.3, 3.4 and 3.5**). These data indicate that expression of Flp^{H305L} from a single chromosomal copy of the *FLPH305L* gene yields levels of protein that are insufficient to achieve a saturating level of cleavage of the *FRT* site. In other words, with this amount of Flp^{H305L}, only a subset of cells in each cell cycle are likely to experience a replication fork-Flp-nick collision. A potential factor affecting the amount of DNA cleavage is the absence of a nucleus localisation signal (*NLS*) on Flp^{H305L}, which could limit its nuclear concentration. Alternatively, Flp^{H305L} may simply have a low DNA nicking activity in fission yeast. Nevertheless, the convenience of using strains with stably integrated chromosomal copies of *FLPH305L*, and the fact that the level of Flp^{H305L} achieved was still sufficient to strongly induce recombination, lead me to use this construct in all my subsequent genetic experiments.

3.3.2 Establishing a system to monitor BIR-associated template switching downstream of protein-bound SSBs.

The induction of direct repeat recombination by Flp-nick SSBs is mostly likely due to replication fork collision with the SSB leading to fork stalling and/or breakage. Replication fork breakage at a Flp-nick SSB in budding yeast has been shown to induce BIR (Mayle et al 2015). A characteristic feature of BIR is a high rate of template switching during its “elongation phase” (Kramara et al., 2018; Mayle et al., 2015; Pham et al., 2021b). Having detected HR-mediated repair in the vicinity of the Flp-nick SSB, I investigated whether recombination is limited to this location or occurs also several kilobases downstream of the nick site, which would indicate template switching associated with BIR. To achieve this, I set up the 12.4 kb reporter system, in which the *ade6* heteroallele reporter is positioned 12.4kb downstream centromere proximal to the *FRT* site. The direct repeat heteroallele reporter in this location measures the template switching events characteristic of BIR, which are distinct from the ectopic recombination induced at the 0 kb reporter (where a SSB is induced within the reporter). With the 12.4 kb reporter, I detected a modest increase in Ade^+ recombinants when the *FRT* site was flanked on both sides by efficient replication origins. I hypothesised that in this experimental setting, converging replication forks may be limiting BIR-mediated mutagenic synthesis. In budding yeast, when SSBs were generated between two efficient origins of replication, mutagenic synthesis was limited to only a few kilobases downstream of the nick site and dropped to spontaneous levels after 15 kb (Mayle et al., 2015). If this phenomenon was conserved in both budding and fission yeast, which are significantly evolutionary distant, it would mean that it is likely conserved also in humans. Consistent with the hypothesis that fork convergence was limiting BIR and, therefore, the amount of template switching at the 12.4 kb

reporter, deletion of the strong replication origin *ori1253*, which is responsible for firing the majority (~70%) of converging replication forks in wild-type cells, resulted in a marked increase in Flp-nick induced recombination at the 12.4 kb reporter. Intriguingly, this increase in Ade$^+$ recombinants was higher (~1.8-fold) when SSBs were generated in the leading template strand (TS) compared to the lagging template strand (BS). The potential significance of this is discussed in Section 3.3.3. In contrast, with the gpII nickase system, I detected slightly more Ade$^+$ recombinants when the SSB was in the lagging template strand (BS) as opposed to the leading template strand (TS). However, this difference was only statistically significant in strains containing *ori1253*.

3.3.3 Lagging-strand nicks can induce BIR

Lagging-strand nicks were previously believed to be successfully skipped over by replication forks leaving behind deDSBs in their wake (Caldecott, 2008). SDSA, which involves only localised HR-mediated repair, is believed to be the most commonly utilised mechanism to repair deDSBs in eukaryotes (See section 1.3) (Pham et al., 2021a). If SDSA was the primary repair mechanism utilised to repair BS SSBs in my experiments, it is very unlikely I would detect template switching 12.4 kb downstream. My finding that both leading and lagging-strand SSBs give rise to similar increased levels of Ade$^+$ recombinants at the 12.4 kb reporter suggests that replication fork collision with both TS and BS nicks gives rise to seDSBs that are repaired by BIR. As mentioned above, with the Flp-nick system when *ori1253* was deleted, there was a marked increase in Ade$^+$ recombinants, especially following the induction of TS nicks, which stimulated more direct repeat recombination compared to BS nicks (**Fig. 3.7**). I confirmed this difference in multiple experiments and two independent sets of isolates (**Fig. 3.7**; **Fig 6.2**).

It has been shown that Flp-nicks are not delivered with absolute strand specificity (Mayle et al 2015) and, therefore, it is possible that the induction of template switching by BS Flp-nicks is in fact due to occasional nicking in the TS. This could explain why BS nicks induce lower levels of template switching. However, my finding that gpII-nicks in either DNA strand induce similar levels of template switching suggests that BIR can be initiated from replication fork encounters with both leading and lagging template strand SSBs. Therefore, I believe that the increase in template switching 12.4kb downstream of a BS Flp-nick, which is detected in both *ori1253*+ and *ori1253*Δ backgrounds, is due to fork encounter with a lagging template strand SSB rather than unwanted Flp^{H305L}-induced SSBs on the DNA strand complementary to the targeted one. Recent *in-vitro* findings in *Xenopus* cell extracts showed that both leading and lagging-strand nicks are converted into seDSBs. Whilst the replisome was shown to run off at leading-strand SSBs, upon encountering lagging-strand SSBs the replisome was shown to stall for some time before being dismantled via a ubiquitination/removal mechanism similar to canonical replication termination (See section 1.1.4) (Vrtis et al., 2021). Should this mechanism be conserved in fission yeast, it could explain the lower frequency of Ade^+ recombinants detected from BS Flp-nick SSBs. BS nicks could cause the replisome to transiently stall, hence increasing the likelihood for a converging replication fork to reach the SSB site. In such scenario, a proportion of seDSB would be converted into a deDSB (**See Fig. 11**) and repaired by error-free SDSA instead of BIR.

3.3.2 A comparison between *RTS1*-induced RDR and Flp/gpII-nick-induced BIR

As mentioned in section 1.2.3, *RTS1* is a polar RFB which blocks the incoming replication forks from one direction. From hereafter I will refer to the *RTS1* blocking orientation as the *RTS1* Active Orientation (*RTS1*-AO) and the non-blocking one as

the *RTS1* Inactive Orientation (*RTS1*-IO). *RTS1* was shown to stimulate direct repeat recombination between *ade6* heteroalleles in a nearly identical experimental setting as my 0 kb reporter system (Ahn et al., 2005). Whilst the spontaneous recombination levels are very similar regardless of whether *FRT* site or *RTS1* are present, Flp-nick SSBs induce several fold higher levels of Ade^+ recombinants than *RTS1*-AO when Flp^{H305L} is expressed from the multicopy pREP1 plasmid. The same is true for gpII-nick SSBs (Osman et al 2016). Given that *RTS1*-AO is a very strong RFB that blocks the incoming fork in almost every cell in each cell cycle, and that the vast majority of these cells exhibit recombination protein foci localizing to the barrier site (Nguyen et al 2015), the fact that Flp/gpII-nicks induce higher levels of recombination suggests that replication fork-SSB encounters are far more liable to drive ectopic recombination than fork collapse at the *RTS1* protein-DNA barrier. It is also intriguing to note that *RTS1*-induced direct repeat recombination is more prone to generate gene conversion recombinants (~55% gene conversions; ~45% deletions) (Ahn et al., 2005), whilst the Flp-nick and gpII-nick SSBs stimulate a higher frequency of deletions (~15% gene conversions; ~85% deletions). A key difference between fork collapse at *RTS1* and at a Flp/gpII-nick is likely the creation of a seDSB at the latter. Fork collapse at *RTS1* is thought to involve the reversal of the replication fork creating a chicken foot-like structure with an exposed DNA end at which recombination proteins load (Ahn et al., 2005). As *RTS1* is a polar RFB, fork convergence at this site can presumably occur with very little hindrance. However, fork convergence at the site of an already broken replication fork can generate a deDSB (**Fig. 3.7A**) (Li et al., 2021).This potential for a seDSB to become a deDSB likely accounts for the ability of Flp/gpII-nicks to induce higher levels of Ade^+ recombinants. Indeed, I suspect that the reason that deletion

recombinants are so prevalent with Flp/gpII-nicks is because the deDSBs are often repaired by SSA.

In a similar fashion to BIR, *RTS1*-AO induced RDR is highly mutagenic and prone to template switching (Nguyen et al., 2015; Jalan et al., 2019). In a system equivalent to my 12.4kb *ori1253*Δ, Nguyen et al., showed that *RTS1*-AO generates a frequency of Ade^+ recombinants of ~1170 x 10^{-4}, which is far higher than Flp^{H305L}-induced recombinants (~30 x 10^{-4}). From these data it would be unfair to assume that *RTS1*-AO induced RDR is far more prone to ectopic template switching compared to Flp^{H305L}-induced BIR. More precisely, in the 0kb setting there was a significant increase in Ade^+ recombinants when Flp^{H305L} was expressed from a multicopy plasmid, compared to expression driven from a chromosomal copy. This indicates that when expression is driven from a chromosomal copy, not every cell experiences a Flp^{H305L}-induced SSB. In contrast, *RTS1* is a strong barrier which blocks replication forks in all cell cycles (Nguyen et al., 2015), as opposed to Flp^{H305L} which may not nick the DNA in every cell cycle. A fair comparison between the two systems could be performed only if the Flp-nick system was to be optimised to induce a SSB in every cell. Otherwise, the high level of template switching detected with *RTS1* could be simply due to a faster restart than BIR, which in budding yeast was shown to be subject to initial delays (Lydeard et al., 2007)

Chapter 4

Investigating the genetic requirements of template switching associated with BIR

4.1 Introduction

As established in Chapter 3, the Flp-nick system stimulates BIR which is associated with high levels of template switching at least 12.4kb downstream of the SSB site. Most of our understanding of BIR comes from studies in budding yeast which identified several key proteins critical in this HR-dependent repair mechanism (Lydeard et al., 2007; Malkova et al., 1996). In this chapter, I use the 12.4 kb reporter system to investigate the genetic requirements for BIR and associated template switching in fission yeast focusing on several genes that have previously been shown to affect RDR in fission yeast or BIR in other organisms. My aim was to determine whether both Rad51-dependent and Rad51-independent pathways hold similar sway in promoting BIR in fission yeast as is the case for RDR (A. Kishkevich & M. C. Whitby, pers. Comm.). I also investigate whether Mus81 is important for BIR in fission yeast like it is in budding yeast (Mayle et al., 2015). In investigating Mus81, I was mindful that it is dispensable for *RTS1*-induced RDR and associated template switching (See section 1.5.7) (Jalan et al., 2019). Intriguingly, the Whitby lab has also recently detected increased template switching associated with RDR in a *ku70*Δ mutant (M. C. Whitby, pers. Comm.). I aimed to test the role of this factor in BIR, which is key in the repair of DSBs by Non Homologous End Joining (NHEJ) (Shibata et al., 2018). Lastly, I investigate whether compromising the ubiquitination-dependent removal of the replisome during replication termination also affects template switching downstream of the SSB site.

4.2 Results

4.2.1 Template switching associated with BIR is dependent on Rad51 and Rad52

In a similar fashion to BIR, which is dependent on Rad52 but can occur independently of Rad51 (Lydeard et al., 2007; Malkova et al., 1996), the Whitby lab previously showed that Rad52-dependent replication restart past *RTS1* is only partially reliant on Rad51 (A. Kishkevich & M. C. Whitby, pers. Comm.). To establish whether in my system of study BIR is dependent on Rad52 and/or Rad51, I constructed strains carrying the 12.4 kb reporter and lacking *ori1253*, *rad51* and/or *rad52*. Prior to measuring the direct repeat recombination frequency in both *rad51*Δ and *rad51*Δ *rad52*Δ mutants, strains were tested for genotoxin sensitivity to ensure they displayed the appropriate phenotypes (**Fig. 6.3**). Consistent with the hyper-recombination phenotype of a *rad51*Δ mutant (Ahn et al., 2005; Doe and Whitby, 2004), the spontaneous Ade$^+$ recombination frequency in strains lacking Flp^{H305L} was ~2.6-fold higher when *rad51* was deleted compared to the equivalent WT strain (**Fig 4.1A**). Upon Flp^{H305L} expression, deletion of *rad51* reduced the Ade$^+$ recombinant frequency to spontaneous levels (~14 x 10^{-4}) regardless of the DNA strand on which SSBs were induced (**Fig 4.1A**). As expected, virtually all gene conversion events were abolished in a *rad51*Δ mutant (**Fig 4.1B**), and when both *rad51* and *rad52* were deleted, very few Ade$^+$ recombinants were observed (**Fig 4.1A,B**).

Rad51 and Rad52 were previously shown to be essential for cell viability following replication fork-*RTS1* encounters (Lambert et al., 2005), and were also found to be important for the repair of Flp-nick SSBs in budding yeast (Mayle et al, 2015). However, evidence from the Whitby lab suggests that deletion of *rad51* and *rad52* in strains carrying *RTS1*-AO does not affect cell viability (Nguyen et al., 2015). In my

experiments, induction of a Flp-nick SSB in a *rad51*Δ or *rad51*Δ *rad52*Δ background did not cause any detectable reduction in growth or cell viability (**Fig. 6.3**). Although, as expected, the *rad51*Δ *rad52*Δ mutant strains did exhibit an overall reduction in growth (**Fig. 6.3B**). Altogether these results show that most, if not all, template switching detected in my experiments is dependent on Rad51 and Rad52. Furthermore, they show that Rad51 and Rad52 are not essential for the viability of cells experiencing a site-specific SSB.

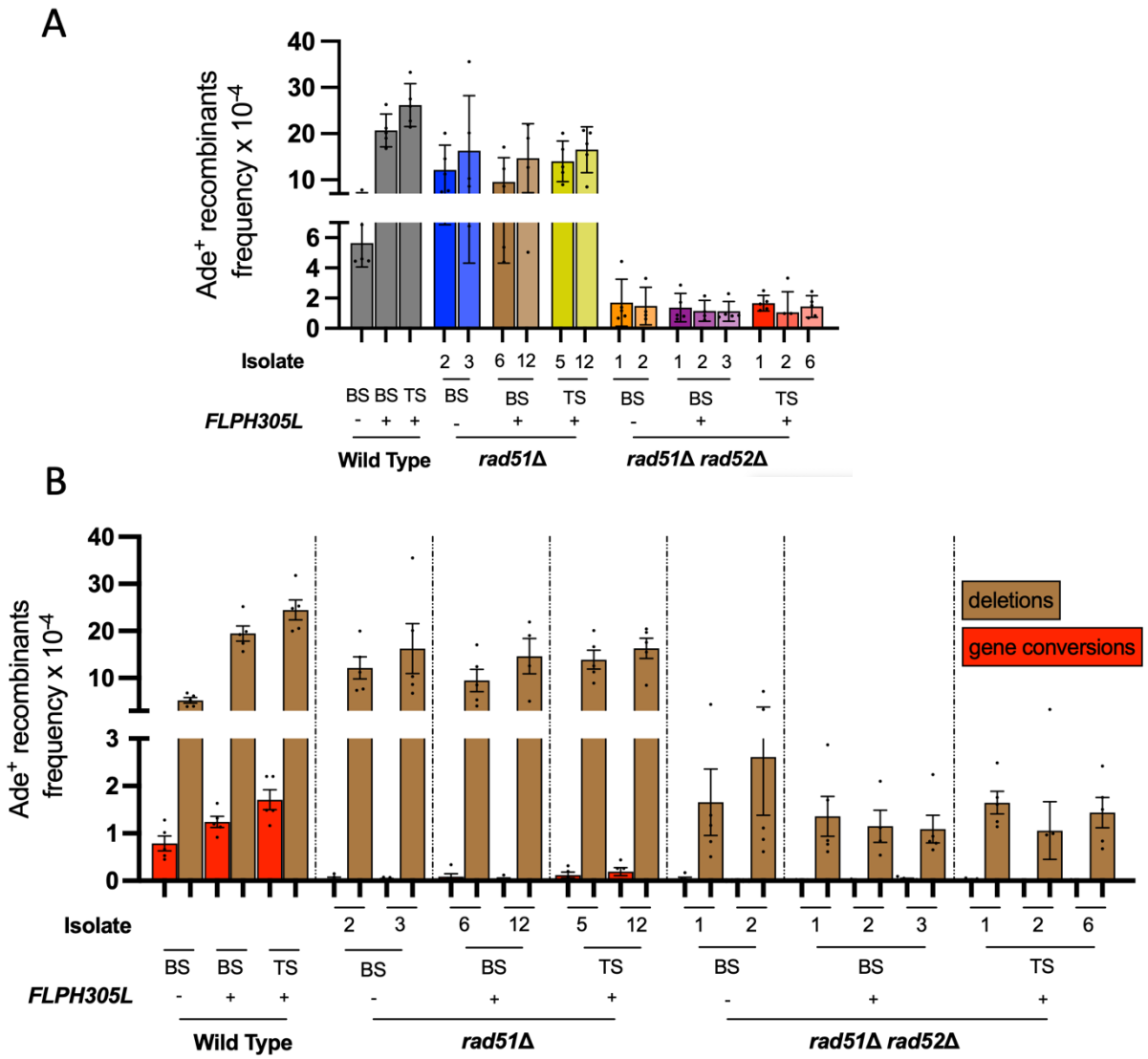

Figure 4.1 BIR-mediated template switching is dependent on Rad51 and Rad52 12.4 kb downstream of the break site. A) *Total frequency of Ade⁺ recombinants.* ***B)*** *Frequency of gene conversions and deletions. All strains carry the 12.4 kb reporter and lack ori1253. TS indicates that the FRT site is orientated so that the majority of SSBs are in the top strand (i.e. leading template strand), whilst BS indicates that FRT is in the opposite orientation such that the majority of SSBs are in the bottom strand (i.e. lagging template strand). Strains are MCW10205, MCW10138, MCW10139, MCW10430, MCW10431, MCW10432, MCW10433, MCW10434, MCW10435, MCW10436, MCW10437, MCW10438, MCW10439, MCW10440, MCW10441, MCW10442 and MCW10443. Error bars represent +/- standard deviation.*

4.2.2 Template switching associated with the repair of leading-strand nicks relies to some extent on the strand annealing activity of Rad52

The Rad51-independent BIR pathway appears to be a minor pathway in budding yeast and has not been investigated in depth (Kramara et al., 2018). This is not the case in human cells, where studies on MiDAS, required to duplicate difficult to replicate DNA regions, suggest that it may proceed via a Rad51-independent BIR pathway (Minocherhomji et al., 2015). Cancer cell lines are also heavily reliant on Rad51-independent BIR due to oncogene overexpression mediated replication stress (Sotiriou et al., 2016). Therefore, it seems that the relative importance of the Rad51-dependent and Rad51-independent pathways varies depending on the organism and/or nature of the DNA lesion.

The data in Section 4.2.1 show that Rad51 is required for BIR-associated template switching in fission yeast. However, as the difference between Flp-nick-induced levels of template switching and *rad51*Δ spontaneous levels is small, it was unclear from my data whether the Rad51-independent pathway contributes to BIR-associated template switching in fission yeast. To investigate this, I determined whether the strand annealing activity of Rad52 was required for Flp-nick-induced template switching. To this end, I introduced the *rad52-R45A* mutant into the 12.4 kb reporter strain background. The *R45A* mutation abolishes Rad52's strand annealing activity without affecting its Rad51 loading role (Pham et al., 2021). The strains were tested for their genotoxin sensitivities (**Fig. 6.5**), and then assayed for recombination (**Fig 4.2A,B**). In a *rad52-R45A* mutant, there was no statistically significant difference in the spontaneous recombination frequency compared to WT (p=0.214) (**Fig 4.2A,B**). Upon Flp^{H305L} expression, the total frequency of Ade^{+} recombinants was also unchanged (p=0.494) when nicks were generated in the BS (**Fig. 4.2A**). However, the

frequency of template switch recombination, induced by nicking in the leading-strand, decreased ~2-fold (p=0.0017) (**Fig. 4.2A**). Intriguingly, although the total frequency of BS nick-induced Ade$^+$ recombinants did not change in a *rad52-R45A*, the ratio between gene conversions and deletions did (**Fig. 4.2B**). Specifically, gene conversions increased from ~10% to ~41% of the total Ade$^+$ recombinants (p=0.0043). A similar change was also seen for TS nick-induced recombination, which shifted from ~8% gene conversions to ~39% (p=0.0062) (**Fig. 4.2B**). These shifts stem from both a reduction in the frequency of deletions and increase in the frequency of gene conversions, which could be due to template switching being driven by Rad51 in the absence of Rad52's strand annealing activity. Altogether, these data indicate that BIR-associated template switching is partially dependent on the strand annealing activity of Rad52.

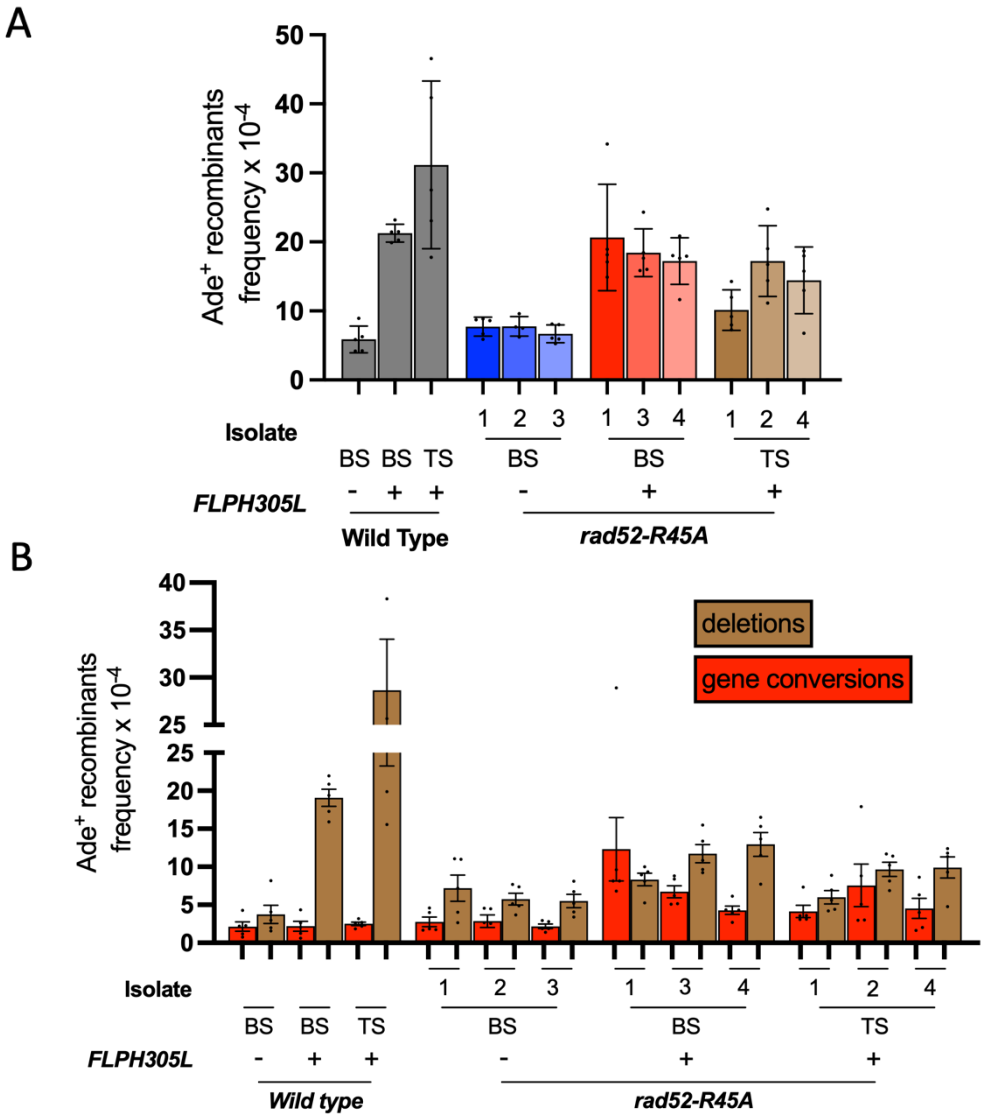

Figure 4.2. The strand annealing activity of Rad52 is responsible for some of the Flp-nick-induced template switch recombination at the 12.4 kb reporter. A) *Total frequency of Ade+ recombinants in strains with ori1253 deleted.* ***B)*** *Frequency of gene conversions and deletions in the same strains as in A. All strains carry the 12.4 kb reporter and lack ori1253. TS indicates that the FRT site is in the orientation where the majority of Flp-nick SSBs are in the top strand (i.e. leading template strand), whilst BS indicates that FRT is in the opposite orientation where the majority of SSBs are in the bottom strand (i.e. lagging template strand). Strains are MCW10453, MCW10454, MCW10455, MCW10456, MCW10457, MCW10458, MCW10459, MCW10460, MCW10461. Error bars represent +/- standard deviation.*

4.2.3 The structure selective endonuclease Mus81 does not affect BIR-associated template switching in fission yeast

Mus81 is part of the XPF/ERCC4 group of structure specific endonucleases which works together with Mms4/Eme1 complex to resolve meiotic and mitotic homologous recombination intermediates such as Holliday junctions and D-loops (Boddy et al., 2001; Osman and Whitby, 2007). Mus81 also plays key roles in processing perturbated, stalled or collapsed replication forks (Doe et al., 2002; Froget et al., 2008; Hanada et al., 2007). As previously mentioned, Mayle et al. (2015) showed that Mus81 limits BIR-mediated mutagenic synthesis, yet previous work in fission yeast showed that *RTS1*-induced template switching does not rely on Mus81 (Jalan et al., 2019). To determine whether Mus81 affects BIR in fission yeast, I constructed strains carrying the 12.4kb reporter in a *ori1253*Δ *mus81*Δ background. After confirming that these strains had the expected sensitivity to genotoxins (**Fig. 6.4**), I measured the frequency of spontaneous and Flp-nick-induced recombination at the 12.4 kb site (**Fig 4.3A**). There was no statistically significant effect on the spontaneous recombination level when *mus81* was deleted (**Fig 4.3A**). There was also hardly any change in the frequency of BS or TS nick-induced Ade^+ recombinants (**Fig. 4.3A**). Regarding the ratio between gene conversion and deletions, this was also unaffected by deletion of *mus81* (**Fig. 4.3B**). In summary, these findings suggest that, unlike in budding yeast, Mus81 plays no role in BIR in fission yeast.

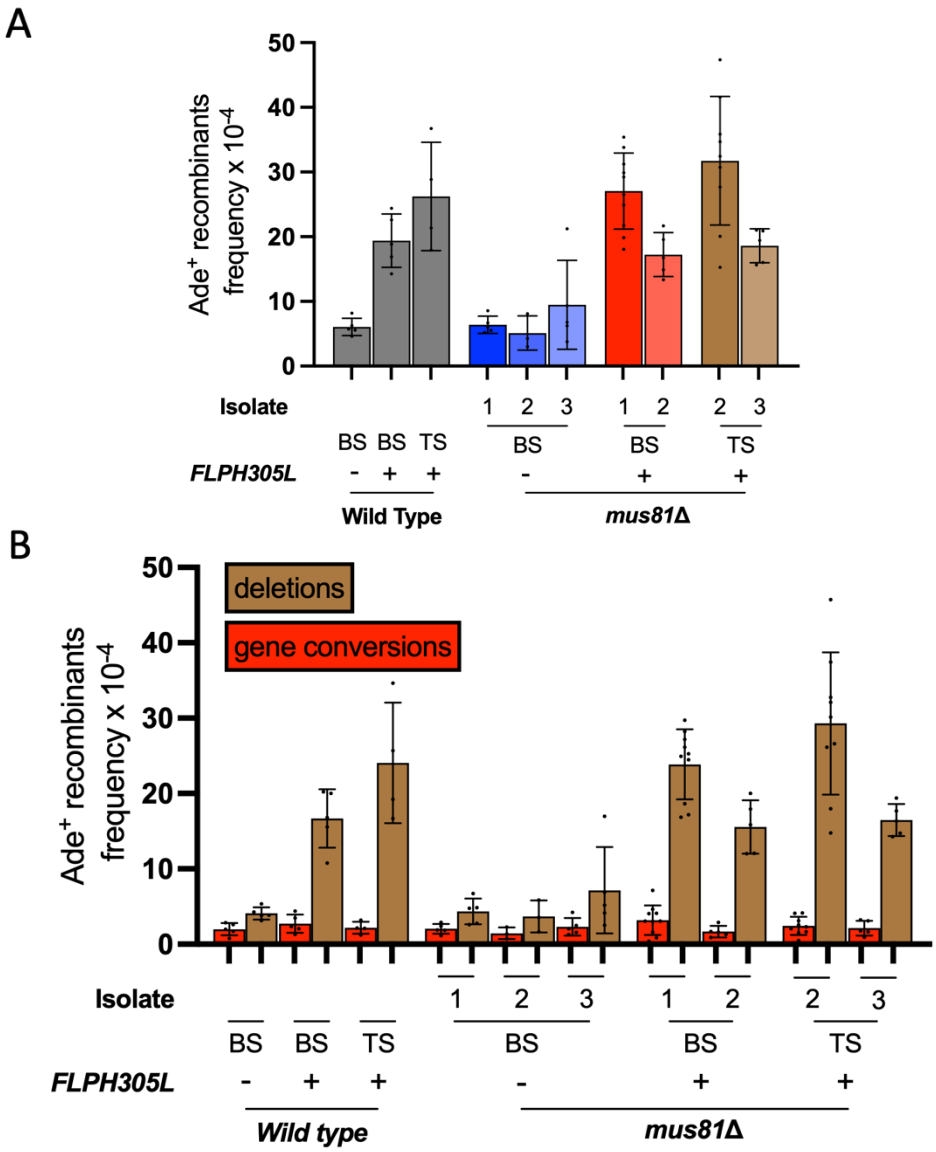

Figure 4.3. Mus81 is not required for template switching associated with BIR. A) *Total frequency of Ade+ recombinants in strains with ori1253 deleted.* ***B)*** *Frequency of gene conversions and deletions in the same strains as in A. All strains carry the 12.4 kb reporter and lack ori1253. TS indicates that the FRT site is in the orientation where the majority of Flp-nick SSBs are in the top strand (i.e. leading template strand), whilst BS indicates that FRT is in the opposite orientation where the majority of SSBs are in the bottom strand (i.e. lagging template strand). Strains are MCW10205, MCW10138, MCW10139, MCW10162, MCW10163, MCW10164, MCW10165, MCW10166, MCW10167, MCW10168. Error bars represent +/- standard deviation.*

4.2.4 Ku70 limits template switching associated with BIR

Ku70 is a subunit of the heterodimeric Ku70/Ku80 complex which binds to DSBs and promotes NHEJ (Shibata et al., 2018). Ku70 has mostly been studied in the context of DSB repair, however there is evidence that it can associate with stalled, collapsed and/or broken replication forks and influence their processing (Teixeira-Silva et al., 2017; Willis et al., 2018; Shao et al., 2012). To investigate whether Ku70 is involved in BIR mediated repair of Flp^{H305L}-induced SSBs, I deleted *pku70* in the *ori1253*Δ background and measured direct repeat recombination utilising the 12.4kb reporter (Fig. 4.4). If anything, there was a slight (~1.7-fold) ($p=0.0246$) increase in spontaneous recombination in the absence of *pku70* (**Fig. 4.4A**), whilst there was a ~3.36-fold ($p<0.0001$) and ~3-fold ($p<0.0001$) increase in direct repeat recombination when nicks where generated predominantly in the BS and TS, respectively (**Fig 4.4A**). The ratio between spontaneous gene conversions and deletions showed little or no variation when Ku70 was absent (**Fig 4.4B**). Upon Flp^{H305L} expression in a *pku70*Δ background, gene conversion increased ~4-fold ($p<0.0001$) when nicks were generated predominantly in the BS, and similarly, ~3.8-fold ($p<0.0001$) when nicks were generated predominantly in the TS. Deletions also increased by similar fold amounts as gene conversions. Expression of Flp^{H305L} stimulated a ~3.3-fold ($p<0.0001$) and a 3.3-fold ($p<0.0001$) increase in deletions when nicks were generated predominantly in the BS and TS, respectively. Altogether these data suggest that Ku70 acts either directly or indirectly to limit BIR-associated template switching induced by leading and lagging-strand SSBs.

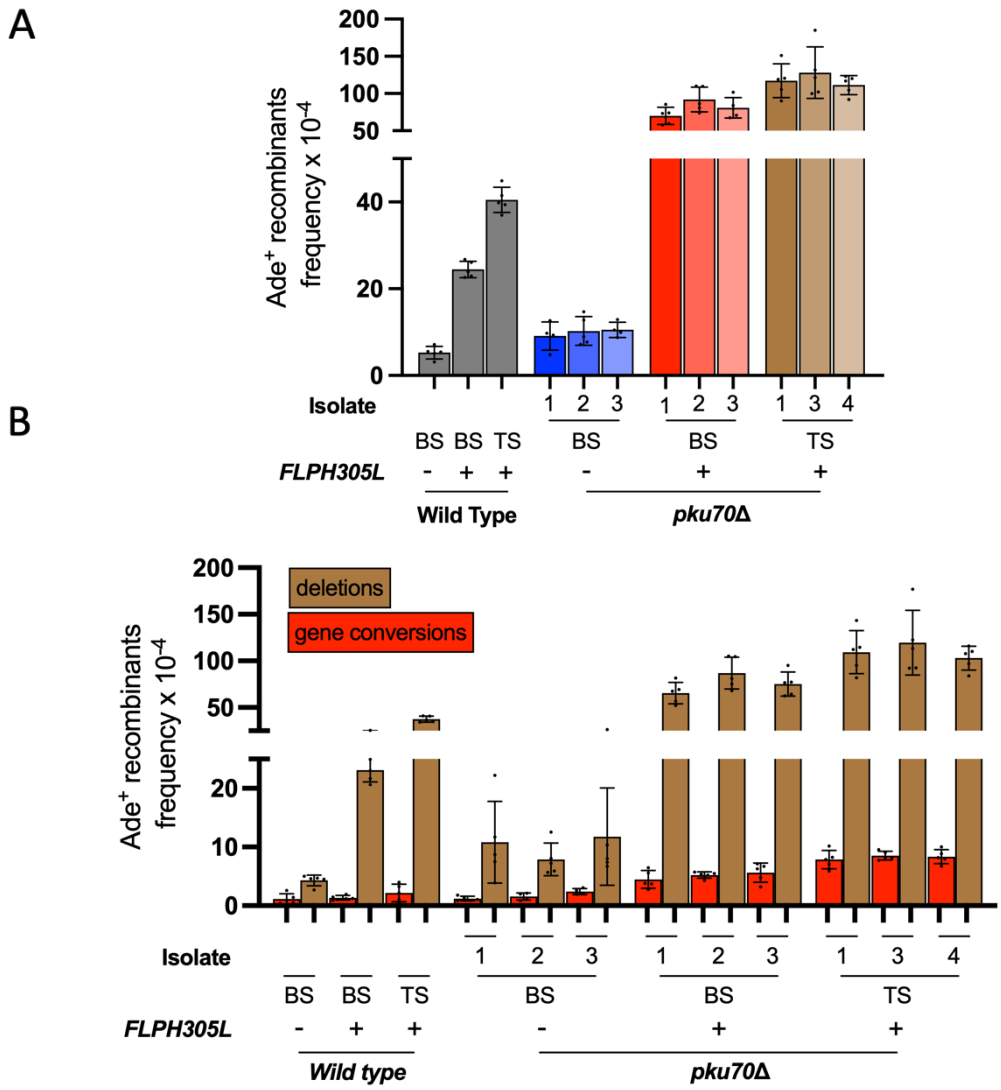

Figure 4.4. Ku70 limits BIR-associated template switch recombination induced by Flp-nick SSBs. A) *Total frequency of Ade+ recombinants in strains with ori1253 deleted.* ***B)*** *Frequency of gene conversions and deletions in the same strains as in A. TS indicates that the FRT site is in the orientation where the majority of Flp-nick SSBs are in the top strand (i.e. leading template strand), whilst BS indicates that FRT is in the opposite orientation where the majority of SSBs are in the bottom strand (i.e. lagging template strand). All strains carry the 12.4 kb reporter and lack ori1253. Strains are MCW10205, MCW10138, MCW10139, MCW10144, MCW10145,* MCW10146, MCW10147, MCW10148, MCW10149, MCW10150, MCW10151, MCW10152. *Error bars represent +/- standard deviation.*

4.2.5 *pof3* deletion compromises BIR-associated template switch recombination.

Pof3 is part of the E3 ubiquitin ligase Skp1-Cullin-1-F-box (SCF) complex (Katayama et al., 2002). The equivalent protein in *Xenopus* egg extracts, $CRL2^{Lrr1}$, was shown to play a role in the disassembly of the CMG replicative helicase upon encountering lagging-strand SSBs. Vrtis et al. showed that the replisome transiently stalls at the lagging-strand SSB site before the CMG helicase is ubiquitinated by $CRL2^{LRR1}$ and disassembled, likely by the p97 segregase/unfoldase. In contrast, upon encountering leading-strand SSBs, the replisome runs off the DNA seemingly without the need for a ubiquitin-mediated disassembly process (Vrtis et al., 2021). I sought to investigate whether inhibiting the ubiquitination-dependent replisome removal process affected the template switching detected 12.4kb downstream of Flp^{H305L}-induced SSBs. Therefore, I constructed strains carrying the 12.4 kb reporter in a *ori1253*Δ *pof3*Δ background. Consistent with the spontaneous hyperrecombination phenotype of *pof3*Δ mutants (M. C. Whitby, pers. Comm.), in my *pof3*Δ strains I detected a ~1.8-fold increase in spontaneous recombination, which stem mainly from an increase in deletion events (**Fig. 4.5A,B**). Upon Flp^{H305L} expression, the template switching detected when nicks were generated in the BS dropped to spontaneous levels (~1.7-fold decrease) (**Fig. 4.5A**) (p=0.0015), whereas when SSBs were induced predominantly in the leading-strand there was a minor ~1.25-fold decrease (p=0.0328) in direct repeat recombination detected using the 12.4 kb reporter. The induced level of direct repeat recombination showed no bias towards either gene conversions or deletion events (**Fig. 4.5B**). In summary, these results suggest that Pof3 deletion slightly inhibits the template switching associated with BIR-mediated repair of TS nicks, but to a higher extent the repair of BS nicks via BIR.

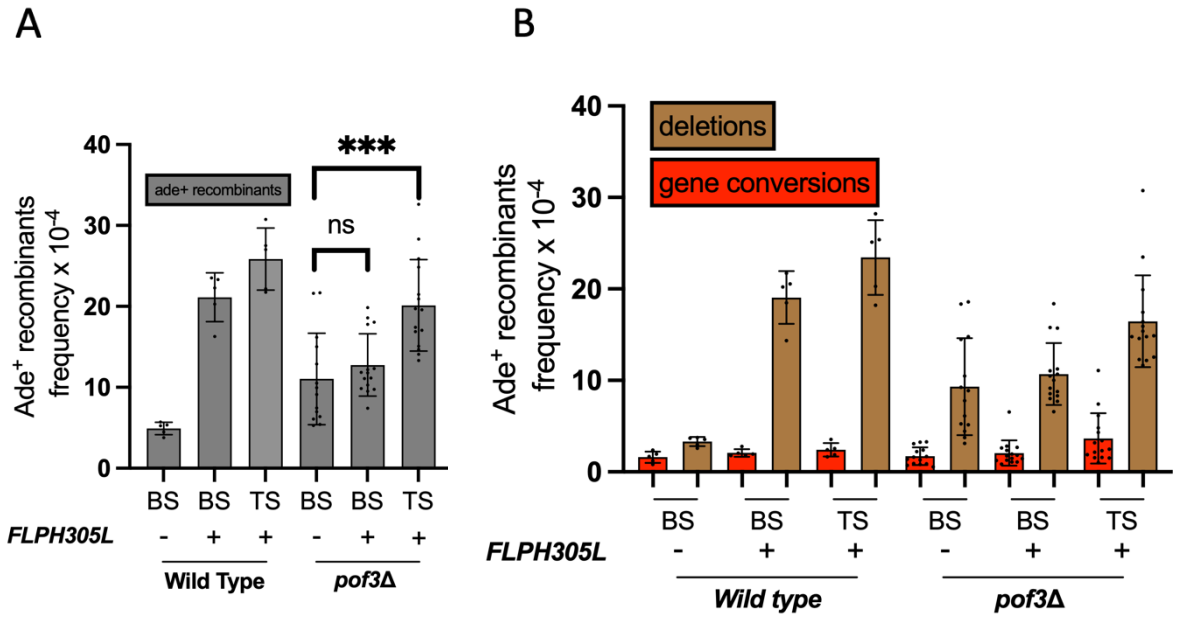

Figure 4.5. Pof3 stimulates direct repeat recombination downstream Flp^{H305L}-induced SSBs. A) *Total frequency of Ade+ recombinants in strains with ori1253 deleted.* ***B)*** *Frequency of gene conversions and deletions in the same strains as in A. TS indicates Top (leading) strand whilst BS indicates bottom (lagging) strand orientation. All strains carry 12kb reporters and lack ori1253. Strains are MCW10205, MCW10138, MCW10139, MCW10169, MCW10170, MCW10172. Error bars represent +/- standard deviation. P<0.001 (***).*

4.3 Discussion

4.3.1 The Rad51-dependent pathway drives BIR-associated template switching in fission yeast

The Whitby lab recently showed that *RTS1*-induced RDR proceeds via both Rad51-dependent and Rad51-independent pathways in fission yeast. However, in contrast to BIR in budding yeast, where the Rad51-independent pathway is thought to be inefficient and rarely used (Lydeard et al., 2007; Malkova et al., 1996), the Whitby lab finds that the RDR-associated template switching events (12.4 kb downstream *RTS1*) rely heavily on the strand annealing activity of Rad52 and much less on Rad51 (A. Kishkevich & M. C. Whitby, pers. Comm.). I performed a similar analysis and, to my surprise, found that BIR-associated template switching in fission yeast, as opposed to the template switch recombination induced by *RTS1*, relies mainly on Rad51 (**Fig. 4.2**). Work in budding yeast from the Haber lab hinted that the strand invasion step to initiate Rad51-dependent BIR is mechanistically different from the template switching downstream, which was relatively less dependent on Rad51 and sequence homology length, and had an increased dependence on Rdh54 (Anand et al., 2014). As Rdh54 is known to be important for Rad51-independent BIR, their data suggests that the initiation and elongation phases of BIR are mechanistically distinct – initiation is driven by the Rad51-dependent pathway, whereas template switching during the elongation phase exhibits a greater dependence on the Rad51-independent pathway. In other words, BIR could potentially mature into a less Rad51-dependent form as the D-loop travels further from the break site.

Owing to the role of Rdh54 in Rad51-independent BIR (See section1.5.4) (Signon et al., 2001), and to the recent finding that the strand annealing activity of Rad52 is required for template switching downstream of *RTS1* (A. Kishkevich & M. C.

Whitby, pers. Comm.), I decided to investigate the role of Rad52's strand annealing activity in BIR in fission yeast. For this purpose, I tested *Rad52-R45A*, a mutated version of Rad52 that is incapable of performing strand annealing, to see if it affected BIR-associated template switching. Intriguingly, leading template strand (TS) nick-induced template switch recombination decreased approximately 2-fold, whereas the total frequency of Ade^+ recombinants induced by a lagging template strand (BS) nick remained unaltered (**Fig. 4.2A**). This result suggests that BIR-associated template switching relies at least in part on the strand annealing activity of Rad52. It is unclear however, why Rad52's strand annealing activity had no effect on the total frequency of Ade^+ recombinants when BIR is induced from a lagging template strand SSB (**Fig. 4.2A**). However, although the total frequency of recombinants did not change the relative proportion of deletions and gene conversions did. Since *Rad52-R45A* is still capable of performing Rad51-loading, this could potentially be due to increased Rad51 mediated template switching when Rad52's strand annealing activity is compromised. Gene conversion events are dependent on Rad51, as evidenced by the striking reduction in gene conversion types in a *rad51*Δ mutant (**Fig. 4.1A**). This effect of *rad52-R45A* is not seen in *RTS1*-induced template switching with an equivalent experimental system (A. Kishkevich & M. C. Whitby, pers. Comm.). In *RTS1*-induced template switching, both gene conversions and deletions decrease in a *rad52-R45A* mutant (A. Kishkevich & M. C. Whitby, pers. Comm.). Although RDR and BIR are related processes, it is no surprise to detect striking differences between them. RDR is associated with an unbroken and reversed replication fork (Nguyen et al., 2015) whilst BIR is initiated from a collapsed broken replication fork. Whilst it is known that BIR proceeds via a migrating D-loop (Davis and Symington, 2004), there is currently no evidence indicating that the same is true for RDR. Even the mode of DNA synthesis is

strikingly different. It is well established that whilst DNA synthesis is conservative in BIR (Donnianni and Symington, 2013; Sakofsky et al., 2012), in RDR it is semiconservative (Miyabe et al., 2015).

4.3.2 Mus81 is dispensable for the maturation of D-loops in BIR

Mus81 is an important Holliday junction resolvase (Boddy et al., 2001) which is known to process perturbated replication forks (Doe et al., 2002). As previously mentioned Mus81 was shown to limit mutagenic repair associated with fork breakage at SSBs, which was particularly evident when converging replication forks were lacking (Mayle et al., 2015). I therefore decided to investigate whether this phenomenon was conserved in fission yeast. Considering that BIR is an evolutionary conserved mechanism to repair seDSBs, I expected the role of Mus81 to be conserved across the two different eukaryotic organisms and, therefore, to detect significantly higher levels of template switching upon *mus81* deletion. Surprisingly, I detected no change in Flp-nick induced template switching in a *mus81*Δ mutant (**Fig. 4.3A**). Even the ratio between gene conversion and deletion was unchanged (**Fig. 4.3B**). I suspect such striking difference to be due to the existence of other mechanisms responsible for the maturation of the D-loop which are either I) utilised by the cell more often than Mus81-mediated cleavage, or II) implemented as backup pathways when Mus81 is lacking. Indeed, in budding yeast, mutagenic synthesis is far greater in a *mus81*Δ *yen1*Δ double mutant than in a *mus81*Δ single mutant; with a y*en1*Δ single mutant exhibiting wild-type levels of template switching (Mayle et al., 2015). Therefore, Yen1 likely acts as a backup pathway to Mus81-mediated cleavage of the D-loop. Fission yeast lacks a Yen1 orthologue. Nevertheless, in this study, I cannot exclude that a backup pathway exists to compensate for the absence of Mus81 in fission yeast. Alternatively, different

pathways responsible for maturing the D-loop into a more robust, less mutagenic structure might have evolved in fission yeast.

4.3.3 Ku70 may limit template switching

Ku70 has mostly been studied in the context of DSB repair by NHEJ and, whilst there have been several published studies that have investigated whether it plays a role in the processing of perturbed replication forks (Teixeira-Silva et al., 2017; Willis et al., 2018; Shao et al., 2012), our understanding of its involvement in this area of biology remains limited. Ku70-mediated binding to DSBs is not sequence specific and it specifically counteracts end resection, the mechanistic step which irreversibly channels DNA repair into HR (Shibata et al., 2018; Davis and Chen, 2013). Removal of the Ku70-Ku80 heterodimer from the DNA ends exposed at a DSB involves nucleolytic processing by the Mre11-Rad50-Nbs1/Xrs2 (MRN) complex in conjunction with Ctp1/CtIP/Sae2 (Foster et al., 2011). Removal of Ku frees up the DNA end for long-range resection by Exo1 and/or Dna2 acting in conjunction with a RecQ-type DNA helicase (Gobbini et al., 2018). A similar two-step end resection process also appears to be required for efficient replication restart at the *RTS1* barrier (Teixeira-Silva et al., 2017a). This prompted Teixeira-Silva et al., to propose that Ku binds to the dsDNA end at a reversed replication fork. However, whilst the presence of Ku was shown to impede replication restart in the absence of MRN-Ctp1, its absence also caused a reduction in restart efficiency seemingly because of more extensive DNA resection and slower recruitment of RPA and Rad51 (Teixeira-Silva et al., 2017). Conversely, the Whitby lab has observed enhanced recruitment of Rad52 foci at the *RTS1* barrier in a *pku70*Δ mutant, as well as increased direct repeat recombination at the barrier and at the 12.4 kb reporter (M. C. Whitby, pers. Comm.). I therefore decided to investigate the role of Ku70 in BIR in fission yeast. Since the literature suggests that Ku70 opposes end

resection (Davis and Chen, 2013; Shibata et al., 2018), I predicted that absence of Ku70 would favour BIR and increase the levels of ectopic template switching detected at the 12.4kb reporter. In line with my expectations, deletion of Ku70 in the *ori1253*Δ background resulted in a significant increase in template switching regardless of the DNA strand targeted by Flp^{H305L} (**Fig. 4.4A**). Presumably, in WT strains Ku70 binds to the seDSBs generated by the replication fork-SSB encounters, hence opposing end resection. Absence of Ku70 presumably enables faster end resection and initiation of BIR leading to a higher proportion of D-loops reaching the 12.4 kb reporter before merging with an opposing replication fork. No change in the ratio of gene conversions and deletions was detected (**Fig. 4.4B**), suggesting that the relative use of Rad51-dependent and Rad51-independent pathways in template switching is not affected by the absence of Ku70. In the future, it would be interesting to investigate whether deletion of proteins involved in end resection in a *pku70*Δ background would restore the low template switching levels detected in WT conditions. It would also be important to establish by fluorescence live cell imaging whether Rad52 recruitment to the break site is faster upon Ku70 deletion. If so, it would mean that a higher proportion of D-loops are initiated sooner and as a consequence, duplicate 12.4kb reporters earlier and before merging with an opposing fork.

4.3.4 Pof3 promotes template switching associated with the BIR-mediated repair of lagging-strand nicks

In *Xenopus* cell extracts both leading and lagging-strand SSBs are converted into seDSBs by the incoming replication fork. However, these findings are based on an *in vitro* system of study (Vrtis et al., 2021) and, whilst leading-strand nicks were shown to be converted into seDSBs *in vivo* (Mayle et al., 2015), the same has not been demonstrated in the context of lagging-strand SSBs and; therefore, it remains unclear

whether lagging-strand SSBs are repaired via BIR. Vrtis et al., reports that lagging-strand nicks, as opposed to leading-strand SSBs, cause the replisome to be disassembled via a ubiquitination-mediated removal mechanism, which importantly is slower than replisome runoff (at leading-strand SSBs) (Vrtis et al., 2021). Owing to these findings *in vitro*, I hypothesised that on the lagging-strand replisome stalling increases the likelihood of a converging fork reaching the SSB site and suppressing BIR (See section 3.3.3). This hypothesis assumes that the CMG helicase ubiquitination/removal mechanism is conserved in fission yeast. Whether this mechanism holds true in fission yeast could be tested by purifying Pof3 and its binding partners via co-immunoprecipitation. Should the CMG helicase be interacting with Pof3, candidate lysine residues onto the Mcm7 subunit (where ubiquitin molecules are attached by E3 ligases) could be mutated. If Pof3 indeed ubiquitinates the Mcm7 subunit, precluding this process would cause the replisome to stall at lagging-strand SSBs. Therefore, with 12.4 kb reporters in an *ori1253*Δ background, similar results to the ones obtained upon Flp^{H305L} expression and Pof3 depletion would be generated (**Fig. 4.5A,B**). This hypothesis could explain why with the Flp-nick system I consistently detected slightly more template switching when nicks were generated predominantly in the leading-strand compared to when SSBs were mainly induced in the bottom strand (**Fig. 3.7B**). In WT cells, I suspect Pof3 to be promoting replisome disassembly, hence improving the kinetics of BIR-mediated restart. Consequently, restarted replication forks could replicate the 12.4 kb reporter more often, before merging with an opposing fork. However, it is important also to note that with the gpII nickase system, there was little or no difference between the template switching detected when nicks were generated in either DNA strand (**Fig. 3.8B,D**). As previously mentioned, in this experiment the gpII nickase was expressed from the multicopy pREP81 plasmid,

which may be retained in different copy numbers in different cells (Karim et al., 2013). It is not feasible to determine exactly how many copies of each plasmid are retained in each strain. In my experiments, expression of Flp^{H305L} in a *ori1253*Δ *pof3*Δ background abolished all template switching recombination events detectable with the 12.4 kb reporter when nicks were generated predominantly in the lagging-strand (**Fig. 4.5A**). A minimal reduction in template switching was also detected when nicks were generated mainly in the leading-strand (**Fig. 4.5A**). This suggests that Pof3 is required for all recombination events following replication fork-BS SSB encounters. The small effect of *Pof3* deletion in strains carrying *FRT TS* is potentially due to the Flp^{H305L} mode of cleavage not targeting a specific strand only (**Fig. 3.2**). Altogether, my results clearly indicate that *Pof3* promotes recombination to repair BS nicks in the context of a replication fork, whilst this is not the case in a TS nick scenario. However, my experiments are not sufficient to demonstrate whether such effect is due to Pof3 not ubiquitinating the CMG helicase, or due to other regulatory mechanisms of Pof3 which have not been discovered yet.

Chapter 5

Concluding remarks

5.1 The Key findings of this study

It has been well established that cells implement sophisticated recombination mechanisms to overcome DNA barriers/lesions and restart replication forks (Carr and Lambert, 2013; Kramara et al., 2018). To investigate these repair mechanisms, a number of research groups utilised site-specific RFBs such as *RTS1* (Ahn et al., 2005; Lambert et al., 2005; Lorenz et al., 2009; Nguyen et al., 2015) or site-specific nucleases to induce DNA breaks (Kramara et al., 2018; Liu et al., 2021; Mayle et al., 2015; Nielsen et al., 2012). It has been demonstrated that BIR is initiated at seDSBs and proceeds via a migrating D-loop, which is significantly unstable and prone to template switching (Kramara et al., 2018; Liu et al., 2021; Sakofsky et al., 2012). In Chapter 3, I established the Flp-nick system to study BIR in fission yeast and detected template switching, which is a well-conserved characteristic of BIR, 12.4kb downstream of the break site. By utilising the Flp-nick and the gpII nickase systems, I demonstrated that both leading and lagging-strands generate high levels of template switching which are associated with BIR. I also showed that converging replication forks limit BIR-mediated mutagenic synthesis in fission yeast, as they do in budding yeast (Mayle et al., 2015).

In Chapter 4, I proceeded to investigate the key genetic requirements of BIR in fission yeast and compared them to RDR in fission yeast and BIR in other organisms. As expected, all template switching detected was dependent on Rad52 and required Rad51. In a similar fashion to RDR (A. Kishkevich & M. C. Whitby, pers. Comm.), I also showed that template switching associated with BIR relies to some extent on the strand annealing activity of Rad52. However, as opposed to *RTS1*-induced RDR (A. Kishkevich & M. C. Whitby, pers. Comm.), BIR in fission yeast is seemingly far more dependent on Rad51 and less dependent on Rad52's strand annealing activity. This difference between RDR and BIR may be attributed to the structure of the replication

fork upon encountering a RFB or SSB being significantly different. In the case of RDR triggered by *RTS1*, the replication fork is unbroken and likely reversed (Nguyen et al., 2015), whilst in the case of BIR induced by a fork-SSB encounter, the fork is broken to form a seDSB (Kramara et al., 2018; Mayle et al., 2015; Vrtis et al., 2021). Conceivably, the Rad51-independent pathway (that depends on Rad52's DNA annealing activity) is more able to initiate RDR from a reversed fork than from a broken fork.

Having established that BIR-associated template switching is dependent on Rad51 and Rad52 in fission yeast, I went on to investigate whether the structure selective endonuclease Mus81 played a role in BIR in fission yeast. Intriguingly, I detected no change in the level of template switching. This is not the case in budding yeast, where Mus81 plays a pivotal role in limiting BIR-mediated mutagenic synthesis (Mayle et al., 2015). In budding yeast, template switching associated with BIR in a *mus81*Δ mutant is largely suppressed by Yen1 (Mayle et al 2015). Unlike budding yeast, there is no Yen1 in fission yeast and thus, there is no obvious alternative to Mus81, which could explain why a *mus81*Δ mutant exhibits no change in template switching. However, I cannot exclude the possibility that there are other backup pathways to Mus81 that are responsible for the maturation of the D-loop as it travels away from the break site.

I also investigated whether Ku70 plays a role in BIR, as it does in RDR. There is contradicting evidence on the role of Ku70 in RDR – studies suggest that it may either promote (Teixeira-Silva et al., 2017), and/or oppose (M. C. Whitby, pers. Comm.) HR in fission yeast. Also, a recent study in mammalian cells indicates that it may play no role at all in the context of a perturbed replication fork (Willis et al., 2018). In my system of study, Ku70 limits the template switching associated with BIR. I suspect this is due to the need to remove Ku70 via short-range end resection (Foster et al., 2011), which

results in slower restart and increased likelihood to merge with an opposing replication fork prior to replicating the 12.4 kb reporter.

Lastly, I aimed to understand whether the mechanism of replisome disassembly at lagging-strand SSBs determined using *Xenopus* egg extracts *in vitro* (Vrtis et. al., 2021), is conserved *in vivo* in fission yeast. I found that Pof3 is required for template switching when BIR is induced by nicks in the lagging-strand (BS), consistent with the findings using the *Xenopus* system *in vitro*. Presumably, when Pof3 is absent, replisome disassembly at lagging-strand SSBs is either slower or fails altogether. In either case, the induction of BIR (and therefore template switching at the 12.4 kb reporter) will be impaired.

The main limitation of my study is that the variations in direct repeat recombination detected 12.4 kb downstream may be due to changes in either template switching or replication restart. If it was possible to determine with accuracy the amount of replication restart, it would be possible to correlate quantitatively the changes in direct repeat recombination to the variations in template switching. To address this limitation, a potentially feasible approach could be to utilise polymerase usage sequencing (Pu-seq) to quantify the amount of replication restart. Pu-seq could determine the proportion of leading and lagging template strands synthesised by Polδ and Polε at any specific genomic locus (Miyabe et al., 2011).

A second limitation is that the increase in template switching detected with 12.4 kb reporters following the induction of the Flp-nick system was only about 4 to 6-fold higher than spontaneous recombination. When I deleted *rad51* or *pof3*, there was also a ~3-fold increase in spontaneous recombination. Therefore, it was difficult to determine whether the template switching detected upon Flp^{H305L} expression was completely dependent on Rad51/Pof3, or whether there was some residual template

switching that was independent of them. In the future, it will be imperative to try to increase the amount of template switching generated following the induction of the Flp-nick. This would increase the sensitivity of my experimental system. Presumably, increasing the number of cells experiencing a site-specific Flp^{H305L}-induced SSB would result in increased replication fork-SSB encounters and thus, increased template switching. The low template switching levels detected in my system are potentially due to low levels of Flp^{H305L} molecules entering the nucleus. The addition of a Nucleus Localisation Sequence (NLS) upstream of the *FLPH305L* coding sequence should, theoretically, increase the number of Flp^{H305L} molecules being imported into the nucleus. Lastly, expression of Flp^{H305L} from the same promoter (*i.e. Pnmt1*) but from a multicopy plasmid would likely increase the number of Flp^{H305L}-induced nicks and thus, template switching downstream. Indeed, with 0kb reporters I detected a ~10-fold increase in direct repeat recombination when Flp^{H305L} was expressed from a multicopy pREP1 plasmid, compared to when expression was driven from a single chromosomal copy (compare data in **Fig. 3.3, 3.4 and 3.5)**.

Finally, it will be important to elucidate whether, in a similar fashion to the findings of Vrtis et. al., 2021, SSBs are converted into seDSBs *in vivo*. To answer this question, it will be necessary to perform direct physical analysis of the DNA at the break site via a combination of neutral and alkaline gel electrophoresis and Southern blotting. However, detection of the SSBs and DSBs may be challenging if they are rapidly processed. It may be necessary to develop improved expression systems for Flp^{H305L} and gpII, which would enable efficient and rapid expression in synchronized populations of cells. In this regard, it is interesting to note the recent success in expressing I-*Ppo*I from the *TET* promoter to generate site-specific DSBs in fission yeast (Yan et al., 2019). It will also be important to consider performing these

experiments in a *rad50S* mutant background, which is known to be deficient in processing protein-bound DNA ends (Osman et al., 2016).

Chapter 6

Appendix

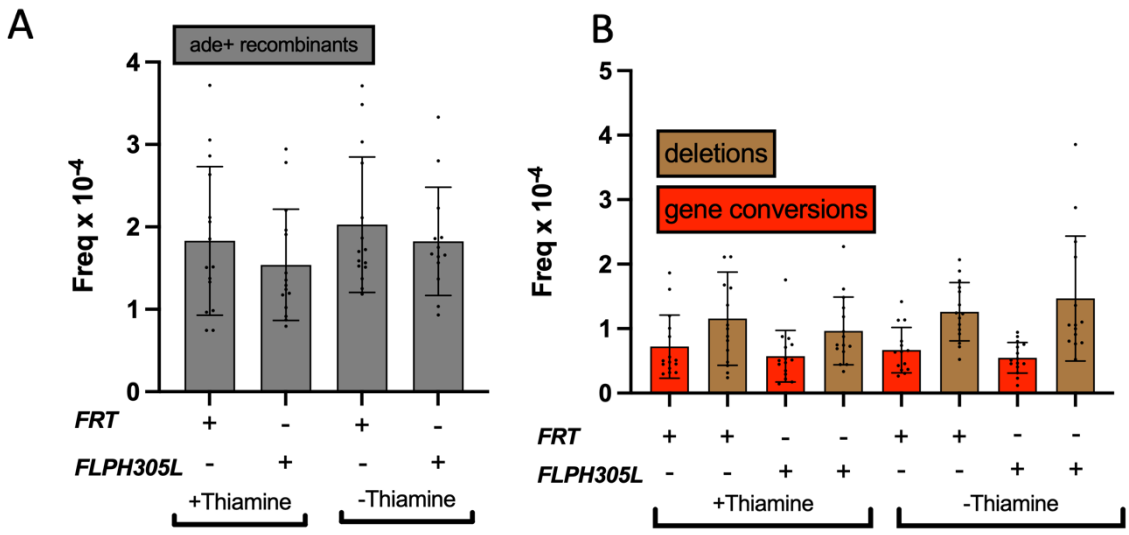

Figure 6.1. High FlpH305L expression per se does not stimulate recombination between ade6 heteroalleles. *Bar charts illustrating the frequency of Ade$^+$ recombinants generated following high expression of FLPH305L from the nmt1 promoter when no FRT site is present, and when the FRT sequence is present but no FLPH305L is expressed.* ***A)*** *illustrates the frequency of total Ade$^+$ recombinants frequency.* ***B)*** *Bar chart showing the proportion of gene conversions and deletions. TS indicates Top (leading) strand whilst BS indicates bottom (lagging) strand orientation. Strains are MCW10107 and MCW10163. Error bars represent +/- standard deviation.*

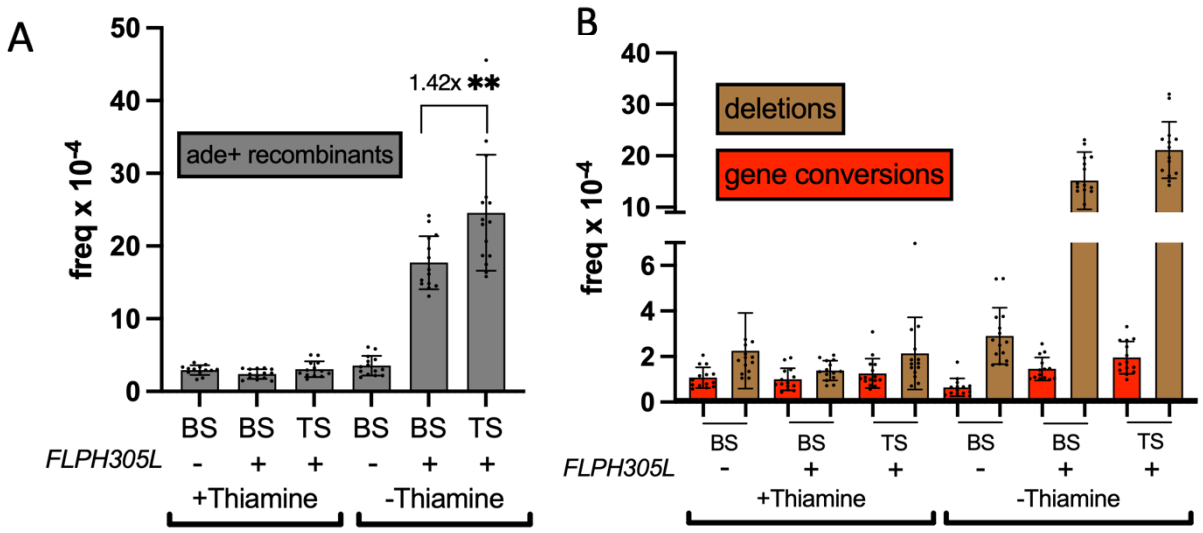

Figure 6.2. ***Both TS and BS Flp^{H305L}-induced SSBs stimulate recombination between direct ade6 heteroalleles to similar frequencies. A)*** *Frequency of Ade^{+} recombinants at 12.4 kb reporter downstream of the FRT site when ori1253 is deleted.* ***B)*** *Calculated proportion of gene conversions and deletions. TS indicates Top (leading) strand whilst BS indicates bottom (lagging) strand orientation. Strains are MCW10205, MCW10137, MCW10140. Error bars represent +/- standard deviation. P<0.01 (**).*

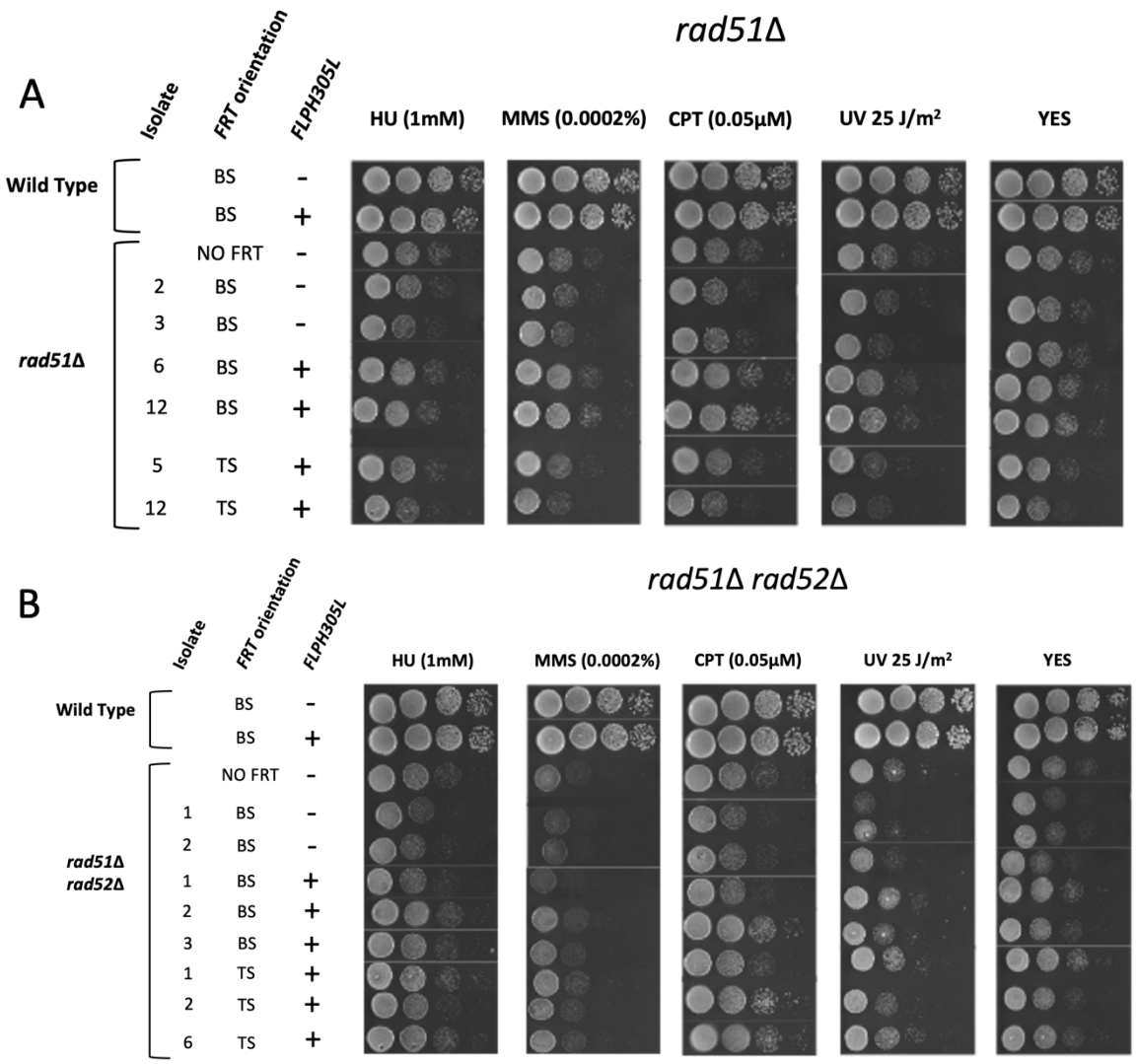

Figure 6.3. Genotoxin sensitivity assay of rad51Δ and rad51Δrad52Δ strains to monitor cell viability. *10µl of serial 10-fold dilutions were spotted on YES plates supplemented with either HU, MMS or CPT at the appropriate concentration or irradiated with UV light.* ***A)*** *Genotoxin sensitivity assay of rad51Δ mutants. Strains are MCW10205, MCW10138, MCW1088, MCW10430, MCW10431, MCW10432, MCW10433, MCW10434 and MCW10435* ***B)*** *Genotoxin sensitivity assay of rad51Δrad52Δ mutants. Strains are MCW10205, MCW10138, MCW9182, MCW10436, MCW10437, MCW10438, MCW10439, MCW10440, MCW10441, MCW10442 and MCW10443. Plates were photographed following 4 days of growth at 30 ℃.*

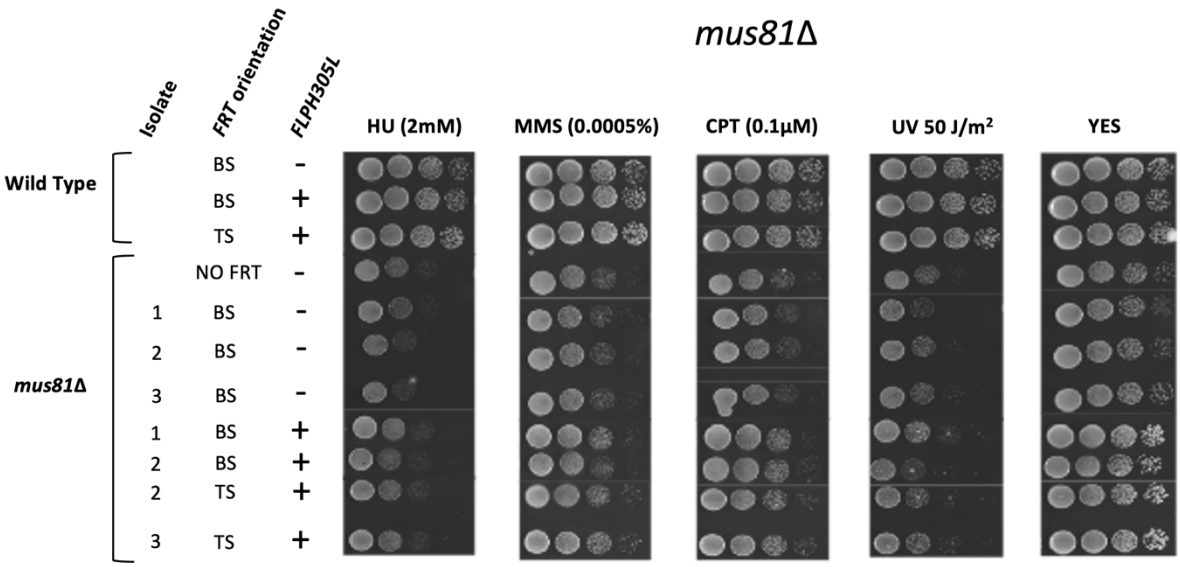

Figure 6.4 Spot assay to assess the genotoxin sensitivity of mus81Δ mutants. *10µl of serial 10-fold dilutions were spotted on YES plates supplemented with HU, MMS or CPT at the appropriate concentration or irradiated with UV light. Strains are MCW10205, MCW10138, MCW10139, FO1366, MCW10162, MCW10163, MCW10164, MCW10165, MCW10166, MCW10167, MCW10168. Plates were photographed following 4 days of growth at 30 ℃.*

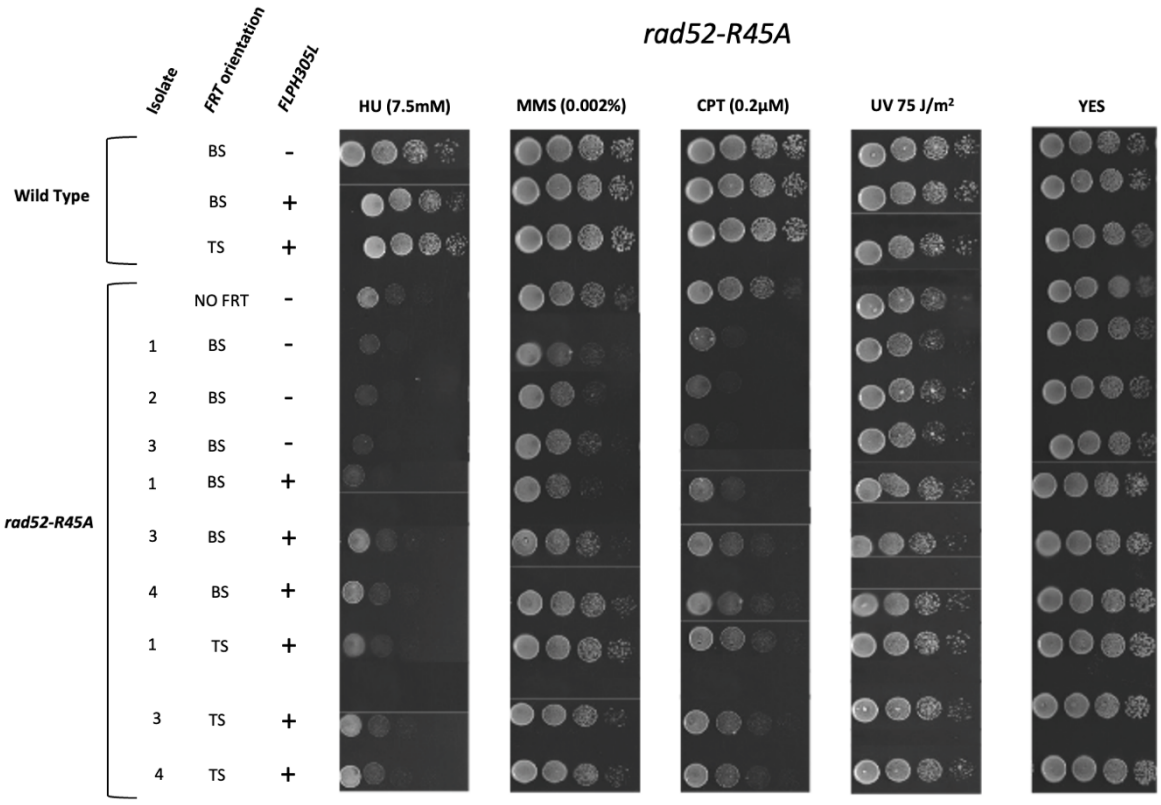

Figure 6.5 Genotoxin sensitivity assay of rad52-R45A mutants to monitor cell viability. *10µl of serial 10-fold dilutions were spotted on YES plates supplemented with HU, MMS or CPT at the appropriate concentration or irradiated with UV light. Strains are MCW10205, MCW10138, MCW10139, MCW9604, MCW10453, MCW10454, MCW10455, MCW10456, MCW10457, MCW10458, MCW10459, MCW10460, MCW1046. Plates were photographed following 4 days of growth at 30 ℃*

Table 6.1 *List of S. pombe strains utilised in this study.*

Strain number		**Mating-type**	***Genotype***	**Source**	**Construction methodology**
FO656	n/a	h+	*ura4-D18 leu1-32 his3-D1 arg3-D4*	Lab strain	n/a
FO652	n/a	h-	*ura4-D18 leu1-32 his3-D1 arg3-D4*	Lab strain	n/a
FO1236	n/a	h-	*ade6-M375 ura4-D18 leu1-32 his3-D1 arg3-D4*	Lab strain	n/a
FO1366	n/a	h-	*Mus81∆::KanMX6 ura4-D18 leu1-32 his3-D1 arg3-D4*	Lab strain	n/a
MCW428	n/a	h-	*ade6-M375 int::pFOX2/his3+/ade6-L469 ura4-D18 leu1-32 his3-D1 arg3-D4*	Lab strain	n/a

MCW1207	n/a	h-	*ku70Δ::KanMX6 ura4-D18 leu1-32 his3-D1 arg3-D4*	Lab strain	n/a
MCW9182	n/a	h-	*Rad51Δ::arg3⁺ Rad52Δ::KanMX6 ura4-D18 leu1-32 his3-D1 arg3-D4*	Lab strain	n/a
MCW9604	n/a	h-	*Rad52-R45A::KanMX6 ura4-D18 leu1-32 his3-D1 arg3-D4*	Lab strain	n/a
MCW10375	n/a	h-	*Pof3Δ::KanMX6 ura4-D18 leu1-32 his3-D1 arg3-D4*	Lab strain	n/a
MCW10107	YL1	h-	*ade6-M375 int::pYL7/his3+ /FRT TS/ade6-L469 ura4-D18 leu1-32 his3-D1 arg3-D4*	This study	BlpI linearised pYL7 was integrated into FO1236. Progeny screened by auxotrophy and colony PCR with o717 ando705. The integrity of the FRT site was checked via Sanger sequencing with 0717.
MCW10108	YL2	h-	*ade6-M375 int::pYL4/his3+ /FRT BS/ade6-L469 ura4-D18 leu1-32 his3-D1 arg3-D4*	This study	BlpI linearised pYL4 was integrated into FO1236. Progeny screened by auxotrophy and colony PCR with o717 ando705. The integrity of the FRT site was checked via Sanger sequencing with 0717.

MCW10109	YL3	h+	*lys1::Pnmt1-FLPH305L-hphMX4 ura4-D18 leu1-32 his3-D1 arg3-D4*	This study	NotI digested pYL1 was integrated into FO656. Progeny screened by drug selection and colony PCR with oMW1938 and oMW1286.
MCW10110	YL4	h+	*lys1::Pnmt41-FLPH305L-hphMX4 ura4-D18 leu1-32 his3-D1 arg3-D4*	This study	NotI digested pYL3 was integrated into FO656. Progeny screened by drug selection and colony PCR with oMW1938 and oMW1286.
MCW10111	YL5	h+	*lys1::Pnmt81-FLPH305L-hphMX4 ura4-D18 leu1-32 his3-D1 arg3-D4*	This study	NotI digested pYL2 was integrated into FO656. Progeny screened by drug selection and colony PCR with oMW1938 and oMW1286.
MCW10112	YL6	h-	*ade6::FRT BS-LEU2 ura4-D18 leu1-32 his3-D1 arg3-D4*	This study	NotI digested pYL6 was integrated into FO652. Progeny screened by auxotrophy and colony PCR with oMW983 and oMW1905. The integrity of the FRT site was checked via Sanger sequencing with oMW983
MCW10114	YL8	h-	*ade6::FRT TS-LEU2 ura4-D18 leu1-32 his3-D1 arg3-D4*	This study	NotI digested pYL5 was integrated into FO652. Progeny screened by auxotrophy and colony PCR with oMW983 and oMW1905. The integrity of the FRT site was checked via Sanger sequencing with oMW983

MCW10116	YL10	h-	*lys1::Pnmt81-FLPH305L-hphMX4 ade6-M375 int::pYL7/his3+ /FRT TS/ade6-L469 ura4-D18 leu1-32 his3-D1 arg3-D4*	This study	Cross between MCW10107 and MCW10111. Progeny was screened by auxotrophy and drug selection.
MCW10117	YL11	h-	*lys1::Pnmt41-FLPH305L-hphMX4 ade6-M375 int::pYL7/his3+ /FRT TS/ade6-L469 ura4-D18 leu1-32 his3-D1 arg3-D4*	This study	Cross between MCW10107 and MCW10110. Progeny was screened by auxotrophy and drug selection.
MCW10118	YL12	h-	*lys1::Pnmt1-FLPH305L-hphMX4 ade6-M375 int::pYL7/his3+ /FRT TS/ade6-L469 ura4-D18 leu1-32 his3-D1 arg3-D4*	This study	Cross between MCW10107 and MCW10109. Progeny was screened by auxotrophy and drug selection.
MCW10121	YL15	h-	*lys1::Pnmt1-FLPH305L-hphMX4 ade6-M375 int::pYL4/his3+ /FRT BS/ade6-L469 ura4-D18 leu1-32 his3-D1 arg3-D4*	This study	Cross between MCW10108 and MCW10109. Progeny was screened by auxotrophy and drug selection.
MCW10128	YL17	h-	*ade6::FRT BS-LEU2 ade6-L469/pUC8/his3+/ade6-M375-ura4MX4-aim1 (12.4 kb) ura4-D18 leu1-32 his3-D1 arg3-D4 ade6-D1*	This study	Cross between MCW10112 and MCW9284. Progeny was screened by auxotrophy and drug selection.
MCW10130	YL19	h-	*ade6::FRT TS-LEU2 ade6-L469/pUC8/his3+/ade6-M375-ura4MX4-aim1 (12.4 kb) ura4-D18 leu1-32 his3-D1 arg3-D4 ade6-D1*	This study	Cross between MCW10114 and MCW9284. Progeny was screened by auxotrophy and drug selection.

MCW10133	YL22	h-	*oriIII-1253Δ::natMX4 ade6::FRT BS-LEU2 ade6-L469/pUC8/his3+/ade6-M375-ura4MX4-aim1 (12.4 kb) ura4-D18 leu1-32 his3-D1 arg3-D4 ade6-D1*	This study	Cross between MCW10127 and MCW9149. Progeny was screened by auxotrophy and drug selection.
MCW10134	YL23	h-	*oriIII-1253Δ::natMX4 ade6::FRT TS-LEU2 ade6-L469/pUC8/his3+/ade6-M375-ura4MX4-aim1 (12.4 kb) ura4-D18 leu1-32 his3-D1 arg3-D4 ade6-D1*	This study	Cross between MCW10129 and MCW9149. Progeny was screened by auxotrophy and drug selection.
MCW10137	YL26	h+	*lys1::Pnmt1-FLPH305L-hphMX4 oriIII-1253Δ::natMX4 ade6::FRT BS-LEU2 ade6-L469/pUC8/his3+/ade6-M375-ura4MX4-aim1 (12.4 kb) ura4-D18 leu1-32 his3-D1 arg3-D4 ade6-D1*	This study	Cross between MCW10133 and MCW10109. Progeny was screened by auxotrophy and drug selection.
MCW10138	YL27	h+	*lys1::Pnmt1-FLPH305L-hphMX4 oriIII-1253Δ::natMX4 ade6::FRT BS-LEU2 ade6-L469/pUC8/his3+/ade6-M375-ura4MX4-aim1 (12.4 kb) ura4-D18 leu1-32 his3-D1 arg3-D4 ade6-D1*	This study	Cross between MCW10133 and MCW10109. Progeny was screened by auxotrophy and drug selection.
MCW10139	YL28	h+	*lys1::Pnmt1-FLPH305L-hphMX4 oriIII-1253Δ::natMX4 ade6::FRT TS-LEU2 ade6-L469/pUC8/his3+/ade6-M375-ura4MX4-aim1 (12.4 kb) ura4-D18 leu1-32 his3-D1 arg3-D4 ade6-D1*	This study	Cross between MCW10134 and MCW10109. Progeny was screened by auxotrophy and drug selection.

MCW10140	YL29	h-	*lys1::Pnmt1-FLPH305L-hphMX4 oriIII-1253Δ::natMX4 ade6::FRT TS-LEU2 ade6-L469/pUC8/his3+/ade6-M375-ura4MX4-aim1 (12.4 kb) ura4-D18 leu1-32 his3-D1 arg3-D4 ade6-D1*	This study	Cross between MCW10134 and MCW10109. Progeny was screened by auxotrophy and drug selection.
MCW10141	YL30	h-	*lys1::Pnmt1-FLPH305L-hphMX4 ade6::FRT BS-LEU2 ade6-L469/pUC8/his3+/ade6-M375-ura4MX4-aim1 (12.4 kb) ura4-D18 leu1-32 his3-D1 arg3-D4 ade6-D1*	This study	Cross between MCW10128 and MCW10109. Progeny was screened by auxotrophy and drug selection.
MCW10144	YL33	h-	*lys1::Pnmt1-FLPH305L-hphMX4 ade6::FRT TS-LEU2 ade6-L469/pUC8/his3+/ade6-M375-ura4MX4-aim1 (12.4 kb) ura4-D18 leu1-32 his3-D1 arg3-D4 ade6-D1*	This study	Cross between MCW10130 and MCW10109. Progeny was screened by auxotrophy and drug selection.
MCW10147	YL36	h-	*ade6::gpII site TS-hphMX4 ura4-D18 leu1-32 his3-D1 arg3-D4*	This study	NotI digested pYL8 integrated into FO652. Progeny screened by drug selection and colony PCR with oMW706 and oMW2263.
MCW10148	YL37	h-	*ade6::gpII site BS-hphMX4 ura4-D18 leu1-32 his3-D1 arg3-D4*	This study	NotI digested pYL9 integrated into FO652. Progeny screened by drug selection and colony PCR with oMW706 and oMW2263.
MCW10151	YL40	h-	*ade6::gpII site BS-hphMX4 ade6-L469/pUC8/his3+/ade6-M375-ura4MX4-aim1 (12.4 kb) ura4-D18 leu1-32 his3-D1 arg3-D4 ade6-D1*	This study	Cross between MCW10148 and MCW9284. Progeny was screened by auxotrophy and drug selection.

MCW10152	YL41	h-	*ade6::gpII site TS-hphMX4 ade6-L469/pUC8/his3+/ade6-M375-ura4MX4-aim1 (12.4 kb) ura4-D18 leu1-32 his3-D1 arg3-D4 ade6-D1*	This study	Cross between MCW10147 and MCW9284. Progeny was screened by auxotrophy and drug selection.
MCW10163	YL52	h+	*lys1::Pnmt1-FLPH305L-hphMX4 ade6-M375/his3+ /ade6-L469 ura4-D18 leu1-32 his3-D1 arg3-D4*	This study	Cross between MCW10109 and MCW428. Progeny was screened by auxotrophy and drug selection.
MCW10164	YL53	h-	*lys1::Pnmt1-FLPH305L-hphMX4 ade6-M375/his3+ /ade6-L469 ura4-D18 leu1-32 his3-D1 arg3-D4*	This study	Cross between MCW10109 and MCW428. Progeny was screened by auxotrophy and drug selection.
MCW10165	YL54	h-	*lys1::Pnmt1-FLPH305L-hphMX4 ade6-M375/his3+ /ade6-L469 ura4-D18 leu1-32 his3-D1 arg3-D4*	This study	Cross between MCW10109 and MCW428. Progeny was screened by auxotrophy and drug selection.
MCW10192	YL57	h+	*oriIII-1253Δ::natMX4 ade6::gpII site TS-hphMX4 ade6-L469/pUC8/his3+/ade6-M375-ura4MX4-aim1 (12.4 kb) ura4-D18 leu1-32 his3-D1 arg3-D4 ade6-D1*	This study	Cross between MCW10154 and MCW9149. Progeny was screened by auxotrophy and drug selection.
MCW10194	YL59	h+	*oriIII-1253Δ::natMX4 ade6::gpII site BS-hphMX4 ade6-L469/pUC8/his3+/ade6-M375-ura4MX4-aim1 (12.4 kb) ura4-D18 leu1-32 his3-D1 arg3-D4 ade6-D1*	This study	Cross between MCW10150 and MCW9149. Progeny was screened by auxotrophy and drug selection.

MCW10205	YL63	h+	*oriIII-1253Δ::natMX4 ade6::FRT BS-LEU2 ade6-L469/pUC8/his3+/ade6-M375-ura4MX4-aim1 (12.4 kb) ura4-D18 leu1-32 his3-D1 arg3-D4 ade6-D1*	This study	Cross between MCW10127 and MCW9149. Progeny was screened by auxotrophy and drug selection.
MCW10430	YL88	h+	*rad51Δ::arg3^{+} oriIII-1253Δ::natMX4 ade6::FRT BS-LEU2 ade6-L469/pUC8/his3+/ade6-M375-ura4MX4-aim1 (12.4 kb) ura4-D18 leu1-32 his3-D1 arg3-D4 ade6-D1*	This study	Cross between MCW10205 and MCW9182. Progeny was screened by auxotrophy and drug selection. Tested via spot assay to confirm sensitivity to genotoxic stress.
MCW10431	YL89	h+	*rad51Δ::arg3^{+} oriIII-1253Δ::natMX4 ade6::FRT BS-LEU2 ade6-L469/pUC8/his3+/ade6-M375-ura4MX4-aim1 (12.4 kb) ura4-D18 leu1-32 his3-D1 arg3-D4 ade6-D1*	This study	Cross between MCW10205 and MCW9182. Progeny was screened by auxotrophy and drug selection. Tested via spot assay to confirm sensitivity to genotoxic stress.
MCW10432	YL90	h+	*rad51Δ::arg3^{+} lys1::Pnmt1-FLPH305L-hphMX4 oriIII-1253Δ::natMX4 ade6::FRT BS-LEU2 ade6-L469/pUC8/his3+/ade6-M375-ura4MX4-aim1 (12.4 kb) ura4-D18 leu1-32 his3-D1 arg3-D4 ade6-D1*	This study	Cross between MCW10138 and MCW9182. Progeny was screened by auxotrophy and drug selection. Tested via spot assay to confirm sensitivity to genotoxic stress.
MCW10433	YL91	h+	*rad51Δ::arg3^{+} lys1::Pnmt1-FLPH305L-hphMX4 oriIII-1253Δ::natMX4 ade6::FRT BS-LEU2 ade6-L469/pUC8/his3+/ade6-M375-ura4MX4-aim1 (12.4 kb) ura4-D18 leu1-32 his3-D1 arg3-D4 ade6-D1*	This study	Cross between MCW10138 and MCW9182. Progeny was screened by auxotrophy and drug selection. Tested via spot assay to confirm sensitivity to genotoxic stress.

MCW10434	YL92	h+	*rad51Δ::arg3⁺ lys1::Pnmt1-FLPH305L-hphMX4 oriIII-1253Δ::natMX4 ade6::FRT TS-LEU2 ade6-L469/pUC8/his3+/ade6-M375-ura4MX4-aim1 (12.4 kb) ura4-D18 leu1-32 his3-D1 arg3-D4 ade6-D1*	This study	Cross between MCW10139 and MCW9182. Progeny was screened by auxotrophy and drug selection. Tested via spot assay to confirm sensitivity to genotoxic stress.
MCW10435	YL93	h+	*rad51Δ::arg3⁺ lys1::Pnmt1-FLPH305L-hphMX4 oriIII-1253Δ::natMX4 ade6::FRT TS-LEU2 ade6-L469/pUC8/his3+/ade6-M375-ura4MX4-aim1 (12.4 kb) ura4-D18 leu1-32 his3-D1 arg3-D4 ade6-D1*	This study	Cross between MCW10139 and MCW9182. Progeny was screened by auxotrophy and drug selection. Tested via spot assay to confirm sensitivity to genotoxic stress.
MCW10436	YL94	h+	*rad51Δ::arg3⁺ rad52Δ::KanMX6 oriIII-1253Δ::natMX4 ade6::FRT BS-LEU2 ade6-L469/pUC8/his3+/ade6-M375-ura4MX4-aim1 (12.4 kb) ura4-D18 leu1-32 his3-D1 arg3-D4 ade6-D1*	This study	Cross between MCW10205 and MCW9182. Progeny was screened by auxotrophy and drug selection. Tested via spot assay to confirm sensitivity to genotoxic stress.
MCW10437	YL95	h-	*rad51Δ::arg3⁺ rad52Δ::KanMX6 oriIII-1253Δ::natMX4 ade6::FRT BS-LEU2 ade6-L469/pUC8/his3+/ade6-M375-ura4MX4-aim1 (12.4 kb) ura4-D18 leu1-32 his3-D1 arg3-D4 ade6-D1*	This study	Cross between MCW10205 and MCW9182. Progeny was screened by auxotrophy and drug selection. Tested via spot assay to confirm sensitivity to genotoxic stress.
MCW10438	YL96	h+	*rad51Δ::arg3⁺ rad52Δ::KanMX6 lys1::Pnmt1-FLPH305L-hphMX4 oriIII-1253Δ::natMX4 ade6::FRT BS-LEU2 ade6-*	This study	Cross between MCW10138 and MCW9182. Progeny was screened by auxotrophy and drug selection. Tested via spot assay to confirm sensitivity to genotoxic stress.

			L469/pUC8/his3+/ade6-M375-ura4MX4-aim1 (12.4 kb) ura4-D18 leu1-32 his3-D1 arg3-D4 ade6-D1		
MCW10439	YL97	h-	*rad51Δ::arg3⁺ rad52Δ::KanMX6 lys1::Pnmt1-FLPH305L-hphMX4 oriII-1253Δ::natMX4 ade6::FRT BS-LEU2 ade6-L469/pUC8/his3+/ade6-M375-ura4MX4-aim1 (12.4 kb) ura4-D18 leu1-32 his3-D1 arg3-D4 ade6-D1*	This study	Cross between MCW10138 and MCW9182. Progeny was screened by auxotrophy and drug selection. Tested via spot assay to confirm sensitivity to genotoxic stress.
MCW10440	YL98	h+	*rad51Δ::arg3⁺ rad52Δ::KanMX6 lys1::Pnmt1-FLPH305L-hphMX4 oriII-1253Δ::natMX4 ade6::FRT BS-LEU2 ade6-L469/pUC8/his3+/ade6-M375-ura4MX4-aim1 (12.4 kb) ura4-D18 leu1-32 his3-D1 arg3-D4 ade6-D1*	This study	Cross between MCW10138 and MCW9182. Progeny was screened by auxotrophy and drug selection. Tested via spot assay to confirm sensitivity to genotoxic stress.
MCW10441	YL99	h-	*rad51Δ::arg3⁺ rad52Δ::KanMX6 lys1::Pnmt1-FLPH305L-hphMX4 oriII-1253Δ::natMX4 ade6::FRT TS-LEU2 ade6-L469/pUC8/his3+/ade6-M375-ura4MX4-aim1 (12.4 kb) ura4-D18 leu1-32 his3-D1 arg3-D4 ade6-D1*	This study	Cross between MCW10139 and MCW9182. Progeny was screened by auxotrophy and drug selection. Tested via spot assay to confirm sensitivity to genotoxic stress.
MCW10442	YL100	h-	*rad51Δ::arg3⁺ rad52Δ::KanMX6 lys1::Pnmt1-FLPH305L-hphMX4 oriII-1253Δ::natMX4 ade6::FRT TS-LEU2 ade6-L469/pUC8/his3+/ade6-M375-ura4MX4-aim1 (12.4 kb) ura4-D18 leu1-32 his3-D1 arg3-D4 ade6-D1*	This study	Cross between MCW10139 and MCW9182. Progeny was screened by auxotrophy and drug selection. Tested via spot assay to confirm sensitivity to genotoxic stress.

MCW10443	YL101	h+	*rad51Δ::arg3⁺ rad52Δ::KanMX6 lys1::Pnmt1-FLPH305L-hphMX4 oriIII-1253Δ::natMX4 ade6::FRT TS-LEU2 ade6-L469/pUC8/his3+/ade6-M375-ura4MX4-aim1 (12.4 kb) ura4-D18 leu1-32 his3-D1 arg3-D4 ade6-D1*	This study	Cross between MCW10139 and MCW9182. Progeny was screened by auxotrophy and drug selection. Tested via spot assay to confirm sensitivity to genotoxic stress.
MCW10444	YL102	h+	*ku70Δ::KanMX6 oriIII-1253Δ::natMX4 ade6::FRT BS-LEU2 ade6-L469/pUC8/his3+/ade6-M375-ura4MX4-aim1 (12.4 kb) ura4-D18 leu1-32 his3-D1 arg3-D4 ade6-D1*	This study	Cross between MCW10205 and MCW1207. Progeny was screened by auxotrophy and drug selection.
MCW10445	YL103	h+	*ku70Δ::KanMX6 oriIII-1253Δ::natMX4 ade6::FRT BS-LEU2 ade6-L469/pUC8/his3+/ade6-M375-ura4MX4-aim1 (12.4 kb) ura4-D18 leu1-32 his3-D1 arg3-D4 ade6-D1*	This study	Cross between MCW10205 and MCW1207. Progeny was screened by auxotrophy and drug selection.
MCW10446	YL104	h+	*ku70Δ::KanMX6 oriIII-1253Δ::natMX4 ade6::FRT BS-LEU2 ade6-L469/pUC8/his3+/ade6-M375-ura4MX4-aim1 (12.4 kb) ura4-D18 leu1-32 his3-D1 arg3-D4 ade6-D1*	This study	Cross between MCW10205 and MCW1207. Progeny was screened by auxotrophy and drug selection.
MCW10447	YL105	h-	*ku70Δ::KanMX6 lys1::Pnmt1-FLPH305L-hphMX4 oriIII-1253Δ::natMX4 ade6::FRT BS-LEU2 ade6-L469/pUC8/his3+/ade6-M375-ura4MX4-aim1 (12.4 kb) ura4-D18 leu1-32 his3-D1 arg3-D4 ade6-D1*	This study	Cross between MCW10138 and MCW1207. Progeny was screened by auxotrophy and drug selection.
MCW10448	YL106	h-	*ku70Δ::KanMX6 lys1::Pnmt1-FLPH305L-hphMX4 oriIII-1253Δ::natMX4 ade6::FRT BS-LEU2 ade6-*	This study	Cross between MCW10138 and MCW1207. Progeny was screened by auxotrophy and drug selection.

			L469/pUC8/his3+/ade6-M375-ura4MX4-aim1 (12.4 kb) ura4-D18 leu1-32 his3-D1 arg3-D4 ade6-D1		
MCW10449	YL107	h-	*ku70Δ::KanMX6 lys1::Pnmt1-FLPH305L-hphMX4 oriIII-1253Δ::natMX4 ade6::FRT BS-LEU2 ade6-L469/pUC8/his3+/ade6-M375-ura4MX4-aim1 (12.4 kb) ura4-D18 leu1-32 his3-D1 arg3-D4 ade6-D1*	This study	Cross between MCW10138 and MCW1207. Progeny was screened by auxotrophy and drug selection.
MCW10450	YL108	h-	*ku70Δ::KanMX6 lys1::Pnmt1-FLPH305L-hphMX4 oriIII-1253Δ::natMX4 ade6::FRT TS-LEU2 ade6-L469/pUC8/his3+/ade6-M375-ura4MX4-aim1 (12.4 kb) ura4-D18 leu1-32 his3-D1 arg3-D4 ade6-D1*	This study	Cross between MCW10139 and MCW1207. Progeny was screened by auxotrophy and drug selection.
MCW10451	YL109	h-	*ku70Δ::KanMX6 lys1::Pnmt1-FLPH305L-hphMX4 oriIII-1253Δ::natMX4 ade6::FRT TS-LEU2 ade6-L469/pUC8/his3+/ade6-M375-ura4MX4-aim1 (12.4 kb) ura4-D18 leu1-32 his3-D1 arg3-D4 ade6-D1*	This study	Cross between MCW10139 and MCW1207. Progeny was screened by auxotrophy and drug selection.
MCW10452	YL110	h+	*ku70Δ::KanMX6 lys1::Pnmt1-FLPH305L-hphMX4 oriIII-1253Δ::natMX4 ade6::FRT TS-LEU2 ade6-L469/pUC8/his3+/ade6-M375-ura4MX4-aim1 (12.4 kb) ura4-D18 leu1-32 his3-D1 arg3-D4 ade6-D1*	This study	Cross between MCW10139 and MCW1207. Progeny was screened by auxotrophy and drug selection.

MCW10453	YL111	h+	*Rad52-R45A::KanMX6 oriIII-1253Δ::natMX4 ade6::FRT BS-LEU2 ade6-L469/pUC8/his3+/ade6-M375-ura4MX4-aim1 (12.4 kb) ura4-D18 leu1-32 his3-D1 arg3-D4 ade6-D1*	This study	Cross between MCW10205 and MCW9604. Progeny was screened by auxotrophy and drug selection. Tested via spot assay to confirm sensitivity to genotoxic stress.
MCW10454	YL112	h-	*Rad52-R45A::KanMX6 oriIII-1253Δ::natMX4 ade6::FRT BS-LEU2 ade6-L469/pUC8/his3+/ade6-M375-ura4MX4-aim1 (12.4 kb) ura4-D18 leu1-32 his3-D1 arg3-D4 ade6-D1*	This study	Cross between MCW10205 and MCW9604. Progeny was screened by auxotrophy and drug selection. Tested via spot assay to confirm sensitivity to genotoxic stress.
MCW10455	YL113	h+	*Rad52-R45A::KanMX6 oriIII-1253Δ::natMX4 ade6::FRT BS-LEU2 ade6-L469/pUC8/his3+/ade6-M375-ura4MX4-aim1 (12.4 kb) ura4-D18 leu1-32 his3-D1 arg3-D4 ade6-D1*	This study	Cross between MCW10205 and MCW9604. Progeny was screened by auxotrophy and drug selection. Tested via spot assay to confirm sensitivity to genotoxic stress.
MCW10456	YL114	h+	*Rad52-R45A::KanMX6 lys1::Pnmt1-FLPH305L-hphMX4 oriIII-1253Δ::natMX4 ade6::FRT BS-LEU2 ade6-L469/pUC8/his3+/ade6-M375-ura4MX4-aim1 (12.4 kb) ura4-D18 leu1-32 his3-D1 arg3-D4 ade6-D1*	This study	Cross between MCW10138 and MCW9604. Progeny was screened by auxotrophy and drug selection. Tested via spot assay to confirm sensitivity to genotoxic stress.
MCW10457	YL115	h+	*Rad52-R45A::KanMX6 lys1::Pnmt1-FLPH305L-hphMX4 oriIII-1253Δ::natMX4 ade6::FRT BS-LEU2 ade6-*	This study	Cross between MCW10138 and MCW9604. Progeny was screened by auxotrophy and drug selection. Tested via spot assay to confirm sensitivity to genotoxic stress.

			L469/pUC8/his3+/ade6-M375-ura4MX4-aim1 (12.4 kb) ura4-D18 leu1-32 his3-D1 arg3-D4 ade6-D1		
MCW10458	YL116	h+	*Rad52-R45A::KanMX6 lys1::Pnmt1-FLPH305L-hphMX4 oriIII-1253Δ::natMX4 ade6::FRT BS-LEU2 ade6-L469/pUC8/his3+/ade6-M375-ura4MX4-aim1 (12.4 kb) ura4-D18 leu1-32 his3-D1 arg3-D4 ade6-D1*	This study	Cross between MCW10138 and MCW9604. Progeny was screened by auxotrophy and drug selection. Tested via spot assay to confirm sensitivity to genotoxic stress.
MCW10459	YL117	h-	*Rad52-R45A::KanMX6 lys1::Pnmt1-FLPH305L-hphMX4 oriIII-1253Δ::natMX4 ade6::FRT TS-LEU2 ade6-L469/pUC8/his3+/ade6-M375-ura4MX4-aim1 (12.4 kb) ura4-D18 leu1-32 his3-D1 arg3-D4 ade6-D1*	This study	Cross between MCW10139 and MCW9604. Progeny was screened by auxotrophy and drug selection. Tested via spot assay to confirm sensitivity to genotoxic stress.
MCW10460	YL118	h+	*Rad52-R45A::KanMX6 lys1::Pnmt1-FLPH305L-hphMX4 oriIII-1253Δ::natMX4 ade6::FRT TS-LEU2 ade6-L469/pUC8/his3+/ade6-M375-ura4MX4-aim1 (12.4 kb) ura4-D18 leu1-32 his3-D1 arg3-D4 ade6-D1*	This study	Cross between MCW10139 and MCW9604. Progeny was screened by auxotrophy and drug selection. Tested via spot assay to confirm sensitivity to genotoxic stress.
MCW10461	YL119	h-	*Rad52-R45A::KanMX6 lys1::Pnmt1-FLPH305L-hphMX4 oriIII-1253Δ::natMX4 ade6::FRT TS-LEU2 ade6-L469/pUC8/his3+/ade6-M375-ura4MX4-aim1 (12.4 kb) ura4-D18 leu1-32 his3-D1 arg3-D4 ade6-D1*	This study	Cross between MCW10139 and MCW9604. Progeny was screened by auxotrophy and drug selection. Tested via spot assay to confirm sensitivity to genotoxic stress.

MCW10462	YL120	h-	*Mus81Δ::KanMX6 oriIII-1253Δ::natMX4 ade6::FRT BS-LEU2 ade6-L469/pUC8/his3+/ade6-M375-ura4MX4-aim1 (12.4 kb) ura4-D18 leu1-32 his3-D1 arg3-D4 ade6-D1*	This study	Cross between MCW10205 and FO1366. Progeny was screened by auxotrophy and drug selection. Tested via spot assay to confirm sensitivity to genotoxic stress.
MCW10463	YL121	h+	*Mus81Δ::KanMX6 oriIII-1253Δ::natMX4 ade6::FRT BS-LEU2 ade6-L469/pUC8/his3+/ade6-M375-ura4MX4-aim1 (12.4 kb) ura4-D18 leu1-32 his3-D1 arg3-D4 ade6-D1*	This study	Cross between MCW10205 and FO1366. Progeny was screened by auxotrophy and drug selection. Tested via spot assay to confirm sensitivity to genotoxic stress.
MCW10464	YL122	h+	*Mus81Δ::KanMX6 oriIII-1253Δ::natMX4 ade6::FRT BS-LEU2 ade6-L469/pUC8/his3+/ade6-M375-ura4MX4-aim1 (12.4 kb) ura4-D18 leu1-32 his3-D1 arg3-D4 ade6-D1*	This study	Cross between MCW10205 and FO1366. Progeny was screened by auxotrophy and drug selection. Tested via spot assay to confirm sensitivity to genotoxic stress.
MCW10465	YL123	h+	*Mus81Δ::KanMX6 lys1::Pnmt1-FLPH305L-hphMX4 oriIII-1253Δ::natMX4 ade6::FRT BS-LEU2 ade6-L469/pUC8/his3+/ade6-M375-ura4MX4-aim1 (12.4 kb) ura4-D18 leu1-32 his3-D1 arg3-D4 ade6-D1*	This study	Cross between MCW10138 and FO1366. Progeny was screened by auxotrophy and drug selection. Tested via spot assay to confirm sensitivity to genotoxic stress.
MCW10466	YL124	h-	*Mus81Δ::KanMX6 lys1::Pnmt1-FLPH305L-hphMX4 oriIII-1253Δ::natMX4 ade6::FRT BS-LEU2 ade6-L469/pUC8/his3+/ade6-M375-ura4MX4-aim1 (12.4 kb) ura4-D18 leu1-32 his3-D1 arg3-D4 ade6-D1*	This study	Cross between MCW10138 and FO1366. Progeny was screened by auxotrophy and drug selection. Tested via spot assay to confirm sensitivity to genotoxic stress.

MCW10467	YL125	h+	*Mus81Δ::KanMX6 lys1::Pnmt1-FLPH305L-hphMX4 oriIII-1253Δ::natMX4 ade6::FRT TS-LEU2 ade6-L469/pUC8/his3+/ade6-M375-ura4MX4-aim1 (12.4 kb) ura4-D18 leu1-32 his3-D1 arg3-D4 ade6-D1*	This study	Cross between MCW10139 and FO1366. Progeny was screened by auxotrophy and drug selection. Tested via spot assay to confirm sensitivity to genotoxic stress.
MCW10468	YL126	h+	*Mus81Δ::KanMX6 lys1::Pnmt1-FLPH305L-hphMX4 oriIII-1253Δ::natMX4 ade6::FRT TS-LEU2 ade6-L469/pUC8/his3+/ade6-M375-ura4MX4-aim1 (12.4 kb) ura4-D18 leu1-32 his3-D1 arg3-D4 ade6-D1*	This study	Cross between MCW10139 and FO1366. Progeny was screened by auxotrophy and drug selection. Tested via spot assay to confirm sensitivity to genotoxic stress.
MCW10469	YL127	h+	*Pof3Δ::KanMX6 oriIII-1253Δ::natMX4 ade6::FRT BS-LEU2 ade6-L469/pUC8/his3+/ade6-M375-ura4MX4-aim1 (12.4 kb) ura4-D18 leu1-32 his3-D1 arg3-D4 ade6-D1*	This study	Cross between MCW10205 and MCW10375. Progeny was screened by auxotrophy and drug selection.
MCW10470	YL128	h+	*Pof3Δ::KanMX6 lys1::Pnmt1-FLPH305L-hphMX4 oriIII-1253Δ::natMX4 ade6::FRT BS-LEU2 ade6-L469/pUC8/his3+/ade6-M375-ura4MX4-aim1 (12.4 kb) ura4-D18 leu1-32 his3-D1 arg3-D4 ade6-D1*	This study	Cross between MCW10138 and MCW10375. Progeny was screened by auxotrophy and drug selection.
MCW10471	YL129	h+	*Pof3Δ::KanMX6 lys1::Pnmt1-FLPH305L-hphMX4 oriIII-1253Δ::natMX4 ade6::FRT BS-LEU2 ade6-L469/pUC8/his3+/ade6-M375-ura4MX4-aim1 (12.4 kb) ura4-D18 leu1-32 his3-D1 arg3-D4 ade6-D1*	This study	Cross between MCW10138 and MCW10375. Progeny was screened by auxotrophy and drug selection.

MCW10472	YL130	h-	*Pof3Δ::KanMX6 lys1::Pnmt1-FLPH305L-hphMX4 oriIII-1253Δ::natMX4 ade6::FRT TS-LEU2 ade6-L469/pUC8/his3+/ade6-M375-ura4MX4-aim1 (12.4 kb) ura4-D18 leu1-32 his3-D1 arg3-D4 ade6-D1*	This study	Cross between MCW10139 and MCW10375. Progeny was screened by auxotrophy and drug selection.

Table 6.2 *List of plasmids utilised in this study.*

Strain number	**Strain background**	**Plasmid name**	**Antibiotic resistance marker**	***S. pombe* marker**	**Plasmid construction strategy**
MW3096	DH5α	**pYL1**	Ampicillin	*hphMX4*	PCR amplified nmt1-FLPH305L (oMW1418, oMW1477) from pPC7; cloned as an AscI fragment into pMJ5. Diagnostic digest performed with SalI-BamHI. Sequence confirmed with (oMW1202, oMW1172, oMW1040).
MW3097	DH5α	**pYL2**	Ampicillin	*hphMX4*	PCR amplified nmt81-FLPH305L (oMW1418, oMW1477) from pPC9; cloned as an AscI fragment into pMJ5. Diagnostic digest performed with SalI-BamHI. Sequence confirmed with (oMW1202, oMW1172, oMW1040).
MW3098	DH5α	**pYL3**	Ampicillin	*hphMX4*	PCR amplified nmt41-FLPH305L (oMW1418, oMW1477) from pPC6; cloned as an AscI fragment into pMJ5. Diagnostic digest performed with SalI-BamHI.Sequence confirmed with (oMW1202, oMW1172, oMW1040).

MW3099	DH5α	**pYL4**	Ampicillin	*HIS3*	Annealed oligos (oMW2068, oMW2069) cloned as SalI-EcoRV fragment into pFOX2. Diagnostic digest performed with XbaI. Sequence confirmed with oMW1604.
MW3100	DH5α	**pYL5**	Ampicillin	*LEU2*	Annealed oligos (oMW2068, oMW2069) cloned as SalI-SmaI fragment into pMW938. Diagnostic digest performed with XhoI and NdeI. Sequence confirmed with Sourcebioscience SP6 promoter primer.
MW3101	DH5α	**pYL6**	Ampicillin	*LEU2*	Annealed oligos (oMW2031, oMW2032) cloned as SalI-SmaI fragment into pMW938. Diagnostic digest performed with XhoI and NdeI. Sequence confirmed with Sourcebioscience SP6 promoter primer.
MW3102	DH5α	**pYL7**	Ampicillin	*HIS3*	Annealed oligos (oMW2031, oMW2032) cloned as SalI-EcoRV fragment into pFOX2. Diagnostic digest performed with XbaI. Sequence confirmed with oMW1604.

MW3105	DH5α	**pYL8**	Ampicillin	*hphMX4*	Annealed oligos (oMW480, oMW481) cloned as SalI-SmaI fragment into pMW921. Diagnostic digest performed with XhoI and NdeI. Sequence confirmed with Sourcebioscience SP6 promoter primer.
MW3106	DH5α	**pYL9**	Ampicillin	*hphMX4*	Annealed oligos (oMW482, oMW483) cloned as SalI-SmaI fragment into pMW921. Diagnostic digest performed with XhoI and NdeI. Sequence confirmed with Sourcebioscience SP6 promoter primer.
MW2918	DH5α	**pPC6**	Ampicillin	*LEU2*	Constructed by PC. PCR amplified FLPH305L gene (oMW2029. oMW2030) from MW2902 and cloned as a BamHI-NdeI fragment into pREP41. Sequence confirmed with oMW1040, oMW2047, oMW1172
MW2924	DH5α	**pPC7**	Ampicillin	*LEU2*	Constructed by PC. PCR amplified FLPH305L gene (oMW2029, oMW2030) from MW2902 and cloned as a BamHI-NdeI fragment into pREP1.Sequence confirmed with oMW1040, oMW2047, oMW1172
MW2926	DH5α	**pPC9**	Ampicillin	*LEU2*	Constructed by PC. PCR amplified FLPH305L gene (oMW2029, oMW2030) from MW2902 and cloned as a BamHI-NdeI fragment

					into pREP81.Sequence confirmed with oMW1040, oMW2047, oMW1172
MW2561	DH5α	**pMJ5**	Ampicillin	*hphMX4*	Constructed by MJ. PCR amplified *Pnmt1-NLS-Mar* from p850 (oMW1418, oMW1477) and cloned as AscI fragment into pSHA4. Sequence confirmed with oMW1172 andoMW1040.
none	DH5α	**pFOX2**	Ampicillin	*HIS3*	Targeting construct to generate recombinant substrates consisting in nontandem direct ade6 heteroallele repeats flanking a functional *his3*+ gene.
MW2839	DH5α	**pMW938**	Ampicillin	*LEU2*	Constructed by MCW. Targeting construct to replace endogenous *ade6* with the *FRT* site.
MW2639	DH5α	**pMW921**	Ampicillin	*hphMX4*	Constructed by MCW. Targeting construct to replace endogenous *ade6* with the *FRT* site.
MW2902	DH5α	**pLB109**	Ampicillin	*none*	Constructed by LB. Plasmid carrying budding yeast Flp recombinase step-arrest mutant FLPH305L

MW1726	DH5α	**pREP1**	Ampicillin	*LEU2*	Empty pREP1 plasmid utilised as negative control.

Constructed by - **MCW**: Matthew Whitby; **LB**: Lotte Bjergbaek; **MJ**: Manisha Jalan; **PC**: Patrick Collins; **YL**: Yassine Laksir

Table 6.3 *List of oligonucleotides utilised in this study*

Oligonucleotide number	**Sequence 5'→ 3'**
oMW285	AATGTACGGGCGACAGTC
oMW480	TTTAAAGTCGACCTCGAGGTTCTTTAATAGTGGACTCTTGTTCCAAACTGGAACAACACCCGGGTTTAAA
oMW481	TTTAAACCCGGGTGTTGTTCCAGTTTGGAACAAGAGTCCACTATTAAAGAACCTCGAGGTCGACTTTAAA
oMW482	TTTAAACCCGGGCTCGAGGTTCTTTAATAGTGGACTCTTGTTCCAAACTGGAACAACAGTCGACTTTAAA
oMW483	TTTAAAGTCGACTGTTGTTCCAGTTTGGAACAAGAGTCCACTATTAAAGAACCTCGAGCCCGGGTTTAAA
oMW706	AAAGGCCTCGCTTCTCGAG
oMW707	AGCAGCATACGCTAAAATC
oMW717	AGAAGAAAGCGATCGATGAG
oMW1040	ATCCCGCACCCGTCTACG
oMW1172	GATAATGGACCTGTTAATCG
oMW1202	ATATCCATGGGATTTAACAAAGCGACTATAAGTC
oMW1418	TATGGCGCGCCCTGCAGGTCGATCGACTC

oMW1477	TATGGCGCGCCCGAATTCGAGCTCGCATTAC
oMW1604	TTCGGCCCAATTGACC
oMW2029	GGGTCGACATGCCACAATTTGGTATATTATGTA
oMW2030	TAGGATCCTAATTATATGCGTCTATTTATGTAGGATGAAA
oMW2031	ATCGAAGTTCCTATACTTTCTAGAGAATAGGAACTTCCGAATAGGAACTTCG
oMW2032	TCGACGAAGTTCCTATTCGGAAGTTCCTATTCTCTAGAAAGTATAGGAACTTCGAT
oMW2047	TACTCGTTGTCGGAGATC
oMW2068	ATCGAAGTTCCTATTCGGAAGTTCCTATTCTCTAGAAAGTATAGGAACTTCG
oMW2069	TCGACGAAGTTCCTATACTTTCTAGAGAATAGGAACTTCCGAATAGGAACTTCGAT

Chapter 7

Bibliography

Ahn, J.S., Osman, F., Whitby, M.C., 2005. Replication fork blockage by RTS1 at an ectopic site promotes recombination in fission yeast. EMBO J 24, 2011–2023.

Ait Saada, A., Lambert, S.A.E., Carr, A.M., 2018. Preserving replication fork integrity and competence via the homologous recombination pathway. DNA Repair, Cutting-edge Perspectives in Genomic Maintenance V 71, 135–147.

Ait Saada, A., Teixeira-Silva, A., Iraqui, I., Costes, A., Hardy, J., Paoletti, G., Fréon, K., Lambert, S.A.E., 2017. Unprotected Replication Forks Are Converted into Mitotic Sister Chromatid Bridges. Molecular Cell 66, 398-410.e4.

Anand, R., Beach, A., Li, K., Haber, J., 2017. Rad51-mediated double-strand break repair and mismatch correction of divergent substrates. Nature 544, 377–380.

Anand, R.P., Tsaponina, O., Greenwell, P.W., Lee, C.-S., Du, W., Petes, T.D., Haber, J.E., 2014. Chromosome rearrangements via template switching between diverged repeated sequences. Genes Dev 28, 2394–2406.

Andersen, S.L., Sekelsky, J., 2010. Meiotic versus Mitotic Recombination: Two Different Routes for Double-Strand Break Repair. Bioessays 32, 1058–1066.

Arcangioli, B., de Lahondès, R., 2000. Fission yeast switches mating type by a replication–recombination coupled process. EMBO J 19, 1389–1396.

Arlt, M.F., Mulle, J.G., Schaibley, V.M., Ragland, R.L., Durkin, S.G., Warren, S.T., Glover, T.W., 2009. Replication stress induces genome-wide copy number changes in human cells that resemble polymorphic and pathogenic variants. Am J Hum Genet 84, 339–350.

Arlt, M.F., Ozdemir, A.C., Birkeland, S.R., Wilson, T.E., Glover, T.W., 2011. Hydroxyurea induces de novo copy number variants in human cells. Proceedings of the National Academy of Sciences 108, 17360–17365.

Asano, S., Higashitani, A., Horiuchi, K., 1999. Filamentous phage replication initiator protein gpII forms a covalent complex with the 5' end of the nick it introduced. Nucleic Acids Res 27, 1882–1889.

Avemann, K., Knippers, R., Koller, T., Sogo, J.M., 1988. Camptothecin, a specific inhibitor of type I DNA topoisomerase, induces DNA breakage at replication forks. Mol Cell Biol 8, 3026–3034.

Bartkova, J., Rezaei, N., Liontos, M., Karakaidos, P., Kletsas, D., Issaeva, N., Vassiliou, L.-V.F., Kolettas, E., Niforou, K., Zoumpourlis, V.C., Takaoka, M., Nakagawa, H., Tort, F., Fugger, K., Johansson, F., Sehested, M., Andersen, C.L., Dyrskjot, L., Ørntoft, T., Lukas, J., Kittas, C., Helleday, T., Halazonetis, T.D., Bartek, J., Gorgoulis, V.G., 2006. Oncogene-induced senescence is part of the tumorigenesis barrier imposed by DNA damage checkpoints. Nature 444, 633–637.

Baumann, P., Benson, F.E., West, S.C., 1996. Human Rad51 Protein Promotes ATP-Dependent Homologous Pairing and Strand Transfer Reactions In Vitro. Cell 87, 757–766.

Baxter, J., Diffley, J.F.X., 2008. Topoisomerase II inactivation prevents the completion of DNA replication in budding yeast. Mol Cell 30, 790–802.

Benson, F.E., Baumann, P., West, S.C., 1998. Synergistic actions of Rad51 and Rad52 in recombination and DNA repair. Nature 391, 401–404.

Bernstein, K.A., Gangloff, S., Rothstein, R., 2010. The RecQ DNA helicases in DNA Repair. Annu Rev Genet 44, 393–417.

Bester, A.C., Roniger, M., Oren, Y.S., Im, M.M., Sarni, D., Chaoat, M., Bensimon, A., Zamir, G., Shewach, D.S., Kerem, B., 2011. Nucleotide Deficiency Promotes

Genomic Instability in Early Stages of Cancer Development. Cell 145, 435–446.

Bhowmick, R., Minocherhomji, S., Hickson, I.D., 2016. RAD52 Facilitates Mitotic DNA Synthesis Following Replication Stress. Mol Cell 64, 1117–1126.

Binz, S.K., Sheehan, A.M., Wold, M.S., 2004. Replication protein A phosphorylation and the cellular response to DNA damage. DNA Repair (Amst) 3, 1015–1024.

Bizard, A.H., Hickson, I.D., 2014. The dissolution of double Holliday junctions. Cold Spring Harb Perspect Biol 6, a016477.

Boddy, M.N., Gaillard, P.-H.L., McDonald, W.H., Shanahan, P., Yates, J.R., Russell, P., 2001. Mus81-Eme1 Are Essential Components of a Holliday Junction Resolvase. Cell 107, 537–548.

Branzei, D., Foiani, M., 2010. Maintaining genome stability at the replication fork. Nat Rev Mol Cell Biol 11, 208–219.

Bugreev, D.V., Yu, X., Egelman, E.H., Mazin, A.V., 2007. Novel pro- and anti-recombination activities of the Bloom's syndrome helicase. Genes Dev. 21, 3085–3094.

Caldecott, K.W., 2020. Mammalian DNA base excision repair: Dancing in the moonlight. DNA Repair 93, 102921.

Caldecott, K.W., 2008. Single-strand break repair and genetic disease. Nat Rev Genet 9, 619–631.

Caldecott, K.W., 2003. DNA Single-Strand Break Repair and Spinocerebellar Ataxia. Cell 112, 7–10.

Campos, L.V., Briana, HG., Darren, R. H., Tamar K., Hayes W. M., Kristie, L. R., Brandt, F. E., James, M. D., 2022. RTEL1 and MCM10 overcome topological

stress during replication termination. BioRxiv. Preprint. doi:https://doi.org/10.1101/2022.01.27.478093

Carr, A.M., Lambert, S., 2013. Replication Stress-Induced Genome Instability: The Dark Side of Replication Maintenance by Homologous Recombination. Journal of Molecular Biology, Replicon Theory, Regulation of DNA Replication and Genomic Instability 425, 4733–4744.

Caunt, P., Impoolsup, A., Greenfield, P.F., 1988. Stability of recombinant plasmids in yeast. Journal of Biotechnology 8, 173–192.

Cimprich, K.A., Cortez, D., 2008. ATR: an essential regulator of genome integrity. Nat Rev Mol Cell Biol 9, 616–627.

Cobb, J.A., Schleker, T., Rojas, V., Bjergbaek, L., Tercero, J.A., Gasser, S.M., 2005. Replisome instability, fork collapse, and gross chromosomal rearrangements arise synergistically from Mec1 kinase and RecQ helicase mutations. Genes Dev 19, 3055–3069.

Dalgaard, J.Z., Klar, A.J.S., 2001. A DNA replication-arrest site RTS1 regulates imprinting by determining the direction of replication at mat1 in S. pombe. Genes Dev 15, 2060–2068.

Das, B.B., Huang, S.N., Murai, J., Rehman, I., Amé, J.-C., Sengupta, S., Das, S.K., Majumdar, P., Zhang, H., Biard, D., Majumder, H.K., Schreiber, V., Pommier, Y., 2014. PARP1–TDP1 coupling for the repair of topoisomerase I–induced DNA damage. Nucleic Acids Res 42, 4435–4449.

Davis, A.J., Chen, D.J., 2013. DNA double strand break repair via non-homologous end-joining. Transl Cancer Res 2, 130–143.

Davis, A.P., Symington, L.S., 2004. RAD51-Dependent Break-Induced Replication in Yeast. Mol Cell Biol 24, 2344–2351.

Deegan, T.D., Baxter, J., Ortiz Bazán, M.Á., Yeeles, J.T.P., Labib, K.P.M., 2019. Pif1-Family Helicases Support Fork Convergence during DNA Replication Termination in Eukaryotes. Molecular Cell 74, 231-244.e9.

Deem, A., Keszthelyi, A., Blackgrove, T., Vayl, A., Coffey, B., Mathur, R., Chabes, A., Malkova, A., 2011. Break-Induced Replication Is Highly Inaccurate. PLOS Biology 9, e1000594.

Demple, B., Harrison, L., 1994. REPAIR OF OXIDATIVE DAMAGE TO DNA: Enzymology and Biology. Annu. Rev. Biochem. 63, 915–948.

Dewar, J.M., Budzowska, M., Walter, J.C., 2015. The mechanism of DNA replication termination in vertebrates. Nature 525, 345–350.

Di Micco, R., Fumagalli, M., Cicalese, A., Piccinin, S., Gasparini, P., Luise, C., Schurra, C., Garre', M., Nuciforo, P.G., Bensimon, A., Maestro, R., Pelicci, P.G., d'Adda di Fagagna, F., 2006. Oncogene-induced senescence is a DNA damage response triggered by DNA hyper-replication. Nature 444, 638–642.

Dilley, R.L., Greenberg, R.A., 2015. ALTernative Telomere Maintenance and Cancer. Trends Cancer 1, 145–156.

Dilley, R.L., Verma, P., Cho, N.W., Winters, H.D., Wondisford, A.R., Greenberg, R.A., 2016. Break-induced telomere synthesis underlies alternative telomere maintenance. Nature 539, 54–58.

*Doe, C.L., Ahn, J.S., Dixon, J., Whitby, M.C., 2002. Mus81-Eme1 and Rqh1 Involvement in Processing Stalled and Collapsed Replication Forks *. Journal of Biological Chemistry 277, 32753–32759.*

Doe, C.L., Whitby, M.C., 2004. The involvement of Srs2 in post-replication repair and homologous recombination in fission yeast. Nucleic Acids Research 32, 1480–1491.

Donnianni, R.A., Symington, L.S., 2013. Break-induced replication occurs by conservative DNA synthesis. Proc Natl Acad Sci U S A 110, 13475–13480.

Donnianni, R.A., Zhou, Z.-X., Lujan, S.A., Al-Zain, A., Garcia, V., Glancy, E., Burkholder, A.B., Kunkel, T.A., Symington, L.S., 2019. DNA Polymerase Delta Synthesizes Both Strands during Break-Induced Replication. Mol Cell 76, 371-381.e4.

Downing, B., Morgan, R., VanHulle, K., Deem, A., Malkova, A., 2008. Large inverted repeats in the vicinity of a single double-strand break strongly affect repair in yeast diploids lacking Rad51. Mutat Res 645, 9–18.

Dupaigne, P., Lavelle, C., Justome, A., Lafosse, S., Mirambeau, G., Lipinski, M., Piétrement, O., Le Cam, E., 2008a. Rad51 polymerization reveals a new chromatin remodeling mechanism. PLoS One 3, e3643.

Dupaigne, P., Le Breton, C., Fabre, F., Gangloff, S., Le Cam, E., Veaute, X., 2008b. The Srs2 Helicase Activity Is Stimulated by Rad51 Filaments on dsDNA: Implications for Crossover Incidence during Mitotic Recombination. Molecular Cell 29, 243–254.

Durkin, S.G., Glover, T.W., 2007. Chromosome fragile sites. Annu Rev Genet 41, 169–192.

Duzdevich, D., Warner, M.D., Ticau, S., Ivica, N.A., Bell, S.P., Greene, E.C., 2015. The Dynamics of Eukaryotic Replication Initiation: Origin Specificity, Licensing, and Firing at the Single-Molecule Level. Molecular Cell 58, 483–494.

Elango, R., Sheng, Z., Jackson, J., DeCata, J., Ibrahim, Y., Pham, N.T., Liang, D.H., Sakofsky, C.J., Vindigni, A., Lobachev, K.S., Ira, G., Malkova, A., 2017.

Break-induced replication promotes formation of lethal joint molecules dissolved by Srs2. Nat Commun 8, 1790.

Errico, A., Costanzo, V., 2012. Mechanisms of replication fork protection: a safeguard for genome stability. Critical Reviews in Biochemistry and Molecular Biology 47, 222–235.

Foster, S.S., Balestrini, A., Petrini, J.H.J., 2011. Functional interplay of the Mre11 nuclease and Ku in the response to replication-associated DNA damage. Mol Cell Biol 31, 4379–4389.

Froget, B., Blaisonneau, J., Lambert, S., Baldacci, G., 2008. Cleavage of Stalled Forks by Fission Yeast Mus81/Eme1 in Absence of DNA Replication Checkpoint. MBoC 19, 445–456.

Gaillard, H., García-Muse, T., Aguilera, A., 2015. Replication stress and cancer. Nat Rev Cancer 15, 276–289.

Gaillard, H., Herrera-Moyano, E., Aguilera, A., 2013. Transcription-Associated Genome Instability. Chem. Rev. 113, 8638–8661.

García-Muse, T., Aguilera, A., 2016. Transcription–replication conflicts: how they occur and how they are resolved. Nat Rev Mol Cell Biol 17, 553–563.

Glover, T.W., Wilson, T.E., Arlt, M.F., 2017. Fragile sites in cancer: more than meets the eye. Nat Rev Cancer 17, 489–501.

Gobbini, E., Cassani, C., Vertemara, J., Wang, W., Mambretti, F., Casari, E., Sung, P., Tisi, R., Zampella, G., Longhese, M.P., 2018. The MRX complex regulates Exo1 resection activity by altering DNA end structure. EMBO J 37, e98588.

Gronostajski, R.M., Sadowski, P.D., 1985. The FLP recombinase of the Saccharomyces cerevisiae 2 microns plasmid attaches covalently to DNA via a phosphotyrosyl linkage. Mol Cell Biol 5, 3274–3279.

Hanada, K., Budzowska, M., Davies, S.L., van Drunen, E., Onizawa, H., Beverloo, H.B., Maas, A., Essers, J., Hickson, I.D., Kanaar, R., 2007. The structure-specific endonuclease Mus81 contributes to replication restart by generating double-strand DNA breaks. Nat Struct Mol Biol 14, 1096–1104.

Hanzlikova, H., Gittens, W., Krejcikova, K., Zeng, Z., Caldecott, K.W., 2017. Overlapping roles for PARP1 and PARP2 in the recruitment of endogenous XRCC1 and PNKP into oxidized chromatin. Nucleic Acids Res 45, 2546–2557.

Hayashi, M., Katou, Y., Itoh, T., Tazumi, A., Tazumi, M., Yamada, Y., Takahashi, T., Nakagawa, T., Shirahige, K., Masukata, H., 2007. Genome-wide localization of pre-RC sites and identification of replication origins in fission yeast. EMBO J 26, 1327–1339.

Heintzman, D. R., Lillian, V., Campos, J. W., Byl, N. O. James, M. D., 2019. Topoisomerase II Is Crucial for Fork Convergence during Vertebrate Replication Termination, Cell Reports 29, 422-436.

Hiasa, H., Marians, K.J., 1994. Tus prevents overreplication of oriC plasmid DNA. J Biol Chem 269, 26959–26968.

Hicks, W.M., Kim, M., Haber, J.E., 2010. Increased mutagenesis and unique mutation signature associated with mitotic gene conversion. Science 329, 82–85.

Hossain, Md.A., Lin, Y., Yan, S., 2018. Single-Strand Break End Resection in Genome Integrity: Mechanism and Regulation by APE2. Int J Mol Sci 19, 2389.

Hsiang, Y.H., Hertzberg, R., Hecht, S., Liu, L.F., 1985. Camptothecin induces protein-linked DNA breaks via mammalian DNA topoisomerase I. Journal of Biological Chemistry 260, 14873–14878.

Hu, J., Sun, L., Shen, F., Chen, Y., Hua, Y., Liu, Y., Zhang, M., Hu, Y., Wang, Q., Xu, W., Sun, F., Ji, J., Murray, J.M., Carr, A.M., Kong, D., 2012. The Intra-S Phase Checkpoint Targets Dna2 to Prevent Stalled Replication Forks from Reversing. Cell 149, 1221–1232.

Hu, Y., Raynard, S., Sehorn, M.G., Lu, X., Bussen, W., Zheng, L., Stark, J.M., Barnes, E.L., Chi, P., Janscak, P., Jasin, M., Vogel, H., Sung, P., Luo, G., 2007. RECQL5/Recql5 helicase regulates homologous recombination and suppresses tumor formation via disruption of Rad51 presynaptic filaments. Genes Dev 21, 3073–3084.

Huertas, P., Cortés-Ledesma, F., Sartori, A.A., Aguilera, A., Jackson, S.P., 2008. CDK targets Sae2 to control DNA-end resection and homologous recombination. Nature 455, 689–692.

Ira, G., Satory, D., Haber, J.E., 2006. Conservative inheritance of newly synthesized DNA in double-strand break-induced gene conversion. Mol Cell Biol 26, 9424–9429.

Iraqui, I., Chekkal, Y., Jmari, N., Pietrobon, V., Fréon, K., Costes, A., Lambert, S.A.E., 2012. Recovery of Arrested Replication Forks by Homologous Recombination Is Error-Prone. PLOS Genetics 8, e1002976.

Ishimi, Y., Sugasawa, K., Hanaoka, F., Eki, T., Hurwitz, J., 1992. Topoisomerase II plays an essential role as a swivelase in the late stage of SV40 chromosome replication in vitro. Journal of Biological Chemistry 267, 462–466.

Jain, S., Sugawara, N., Lydeard, J., Vaze, M., Gac, N.T.L., Haber, J.E., 2009. A recombination execution checkpoint regulates the choice of homologous recombination pathway during DNA double-strand break repair. Genes Dev. 23, 291–303.

Jalan, M., Oehler, J., Morrow, C.A., Osman, F., Whitby, M.C., 2019. Factors affecting template switch recombination associated with restarted DNA replication. Elife 8, e41697.

Jasin, M., Rothstein, R., 2013. Repair of Strand Breaks by Homologous Recombination. Cold Spring Harb Perspect Biol 5, a012740.

Jenkyn-Bedford, M., Jones, M.L., Baris, Y., Labib, K.P.M., Cannone, G., Yeeles, J.T.P., Deegan, T.D., 2021. A conserved mechanism for regulating replisome disassembly in eukaryotes. Nature 600, 743–747.

Johnson, R.E., Klassen, R., Prakash, L., Prakash, S., 2015. A Major Role of DNA Polymerase δ in Replication of Both the Leading and Lagging DNA Strands. Mol Cell 59, 163–175.

Jones, R.M., Mortusewicz, O., Afzal, I., Lorvellec, M., García, P., Helleday, T., Petermann, E., 2013. Increased replication initiation and conflicts with transcription underlie Cyclin E-induced replication stress. Oncogene 32, 3744–3753.

Kang, H.Y., Choi, E., Bae, S.H., Lee, K.H., Gim, B.S., Kim, H.D., Park, C., MacNeill, S.A., Seo, Y.S., 2000. Genetic analyses of Schizosaccharomyces pombe dna2(+) reveal that dna2 plays an essential role in Okazaki fragment metabolism. Genetics 155, 1055–1067.

Karim, A.S., Curran, K.A., Alper, H.S., 2013. Characterization of plasmid burden and copy number in Saccharomyces cerevisiae for optimization of metabolic engineering applications. FEMS Yeast Res 13, 10.1111/1567-1364.12016.

Katayama, S., Kitamura, K., Lehmann, A., Nikaido, O., Toda, T., 2002. Fission yeast F-box protein Pof3 is required for genome integrity and telomere function. Mol Biol Cell 13, 211–224.

Kearsey, S.E., Cotterill, S., 2003. Enigmatic variations: divergent modes of regulating eukaryotic DNA replication. Mol Cell 12, 1067–1075.

Kogoma, T., 1997. Stable DNA replication: interplay between DNA replication, homologous recombination, and transcription. Microbiol Mol Biol Rev 61, 212–238.

Kramara, J., Osia, B., Malkova, A., 2018. Break-Induced Replication: The Where, The Why, and The How. Trends in Genetics 34, 518–531.

Krejci, L., Van Komen, S., Li, Y., Villemain, J., Reddy, M.S., Klein, H., Ellenberger, T., Sung, P., 2003. DNA helicase Srs2 disrupts the Rad51 presynaptic filament. Nature 423, 305–309.

Kurokawa, Y., Murayama, Y., Haruta-Takahashi, N., Urabe, I., Iwasaki, H., 2008. Reconstitution of DNA Strand Exchange Mediated by Rhp51 Recombinase and Two Mediators. PLOS Biology 6, e88.

Kuzminov, A., 2001. Single-strand interruptions in replicating chromosomes cause double-strand breaks. Proc Natl Acad Sci U S A 98, 8241–8246.

Labib, K., Hodgson, B., 2007. Replication fork barriers: pausing for a break or stalling for time? EMBO Rep 8, 346–353.

Lambert, S., Watson, A., Sheedy, D.M., Martin, B., Carr, A.M., 2005. Gross Chromosomal Rearrangements and Elevated Recombination at an Inducible Site-Specific Replication Fork Barrier. Cell 121, 689–702.

Larsen, N.B., Hickson, I.D., Mankouri, H.W., 2014. Tus-Ter as a tool to study site-specific DNA replication perturbation in eukaryotes. Cell Cycle 13, 2994–2998.

Laurent, J.M., Garge, R.K., Teufel, A.I., Wilke, C.O., Kachroo, A.H., Marcotte, E.M., 2020. Humanization of yeast genes with multiple human orthologs reveals functional divergence between paralogs. PLOS Biology 18, e3000627.

Le, S., Moore, J.K., Haber, J.E., Greider, C.W., 1999. RAD50 and RAD51 Define Two Pathways That Collaborate to Maintain Telomeres in the Absence of Telomerase. Genetics 152, 143–152.

Le, T.T., Ainsworth, J., Polo Rivera, C., Macartney, T., Labib, K.P.M., 2021. Reconstitution of human CMG helicase ubiquitylation by CUL2LRR1 and multiple E2 enzymes. Biochem J 478, 2825–2842.

Leonard, A.C., Méchali, M., 2013. DNA Replication Origins. Cold Spring Harb Perspect Biol 5, a010116.

Li, S., Wang, H., Jehi, S., Li, J., Liu, S., Wang, Zi, Truong, L., Chiba, T., Wang, Zefeng, Wu, X., 2021. PIF1 helicase promotes break-induced replication in mammalian cells. EMBO J 40, e104509.

Lieber, M.R., 1997. The FEN-1 family of structure-specific nucleases in eukaryotic dna replication, recombination and repair. BioEssays 19, 233–240.

Liu, J., Renault, L., Veaute, X., Fabre, F., Stahlberg, H., Heyer, W.-D., 2011. Rad51 paralogues Rad55–Rad57 balance the antirecombinase Srs2 in Rad51 filament formation. Nature 479, 245–248.

Liu, L., Yan, Z., Osia, B.A., Twarowski, J., Sun, L., Kramara, J., Lee, R.S., Kumar, S., Elango, R., Li, H., Dang, W., Ira, G., Malkova, A., 2021. Tracking break-induced replication shows that it stalls at roadblocks. Nature 590, 655–659.

Liu, L.F., 1989. Dna Topoisomerase Poisons as Antitumor Drugs. Annual Review of Biochemistry 58, 351–375.

Lorenz, A., Osman, F., Folkyte, V., Sofueva, S., Whitby, M.C., 2009. Fbh1 Limits Rad51-Dependent Recombination at Blocked Replication Forks. Molecular and Cellular Biology 29, 4742–4756.

Lorenz, A., Osman, F., Sun, W., Nandi, S., Steinacher, R., Whitby, M.C., 2012. The Fission Yeast FANCM Ortholog Directs Non-Crossover Recombination During Meiosis. Science 336, 1585–1588.

Low, E., Chistol, G., Zaher, M.S., Kochenova, O.V., Walter, J.C., 2020. The DNA replication fork suppresses CMG unloading from chromatin before termination. Genes Dev 34, 1534–1545.

Lundblad, V., Blackburn, E.H., 1993. An alternative pathway for yeast telomere maintenance rescues est1- senescence. Cell 73, 347–360.

Lydeard, J.R., Jain, S., Yamaguchi, M., Haber, J.E., 2007. Break-induced replication and telomerase-independent telomere maintenance require Pol32. Nature 448, 820–823.

Ma, C.-H., Kwiatek, A., Bolusani, S., Voziyanov, Y., Jayaram, M., 2007. Unveiling hidden catalytic contributions of the conserved His/Trp-III in tyrosine recombinases: assembly of a novel active site in Flp recombinase harboring alanine at this position. J Mol Biol 368, 183–196.

MacAlpine, D.M., Bell, S.P., 2005. A genomic view of eukaryotic DNA replication 18.

Macheret, M., Halazonetis, T.D., 2018. Intragenic origins due to short G1 phases underlie oncogene-induced DNA replication stress. Nature 555, 112–116.

Majka, J., Burgers, P.M.J., 2004. The PCNA–RFC Families of DNA Clamps and Clamp Loaders, in: Progress in Nucleic Acid Research and Molecular Biology. Academic Press, pp. 227–260.

Malkova, A., Ivanov, E.L., Haber, J.E., 1996. Double-strand break repair in the absence of RAD51 in yeast: a possible role for break-induced DNA replication. Proc Natl Acad Sci U S A 93, 7131–7136.

Malkova, A., Naylor, M.L., Yamaguchi, M., Ira, G., Haber, J.E., 2005. RAD51-Dependent Break-Induced Replication Differs in Kinetics and Checkpoint Responses from RAD51-Mediated Gene Conversion. Mol Cell Biol 25, 933–944.

Marians, K.J., 2000. PriA-directed replication fork restart in Escherichia coli. Trends Biochem Sci 25, 185–189.

Maric, M., Maculins, T., De Piccoli, G., Labib, K., 2014. Cdc48 and a ubiquitin ligase drive disassembly of the CMG helicase at the end of DNA replication. Science 346, 1253596.

Mayle, R., Campbell, I.M., Beck, C.R., Yu, Y., Wilson, M., Shaw, C.A., Bjergbaek, L., Lupski, J.R., Ira, G., 2015. Mus81 and converging forks limit the mutagenicity of replication fork breakage. Science 349, 742–747.

McEachern, M.J., Haber, J.E., 2006. Break-induced replication and recombinational telomere elongation in yeast. Annu Rev Biochem 75, 111–135.

McGill, C., Shafer, B., Strathern, J., 1989. Coconversion of flanking sequences with homothallic switching. Cell 57, 459–467.

McVey, M., Khodaverdian, V.Y., Meyer, D., Cerqueira, P.G., Heyer, W.-D., 2016. Eukaryotic DNA Polymerases in Homologous Recombination. Annu Rev Genet 50, 393–421.

Mehta, A., Beach, A., Haber, J.E., 2017. Homology Requirements and Competition between Gene Conversion and Break-Induced Replication during Double-Strand Break Repair. Mol Cell 65, 515-526.e3.

Mimitou, E.P., Symington, L.S., 2011. DNA end resection - unraveling the tail. DNA Repair (Amst) 10, 344–348.

Minocherhomji, S., Ying, S., Bjerregaard, V.A., Bursomanno, S., Aleliunaite, A., Wu, W., Mankouri, H.W., Shen, H., Liu, Y., Hickson, I.D., 2015. Replication stress activates DNA repair synthesis in mitosis. Nature 528, 286–290.

Mitra, S., Hazra, T.K., Roy, R., Ikeda, S., Biswas, T., Lock, J., Boldogh, I., Izumi, T., 1997. Complexities of DNA base excision repair in mammalian cells. Mol Cells 7, 305–312.

Miyabe, I., Kunkel, T.A., Carr, A.M., 2011. The Major Roles of DNA Polymerases Epsilon and Delta at the Eukaryotic Replication Fork Are Evolutionarily Conserved. PLoS Genet 7, e1002407.

Miyabe, I., Mizuno, K., Keszthelyi, A., Daigaku, Y., Skouteri, M., Mohebi, S., Kunkel, T.A., Murray, J.M., Carr, A.M., 2015. Polymerase δ replicates both strands after homologous recombination-dependent fork restart. Nat Struct Mol Biol 22, 932–938.

Mizuno, K., Lambert, S., Baldacci, G., Murray, J.M., Carr, A.M., 2009. Nearby inverted repeats fuse to generate acentric and dicentric palindromic chromosomes by a replication template exchange mechanism. Genes Dev. 23, 2876–2886.

Mosig, G., 1998. Recombination and recombination-dependent DNA replication in

Neumann, A.A., Reddel, R.R., 2002. Telomere maintenance and cancer ? look, no telomerase. Nat Rev Cancer 2, 879–884.

Nguyen, M.O., Jalan, M., Morrow, C.A., Osman, F., Whitby, M.C., 2015. Recombination occurs within minutes of replication blockage by RTS1 producing restarted forks that are prone to collapse. Elife 4, e04539.

Nieduszynski, C.A., Hiraga, S., Ak, P., Benham, C.J., Donaldson, A.D., 2007. OriDB: a DNA replication origin database. Nucleic Acids Res 35, D40–D46.

Nielsen, I., Andersen, A.H., Bjergbæk, L., 2012. Studying repair of a single protein-bound nick in vivo using the Flp-nick system. Methods Mol Biol 920, 393–415.

Nielsen, I., Bentsen, I.B., Lisby, M., Hansen, S., Mundbjerg, K., Andersen, A.H., Bjergbaek, L., 2009. A Flp-nick system to study repair of a single protein-bound nick in vivo. Nat Methods 6, 753–757.

Oakley, A.J., 2019. A structural view of bacterial DNA replication. Protein Science 28, 990–1004.

Osman, F., Ahn, J.S., Lorenz, A., Whitby, M.C., 2016. The RecQ DNA helicase Rqh1 constrains Exonuclease 1-dependent recombination at stalled replication forks. Sci Rep 6, 22837.

Osman, F., Whitby, M.C., 2009a. Monitoring Homologous Recombination Following Replication Fork Perturbation in the Fission Yeast Schizosaccharomyces pombe, in: Vengrova, S., Dalgaard, J.Z. (Eds.), DNA Replication: Methods and Protocols, Methods in Molecular Biology. Humana Press, Totowa, NJ, pp. 535–552.

Osman, F., Whitby, M.C., 2009b. Monitoring homologous recombination following replication fork perturbation in the fission yeast Schizosaccharomyces pombe. Methods Mol Biol 521, 535–552.

Osman, F., Whitby, M.C., 2007. Exploring the roles of Mus81-Eme1/Mms4 at perturbed replication forks. DNA Repair (Amst) 6, 1004–1017.

Paalme, V., Speek, M., 2021. Simple, inexpensive and RNase-free purification of plasmid DNA by fractional precipitation with isopropanol. BioTechniques 71, 490–494.

Pardo, B., Moriel-Carretero, M., Vicat, T., Aguilera, A., Pasero, P., 2020. Homologous recombination and Mus81 promote replication completion in response to replication fork blockage. EMBO reports 21, e49367.

Parker, M.W., Botchan, M.R., Berger, J.M., 2017. Mechanisms and regulation of DNA replication initiation in eukaryotes. Crit Rev Biochem Mol Biol 52, 107–144.

Pham, N., Yan, Z., Yu, Y., Faria Afreen, M., Malkova, A., Haber, J.E., Ira, G., 2021a. Mechanisms restraining break-induced replication at two-ended DNA double-strand breaks. The EMBO Journal 40, e104847.

Pham, N., Yan, Z., Yu, Y., Faria Afreen, M., Malkova, A., Haber, J.E., Ira, G., 2021b. Mechanisms restraining break-induced replication at two-ended DNA double-strand breaks. EMBO J 40, e104847.

Pommier, Y., Sun, Y., Huang, S.N., Nitiss, J.L., 2016. Roles of eukaryotic topoisomerases in transcription, replication and genomic stability. Nat Rev Mol Cell Biol 17, 703–721.

Ponder, R.G., Fonville, N.C., Rosenberg, S.M., 2005. A switch from high-fidelity to error-prone DNA double-strand break repair underlies stress-induced mutation. Mol Cell 19, 791–804.

Pouliot, J.J., Robertson, C.A., Nash, H.A., 2001. Pathways for repair of topoisomerase I covalent complexes in Saccharomyces cerevisiae. Genes to Cells 6, 677–687.

Pratt, D., Erdahl, W.S., 1968. Genetic control of bacteriophage M13 DNA synthesis. J Mol Biol 37, 181–200.

Pryce, D.W., Ramayah, S., Jaendling, A., McFarlane, R.J., 2009. Recombination at DNA replication fork barriers is not universal and is differentially regulated by Swi1. Proc Natl Acad Sci U S A 106, 4770–4775.

Qi, Z., Redding, S., Lee, J.Y., Gibb, B., Kwon, Y., Niu, H., Gaines, W.A., Sung, P., Greene, E.C., 2015. DNA Sequence Alignment by Microhomology Sampling during Homologous Recombination. Cell 160, 856–869.

Rai, S.K., Atwood-Moore, A., Levin, H.L., 2018. High-Frequency Lithium Acetate Transformation of Schizosaccharomyces pombe. Methods Mol Biol 1721, 167–177.

Ray Chaudhuri, A., Hashimoto, Y., Herrador, R., Neelsen, K.J., Fachinetti, D., Bermejo, R., Cocito, A., Costanzo, V., Lopes, M., 2012. Topoisomerase i poisoning results in PARP-mediated replication fork reversal. Nature Structural and Molecular Biology 19, 417–423.

Roumelioti, F.-M., Sotiriou, S.K., Katsini, V., Chiourea, M., Halazonetis, T.D., Gagos, S., 2016. Alternative lengthening of human telomeres is a conservative DNA replication process with features of break-induced replication. EMBO Rep 17, 1731–1737.

Sabatinos, S.A., Forsburg, S.L., 2010. Molecular genetics of Schizosaccharomyces pombe. Methods Enzymol 470, 759–795.

Saini, N., Giacobone, C.K., Klimczak, L.J., Papas, B.N., Burkholder, A.B., Li, J.-L., Fargo, D.C., Bai, R., Gerrish, K., Innes, C.L., Schurman, S.H., Gordenin, D.A., 2021. UV-exposure, endogenous DNA damage, and DNA replication errors shape the spectra of genome changes in human skin. PLOS Genetics 17, e1009302.

Saini, N., Ramakrishnan, S., Elango, R., Ayyar, S., Zhang, Y., Deem, A., Ira, G., Haber, J.E., Lobachev, K.S., Malkova, A., 2013. Migrating bubble during break-induced replication drives conservative DNA synthesis. Nature 502, 389–392.

Sakofsky, C.J., Ayyar, S., Malkova, A., 2012. Break-Induced Replication and Genome Stability. Biomolecules 2, 483–504.

Sakofsky, C.J., Roberts, S.A., Malc, E., Mieczkowski, P.A., Resnick, M.A., Gordenin, D.A., Malkova, A., 2014. Break-induced replication is a source of mutation clusters underlying kataegis. Cell Rep 7, 1640–1648.

Sambrook, J., Russell, D.W., 2001. Molecular cloning: a laboratory manual, 3rd ed. ed. Cold Spring Harbor Laboratory Press, Cold Spring Harbor, N.Y.

Sanchez, A., Gadaleta, M.C., Limbo, O., Russell, P., 2017. Lingering single-strand breaks trigger Rad51-independent homology-directed repair of collapsed replication forks in the polynucleotide kinase/phosphatase mutant of fission yeast. PLOS Genetics 13, e1007013.

Shao, Z., Davis, A.J., Fattah, K.R., So, S., Sun, J., Lee, K.-J., Harrison, L., Yang, J., Chen, D.J., 2012. Persistently bound Ku at DNA ends attenuates DNA end resection and homologous recombination. DNA Repair (Amst) 11, 310–316.

Shibata, A., Jeggo, P., Löbrich, M., 2018. The pendulum of the Ku-Ku clock. DNA Repair (Amst) 71, 164–171.

Signon, L., Malkova, A., Naylor, M.L., Klein, H., Haber, J.E., 2001. Genetic Requirements for RAD51- and RAD54-Independent Break-Induced Replication Repair of a Chromosomal Double-Strand Break. Mol Cell Biol 21, 2048–2056.

Sipiczki, M., 2000. Where does fission yeast sit on the tree of life? Genome Biol 1, reviews1011.1-reviews1011.4.

Smith, C.E., Llorente, B., Symington, L.S., 2007a. Template switching during break-induced replication. Nature 447, 102–105.

Smith, C.E., Llorente, B., Symington, L.S., 2007b. Template switching during break-induced replication. Nature 447, 102–105.

Smith, O.K., Aladjem, M.I., 2014. Chromatin Structure and Replication Origins: Determinants of Chromosome Replication and Nuclear Organization. Journal of Molecular Biology, Emerging Concepts in Epigenetic Signaling 426, 3330–3341.

Sotiriou, S.K., Kamileri, I., Lugli, N., Evangelou, K., Da-Ré, C., Huber, F., Padayachy, L., Tardy, S., Nicati, N.L., Barriot, S., Ochs, F., Lukas, C., Lukas, J., Gorgoulis, V.G., Scapozza, L., Halazonetis, T.D., 2016. Mammalian RAD52 Functions in Break-Induced Replication Repair of Collapsed DNA Replication Forks. Mol Cell 64, 1127–1134.

Srinivasan, S.V., Dominguez-Sola, D., Wang, L.C., Hyrien, O., Gautier, J., 2013. Cdc45 is a critical effector of myc-dependent DNA replication stress. Cell Rep 3, 1629–1639.

Štafa, A., Donnianni, R.A., Timashev, L.A., Lam, A.F., Symington, L.S., 2014. Template Switching During Break-Induced Replication Is Promoted by the Mph1 Helicase in Saccharomyces cerevisiae. Genetics 196, 1017–1028.

Stewart, J.A., Miller, A.S., Campbell, J.L., Bambara, R.A., 2008. Dynamic Removal of Replication Protein A by Dna2 Facilitates Primer Cleavage during Okazaki Fragment Processing in Saccharomyces cerevisiae. Journal of Biological Chemistry 283, 31356–31365.*

Stewart, L., Redinbo, M.R., Qiu, X., Hol, W.G., Champoux, J.J., 1998. A model for the mechanism of human topoisomerase I. Science 279, 1534–1541.

Stivison, E.A., Young, K.J., Symington, L.S., 2020. Interstitial telomere sequences disrupt break-induced replication and drive formation of ectopic telomeres. Nucleic Acids Res 48, 12697–12710.

Strumberg, D., Pilon, A.A., Smith, M., Hickey, R., Malkas, L., Pommier, Y., 2000. Conversion of topoisomerase I cleavage complexes on the leading strand of ribosomal DNA into 5'-phosphorylated DNA double-strand breaks by replication runoff. Molecular and Cellular Biology 20, 3977–3987.

Teixeira-Silva, A., Ait Saada, A., Hardy, J., Iraqui, I., Nocente, M.C., Fréon, K., Lambert, S.A.E., 2017a. The end-joining factor Ku acts in the end-resection of double strand break-free arrested replication forks. Nat Commun 8, 1982.

Teixeira-Silva, A., Ait Saada, A., Hardy, J., Iraqui, I., Nocente, M.C., Fréon, K., Lambert, S.A.E., 2017b. The end-joining factor Ku acts in the end-resection of double strand break-free arrested replication forks. Nat Commun 8, 1982.

Teng, S.-C., Chang, J., McCowan, B., Zakian, V.A., 2000. Telomerase-Independent Lengthening of Yeast Telomeres Occurs by an Abrupt Rad50p-Dependent, Rif-Inhibited Recombinational Process. Molecular Cell 6, 947–952.

Teng, S.-C., Zakian, V.A., 1999. Telomere-Telomere Recombination Is an Efficient Bypass Pathway for Telomere Maintenance in Saccharomyces cerevisiae. Mol Cell Biol 19, 8083–8093.

Thomas, A., Pommier, Y., 2019. Targeting Topoisomerase I in the Era of Precision Medicine. Clinical Cancer Research 25, 6581–6589.

Trujillo, K.M., Roh, D.H., Chen, L., Van Komen, S., Tomkinson, A., Sung, P., 2003. Yeast Xrs2 Binds DNA and Helps Target Rad50 and Mre11 to DNA Ends. Journal of Biological Chemistry 278, 48957–48964.*

VanHulle, K., Lemoine, F.J., Narayanan, V., Downing, B., Hull, K., McCullough, C., Bellinger, M., Lobachev, K., Petes, T.D., Malkova, A., 2007. Inverted DNA Repeats Channel Repair of Distant Double-Strand Breaks into Chromatid Fusions and Chromosomal Rearrangements. Mol Cell Biol 27, 2601–2614.

Vasan, S., Deem, A., Ramakrishnan, S., Argueso, J.L., Malkova, A., 2014. Cascades of Genetic Instability Resulting from Compromised Break-Induced Replication. PLOS Genetics 10, e1004119.

Verma, P., Greenberg, R.A., 2016. Noncanonical views of homology-directed DNA repair. Genes Dev 30, 1138–1154.

Vrtis, K.B., Dewar, J.M., Chistol, G., Wu, R.A., Graham, T.G.W., Walter, J.C., 2021. Single-strand DNA breaks cause replisome disassembly. Molecular Cell 81, 1309-1318.e6.

Vu, T.V., Das, S., Nguyen, C.C., Kim, J., Kim, J.-Y., 2022. Single-strand annealing: Molecular mechanisms and potential applications in CRISPR-Cas-based precision genome editing. Biotechnology Journal 17, 2100413.

Wang, J.C., 2002. Cellular roles of DNA topoisomerases: a molecular perspective. Nat Rev Mol Cell Biol 3, 430–440.

Waseem, N.H., Labib, K., Nurse, P., Lane, D.P., 1992. Isolation and analysis of the fission yeast gene encoding polymerase δ accessory protein PCNA. EMBO Journal 11, 5111–5120.

Whitehouse, C.J., Taylor, R.M., Thistlethwaite, A., Zhang, H., Karimi-Busheri, F., Lasko, D.D., Weinfeld, M., Caldecott, K.W., 2001. XRCC1 stimulates human polynucleotide kinase activity at damaged DNA termini and accelerates DNA single-strand break repair. Cell 104, 107–117.

Willis, N.A., Panday, A., Duffey, E.E., Scully, R., 2018. Rad51 recruitment and exclusion of non-homologous end joining during homologous recombination at a Tus/Ter mammalian replication fork barrier. PLoS Genet 14, e1007486.

Wilson, M.A., Kwon, Y., Xu, Y., Chung, W.-H., Chi, P., Niu, H., Mayle, R., Chen, X., Malkova, A., Sung, P., Ira, G., 2013. Pif1 helicase and Polδ promote recombination-coupled DNA synthesis via bubble migration. Nature 502, 393–396.

Woodward, A.M., Göhler, T., Luciani, M.G., Oehlmann, M., Ge, X., Gartner, A., Jackson, D.A., Blow, J.J., 2006. Excess Mcm2-7 license dormant origins of replication that can be used under conditions of replicative stress. J Cell Biol 173, 673–683.

Wyatt, M.D., Pittman, D.L., 2006. Methylating Agents and DNA Repair Responses: Methylated Bases and Sources of Strand Breaks. Chem. Res. Toxicol. 19, 1580–1594.

Wyrick, J.J., Aparicio, J.G., Chen, T., Barnett, J.D., Jennings, E.G., Young, R.A., Bell, S.P., Aparicio, O.M., 2001. Genome-wide distribution of ORC and MCM proteins in S. cerevisiae: high-resolution mapping of replication origins. Science 294, 2357–2360.

Yan, Z., Xue, C., Kumar, S., Crickard, J.B., Yu, Y., Wang, W., Pham, N., Li, Y., Niu, H., Sung, P., Greene, E.C., Ira, G., 2019. Rad52 Restrains Resection at DNA Double-Strand Break Ends in Yeast. Mol Cell 76, 699-711.e6.

Yeeles, J.T.P., Deegan, T.D., Janska, A., Early, A., Diffley, J.F.X., 2015. Regulated eukaryotic DNA replication origin firing with purified proteins. Nature 519, 431–435.

Yoder, B.L., Burgers, P.M., 1991. Saccharomyces cerevisiae replication factor C. I. Purification and characterization of its ATPase activity. Journal of Biological Chemistry 266, 22689–22697.

Yuan, Z., Li, H., 2020. Molecular mechanisms of eukaryotic origin initiation, replication fork progression, and chromatin maintenance. Biochemical Journal 477, 3499–3525.

Zhao, F., Kim, W., Kloeber, J.A., Lou, Z., 2020. DNA end resection and its role in DNA replication and DSB repair choice in mammalian cells. Exp Mol Med 52, 1705–1714.

Zhu, Z., Chung, W.-H., Shim, E.Y., Lee, S.E., Ira, G., 2008. Sgs1 helicase and two nucleases Dna2 and Exo1 resect DNA double strand break ends. Cell 134, 981–994.